UNCLASSIFIED

SECURITY CLASSIFICATION OF THIS PAGE *(When Data Entered)*

REPORT DOCUMENTATION PAGE		READ INSTRUCTIONS BEFORE COMPLETING FORM
1. REPORT NUMBER AFFDL-TR-73-95	2. GOVT ACCESSION NO.	3. RECIPIENT'S CATALOG NUMBER
4. TITLE *(and Subtitle)* EXPLORATORY INVESTIGATION OF RAPID CRACK PROPAGATION AND CRACK ARREST		5. TYPE OF REPORT & PERIOD COVERED FINAL REPORT 15 DEC 1971 - 7 FEB 1973 6. PERFORMING ORG. REPORT NUMBER D180-17529-1
7. AUTHOR(s) R. C. SHAH		8. CONTRACT OR GRANT NUMBER(s) F33615-72-C-1063
9. PERFORMING ORGANIZATION NAME AND ADDRESS BOEING AEROSPACE COMPANY SEATTLE, WASHINGTON 98124		10. PROGRAM ELEMENT, PROJECT, TASK AREA & WORK UNIT NUMBERS
11. CONTROLLING OFFICE NAME AND ADDRESS AIR FORCE FLIGHT DYNAMICS LABORATORY AIR FORCE SYSTEMS COMMAND WRIGHT-PATTERSON AIR FORCE BASE, OHIO 45433		12. REPORT DATE AUGUST 1973 13. NUMBER OF PAGES 104
14. MONITORING AGENCY NAME & ADDRESS *(if different from Controlling Office)* SAME		15. SECURITY CLASS. *(of this report)* UNCLASSIFIED 15a. DECLASSIFICATION/DOWNGRADING SCHEDULE

16. DISTRIBUTION STATEMENT *(of this Report)*

APPROVED FOR PUBLIC RELEASE; DISTRIBUTION UNLIMITED.

17. DISTRIBUTION STATEMENT *(of the abstract entered in Block 20, if different from Report)*

18. SUPPLEMENTARY NOTES

19. KEY WORDS *(Continue on reverse side if necessary and identify by block number)*

FRACTURE MECHANICS	2219-T851 ALUMINUM
CRACK VELOCITY	7075-T6-ALUMINUM
RAPID CRACK PROPAGATION	6Al-4V β TITANIUM
CRACK ARREST	9Ni-4Co-02C STEEL
DCB SPECIMENS	4340 STEEL

20. ABSTRACT *(Continue on reverse side if necessary and identify by block number)*

THIS EXPERIMENTAL PROGRAM WAS UNDERTAKEN TO STUDY AND INVESTIGATE THE EFFECTS OF CRACK VELOCITY AND MATERIAL PARAMETERS ON THE CRACK ARREST CHARACTERISTICS OF AIRCRAFT STRUCTURAL ALLOYS. MATERIALS TESTED INCLUDED 2219-T851 AND 7075-T6 ALUMINUM, 6Al-4V BETA-ANNEALED TITANIUM, 9Ni-4Co-0.2C AND 4340 STEEL ALLOYS. TESTS WERE CONDUCTED WITH RADIALLY FLARED AND UNIFORM HEIGHT DCB (DOUBLE CANTILER BEAM) SPECIMENS CONTAINING EITHER SHARP CRACKS OR NOTCHES WITH FINITE ROOT RADII. THE SPECIMENS WERE

DD FORM 1 JAN 73 1473 EDITION OF 1 NOV 65 IS OBSOLETE

UNCLASSIFIED

SECURITY CLASSIFICATION OF THIS PAGE *(When Data Entered)*

BLOCK 20 - ABSTRACT (CONTINUED.)

INSTRUMENTED TO MEASURE CRACK VELOCITY, CRACK LENGTH, CRACK OPENING DISPLACEMENT, INSTANTANEOUS LOAD, STRAIN AND CRACK LENGTHS AND THE STRESS INTENSITY FACTORS AT THE INITIATION AND THE ARREST OF THE CRACK PROPAGATION. AN INSTRUMENTATION SYSTEM FOR THE MEASUREMENT OF CRACK VELOCITIES FROM ZERO TO SEVERAL THOUSANDS OF FEET PER SECOND IS PRESENTED. EXPERIMENTAL RESULTS ARE PRESENTED AND ARE EVALUATED WITH FRACTURE MECHANICS PARAMETERS. THE TEST RESULTS INDICATE THAT A CRACKED DCB SPECIMEN OF ANY CONFIGURATION UNDER STATIC LOADING IS NOT SUITABLE FOR INVESTIGATING THE DYNAMIC BEHAVIOR OF RAPIDLY RUNNING CRACKS OR CRACK ARREST CONDITIONS. RECOMMENDATIONS FOR SUITABLE TEST SPECIMENS ARE PROVIDED.

FOREWORD

This report was prepared by the Boeing Aerospace Corporation, Seattle, Washington, under Air Force Contract F33615-72-C-1063, "Analysis and Verification of Dynamic Crack Growth Arrest." Technical monitor on this program was Howard A. Wood from December 1971 through April 1972 and Major Rodney A. Bartholomew from April 1972 through February 1973.

This report covers work conducted from 15 December 1971 through 7 February 1973. This report was submitted by the author 29 June 1973, for AFFDL review. This report is also released as Boeing Document D180-17529-1 for internal control at The Boeing Company.

This program was conducted by the Research and Engineering Division of The Boeing Aerospace Company, Seattle, Washington under the supervision of H. W. Klopfenstein, Structures Research and Development Manager. The Program Leader was Mr. J. N. Masters, Supervisor, Failure Mechanisms Group. The Technical Leader was Dr. R. C. Shah. Other Failure Mechanisms personnel who contributed to the technical effort were Drs. L. R. Hall and A. S. Kobayashi and Mr. D. D. Miller. Specimen testing was done by A. A. Ottlyk and technical illustrations and art work by D. G. Good.

This technical report has been reviewed and is approved.

FRANCIS J. JANIK, JR.
Chief, Solid Mechanics Branch
Structures Division
Air Force Flight Dynamics Laboratory

TABLE OF CONTENTS

Section		Page
1.0	INTRODUCTION	1
2.0	BACKGROUND	3
	2.1 Dynamic Crack Propagation and Arrest	3
3.0	MATERIALS AND PROCEDURES	5
	3.1 Materials	5
	3.2 Specimen Fabrication Procedures	6
	3.3 Experimental Procedures	7
4.0	STRESS INTENSITY FACTORS FOR DCB SPECIMENS	9
	4.1 Stress Intensity Factors from Simple Beam Analysis	9
	4.2 Stress Intensity Factors from Finite Element Analysis	10
	4.3 Selection of a Specimen for Rapid Crack Propagation and Arrest	13
5.0	DESCRIPTION AND ANALYSIS OF RESULTS	15
	5.1 Mechanical Property Test Results	15
	5.2 DCB Specimen Tests Using a Conventional Loading Machine	15
	5.3 DCB Specimen Tests Using a Flexible Loading System	21
	5.4 Tests Using a Sensitive Instrumentation System	26
	5.4.1 Instrumentation System	28
	5.4.2 Edge Cracked Panel Test	29
	5.4.3 4340 Steel DCB Specimen Tests	31
6.0	CONCLUSIONS AND RECOMMENDATIONS	35
	6.1 Conclusions	35
	6.2 Recommendations	36

TABLE OF CONTENTS (Continued)

Section	Page
REFERENCES	37
TABLES	39
FIGURES	43

LIST OF TABLES

Number		Page
I	Chemical Composition of Materials Tested	39
II	Mechanical Properties of Materials at Room Temperature	40
III	Results of DCB Specimens Tested Using a Conventional Loading Machine at Room Temperature	41
IV	Results of DCB Specimens Tested Using a Flexible Loading System at Room Temperature	42

LIST OF ILLUSTRATIONS

Figure		Page
1	Static Strain Energy Release Rate Versus Crack Length For The Specimen (Schematic)	43
2	Tensile Specimen For Mechanical Property Measurements	44
3	Uniform Height DCB Specimen	45
4	Flared DCB Specimen For Exploratory Tests	46
5	Flared DCB Specimen For Crack Velocity And Arrest Tests	47
6	Flared DCB Specimen for Crack Velocity and Arrest Tests	48
7	Single Edge Cracked Specimen Of 7075-T6 Aluminum For Crack Velocity Measurement	49
8	Approximate Normalized Strain Energy Release Rate For The Flared DCB Specimen Of Figure 6	50
9	Finite Element Idealization For A Flared DCB Specimen Of Figure 4 With A Crack Length Of 1.0 and 1.05 Inch	51
10	Finite Element Idealization For A Flared DCB Specimen Of Figure 5 With A Crack Length Of 1.00 and 1.05 Inch	52
11	Load-Displacement Diagram For A 9Ni-4Co-0.2C Steel Specimen S14-1	53
12	Load-Displacement Record For 2219-T851 Aluminum Flared DCB Specimens A14-1 and A14-2	54
13	Load-Time Diagram For A 7075-T6 Aluminum Flared DCB Specimen - A14-3	55
14	Displacement Time Diagram For A 7075-T6 Aluminum Flared DCB Specimen - A14-3	56
15	Load-Displacement Diagram For A 7075-T6 Aluminum Flared DCB Specimen - A14-3	57
16	Crack-Growth-Resistance Curve And Crack Driving Force For Load Controlled Test	58

LIST OF ILLUSTRATIONS (CONT.)

Figure		Page
17	Crack-Growth-Resistance Curve And Crack Driving Force Curves For Displacement Controlled Test	59
18	Load-Displacement Diagram For A 9Ni-4Co-0.2C Steel Uniform Height DCB Specimen - S3-1	60
19	Crack Growth Resistance Curve Obtained From Testing 9Ni-4Co-0.2C Steel Uniform Height DCB Specimen - S3-1	61
20	Load-Displacement Diagram For A 6Al-4V β Titanium Uniform Height DCB Specimen - T3-1	62
21	Crack Growth Resistance Curve Obtained From Testing A6Al-4V β Titanium Uniform Height DCB Specimen - T3-1	63
22	6Al-4V β Titanium Specimen - T3-1 - Showing Crack Lengths Before Propagation And At Arrest	64
23	Load-Displacement Diagram For A 2219-T851 Aluminum Uniform Height DCB Specimen A3-2	65
24	Crack Growth Resistance Curve Obtained From Testing A 2219-T851 Aluminum Uniform Height DCB Specimen A3-2	66
25	2219-T851 Aluminum Specimen - A3-2 - Showing Crack Lengths Before Propagation And At Arrest	67
26	A Flexible Loading System	68
27	Load-Time and Displacement-Time Records Obtained For A 7075-T6 Aluminum Flared DCB Specimen A14-4	69
28	Load-Displacement Record Obtained For A 7075-T6 Aluminum Flared DCB Specimen A14-4	70
29	7075-T6 Aluminum Specimen Showing Crack Lengths Before Propagation And At Arrest	71
30	Load-Displacement Record For A 1.50 Inch Thick 2219-T851 Aluminum Uniform Height DCB Specimen A3-4	72
31	Load-Displacement Record For A 1.50 Inch Thick 2219-T851 Aluminum Flared DCB Specimen A14-5	73

LIST OF ILLUSTRATIONS (CONT.)

Figure		Page
32	Load-Time and Displacement-Time Records For A 1.0 Inch Thick 2219-T851 Aluminum Flared DCB Specimen Al4-6	74
33	2219-T851 Aluminum Specimen Al4-6 Showing Crack Lengths Before Propagation And At Arrest	75
34	Load-Displacement Record Obtained For A 6Al-4V β Titanium Uniform Height DCB Specimen T3-2	76
35	Load-Displacement Record For A 9Ni-4Co-0.2C Steel Uniform Height DCB Specimen S3-2	77
36	Load Versus Displacement Record For A 9Ni-4Co-0.2C Steel Flared DCB Specimen Sl4-2	78
37	Instrumentation System And Hook-up For Dynamic Crack Velocity And Arrest Tests	79
38	Strain Gage And Crack Propagation Gage Locations For The Single Edge Cracked Panel Of 7075-T6 Aluminum	80
39	Load Vs. Crack Opening Displacement Record for the 7075-T6 Aluminum Single Edge Cracked Panel	81
40	Crack Velocity As A Function Of Crack Length For The 7075-T6 Aluminum Single Edge Cracked Panel	82
41	Strain Versus Crack Length For A Strain Gage Located at 2.10 Inch Away from the Edge of a Single Edge Cracked Panel of 7075-T6 Aluminum	83
42	A 4340 Steel DCB Specimen Containing A Blunt Notch	84
43	Strain Gage and Crack Propagation Gage Locations for the Flared DCB Specimen of 4340 Steel	85
44	Increase In Crack Length Versus Time For The Flared DCB Specimen of 4340 Steel	86
45	Crack Velocity Versus Distance For The Flared DCB Specimen Of 4340 Steel	87

LIST OF ILLUSTRATIONS (CONT.)

Figure		Page
46	Wedge Loading of a DCB Specimen	88
47	Strain Gage and Crack Propagation Gage Locations for the Notched DCB Specimen	89
48	Increase in Crack Length Versus Time For A DCB Specimen of 4340 Steel Containing a Blunt Notch	90
49	Increase in Crack Length Versus Crack Velocity For A DCB Specimen Of 4340 Steel Containing A Blunt Notch	91

1.0 INTRODUCTION

The desire for high payload/range/performance capabilities in aircraft has led to the use of high strength metallic materials that are prone to fracture problems. Within the past decade, material selection and design approaches have been developed for the design of fracture resistant spacecraft and booster hardware.[1] These approaches have used the linear elastic theory of fracture mechanics to correlate experimental fracture and crack growth data and to relate the data to the performance of full sized structures; such approaches serve as a sound basis for the development of design techniques for aircraft components. Both performance requirements and load/environment histories for aircraft components can be considerably more severe than for spacecraft and booster components. Although a great deal of emphasis is currently being placed on the development of methods for design against fracture, the possibility of fractures originating at undetected flaws or from in-service damage must be considered and damage containment capability incorporated in aircraft structural designs. Unfortunately, very little is known of the phenomena of fast fracture resistance and crack arrest. In fact, the present state of knowledge of dynamic crack propagation, both theoretical and experimental, is in a rather primitive stage when compared to other areas of fracture mechanics such as the prediction of the onset of rapid fracture. Available design procedures for crack arrest are thus based on empirical relations that are established through elaborate and expensive tests of prototype structures.

This experimental program was undertaken to study and investigate the effects of crack velocity and material parameters on the crack arrest characteristics

of aircraft structural alloys and to establish a criterion for crack arrest based on a static analysis. The available information indicated that the static stress intensity factor at arrest, K_a, would be equal to or less than the stress intensity factor at the initiation of a rapidly propagating crack, K_{cr}. The intent of the program was to relate K_a and K_{cr} by means of a new material parameter $\dot{C}_d$ dependent upon crack velocity, material, and material thickness. For this purpose, tests were performed on alloys that are candidates for the tension structure of advanced military aircraft. These alloys include 2219-T851 aluminum, 6Al-4V beta-annealed titanium and 9Ni-4Co-0.2C steel. Other alloys tested were 7075-T6 aluminum and 4340 steel. Tests were conducted with flared and uniform height double cantilever beam (DCB) specimens containing either sharp cracks or notches with finite root radii. The DCB specimens were instrumented with crack opening displacement (COD) gages, crack propagation gages, strain gages and a load cell to measure crack velocity versus crack length; strain, crack length, and load versus time; and crack length and stress intensity factor at the onset of fracture, during rapid crack propagation, and at crack arrest.

Background information for this study is given in Section 2, a description of materials used is given in Section 3, and static stress intensity factor solutions are presented in Section 4. The results of these tests are presented and analyzed in Section 5, and conclusions and recommendations are included in Section 6.

2.0 BACKGROUND

In this section, the information on running cracks and the arrest of running cracks pertinent to the analysis of the test results and available at the time of the initiation of the program is briefly summarized. The potential of various specimen configurations for evaluating the effects of crack velocity and material parameters on crack arrest conditions is then briefly described. The selection of the basic specimen and loading configuration used in this study was heavily influenced by the state of knowledge existing at that time.

2.1 Dynamic Crack Propagation and Arrest

Probably the most comprehensive review of dynamic crack propagation and arrest is the article by Bluhm in Reference 2. This article discusses stress intensity factor (fracture toughness) at the initiation of crack propagation and its relation to static stress intensity factor at crack arrest. The discussion is based on Hoagland's data[3] generated by uniform height DCB specimens and on Yoshiki's data[4] generated by double tension specimens of 0.5 in. thick large steel plates with welded patches or riveted stiffeners. These limited experimental data and data obtained with stiffened thin aluminum plates[5] and double tension specimens of 0.5 in. thick large steel plates with welded stiffeners[6] suggest that arrest occurs if and when the static stress intensity factor becomes equal to or less than the fracture toughness at initiation. This confirmed the concept advanced by Irwin[7] that crack arrest is a reverse phenomenon of the onset of crack propagation. Available information[2] also suggested that rapid crack propagation and crack arrest can be expected for a specimen of strain

rate insensitive material if it has a distribution of the static strain energy release rate $\mathcal{G}$ versus crack length, as schematically illustrated by Figure 1. This information played a vital role in the design and the selection of a specimen for evaluation of the effects of crack velocity and material parameters on the crack arrest conditions.

A number of different specimen-loading-crack configurations, such as linearly tapered DCB specimens, double tension specimens[4,6], combined wedge and remote loaded center cracked panels, and radially flared DCB specimens, to some extent, have the $\mathcal{G}$ versus crack length distribution shown in Figure 1. However, the drawback of the linearly tapered DCB specimens is the very short distances over which the crack propagates prior to arrest and the resultant inability to evaluate possible crack velocity effects on arrest conditions. The double-tension specimen[4,6] requires a special test set-up and for a uniform temperature test, crack arrest can be accomplished only by using mechanical attachments to effect a change in stress level. For the combined wedge and remote loaded center cracked panel, crack propagation and arrest could possibly be induced for very short cracks. On the other hand, at the onset of this program, a radially flared DCB specimen under constant load appeared to have numerous desirable characteristics for studying the effects of crack velocity and material parameters on crack arrest. This is described in detail in Section 4.3.

3.0 MATERIALS AND PROCEDURES

This section includes descriptions of the materials, the specimen fabrication procedures, and the experimental procedures used in this study.

3.1 Materials

Plates of 2219 aluminum, 0.5 by 48.0 by 84.0 in. and 1.5 by 24.0 by 72.0 in. were purchased in T851 condition per MIL-A-8920A-1 specifications. All aluminum plates came from the same heat and rolling batch. Specified limits on chemical composition are listed in Table I. Mechanical properties for the 0.5 and 1.5 inch thick plates are given in Table II. Half inch thick uniform height and flared DCB specimens were machined from the 0.5 inch thick aluminum plate. One inch and 1.5 inch thick aluminum specimens were machined from the 1.5 inch thick plate.

Hot rolled plates of 9Ni-4Co-0.2C steel, 0.5 by 36.0 by 18.0 in. were purchased in annealed condition. The chemical composition of the material, as supplied by the vendor, is listed in Table I. These plates were subjected to heat treatment according to the following specifications so that the ultimate strength of the heat treated 9Ni-4Co-0.2C steel was approximately 200 ksi at room temperature:

Normalize at	$1650^{\circ} \pm 25^{\circ}F$ for 1 hour
Air cool to	Room Temperature
Austenitize at	$1525^{\circ} \pm 25^{\circ}F$ for 1 hour
Oil Quench at	60° to $150^{\circ}F$
Cool to	$-100^{\circ} \pm 25^{\circ}F$ for 1 hour within 2 hours of quenching

Temper at	1025° ±10°F for 4 hours

The mechanical properties of the heat treated steel are listed in Table II.

6Al-4V beta-annealed titanium plates, 0.5 by 34.0 by 206.0 in. were obtained per BMS 7-174B Condition 1, Type E specifications. These plates were obtained from the Department of Transportation, SST Surplus Material. The chemical composition was neither provided nor determined. Mechanical properties are listed in Table II.

The 4340 steel DCB specimens were machined from 0.625 inch thick hot-rolled annealed plate obtained per AMS 6359B specifications. The chemical composition is listed in Table I. The DCB specimens of 4340 steel were finish-machined prior to heat treatment and were then subjected to a heat treatment according to BAC 5617 specifications so that the ultimate strength of the heat treated 4340 was around 280 ksi at room temperature. The heat treatment is to:

Normalize at	1650° ±25°F for 1 hour
Air cool to	Room Temperature
Austenitize at	1550° ±25°F for 45 minutes
Oil Quench at	140°F maximum
Double Temper at	400° ±25°F for 2 1/2 hours

The 7075-T6 aluminum, used for the DCB specimens and for the SEN (single edge notch) specimen, was obtained from Boeing material stores.

3.2 Specimen Fabrication Procedures

Four different types of test specimens were fabricated in this program. The smooth tensile specimens used for determining mechanical properties are shown

in Figure 2. The uniform height and flared DCB specimens used to evaluate fracture toughness, crack velocity, and arrest conditions are shown in Figures 3 to 6. All DCB test specimens, except initial exploratory specimens used to determine the minimum side groove requirements for directed crack propagation and fabricated according to Figure 4, contained side grooves on both sides of the specimen. The depth of each groove was 10 percent of the thickness of the specimen. The SEN specimen of 7075-T6 aluminum, used for evaluation of crack velocity with increasing crack length, is shown in Figure 7.

Starter slots with dimensions about 0.2 in. less than the required final crack dimensions were machined in the specimen, as shown in Figures 3 through 7. The starter slots were then extended using low stress/high cycle tension fatigue. For the DCB specimens which contained a finite root radius notch instead of a crack, the notch of required length was introduced with a cutter of appropriate root radius or with a cutter and an EDM (electric discharge machined) notch. The crack propagation direction was LT for all steel, titanium and 7075-T6 aluminum specimens and TL for all 2219-T851 aluminum specimens.

3.3 Experimental Procedures

Mechanical property tests were conducted per ASTM standards for tensile testing with the test specimens shown in Figure 2. All mechanical property specimens were instrumented with a 2.0 inch gage length extensometer. The field strength (at 0.2% offset), ultimate strength, and elongation were determined. A strain rate of 0.005 in/in/minute was used during the tensile tests until the yield strain was exceeded, then the strain rate was increased to 0.02 in/in/minute until failure.

The DCB specimens and the SEN specimen were loaded in tension until either 1) the crack grew suddenly and arrested, or 2) the excessive tearing type slow crack growth took place, or 3) the specimen fractured and separated in two pieces. All DCB specimens were tested in a 120 kip capacity Baldwin universal test machine with or without a special flexible spring system. The load applied to every specimen was monitored by a load cell placed in series between the specimen and the stationary head of the test machine. The load was monitored on a Visicorder. The load at the specimen was measured to observe any abrupt change in load with crack propagation. All DCB specimens, except two flared DCB specimens of 9Ni-4Co-0.2C steel fabricated per Figure 5, were instrumented with a clip gage to measure the crack opening displacement. The crack opening displacement (COD), like the load, was also monitored on a Visicorder. The chart speed of the Visicorder was 1.0 in/sec or 2.5 in/sec until the applied K based on initial crack length reached approximately 75 percent of K_{cr}. The chart speed was then increased to 20 in/sec or 25 in/sec. To facilitate the data reduction, the Visicorder paper was marked by an electronic pulse at the rate of ten pulses per second. The COD and load at the specimen were used to infer crack length, crack velocity, and the stress intensity factor.

Two 4340 steel DCB specimens and the 7075-T6 aluminum SEN specimen were instrumented with COD, strain gages, and crack propagation gages to measure crack velocities over a wide range. Signals from the load cell, the COD gage, the strain gages, and the crack propagation gages were recorded on different channels of a high speed tape recorder. Details of the instrumentation are given, along with the test results, in Section 5.4.

4.0 STRESS INTENSITY FACTORS FOR DCB SPECIMENS

In this section, the stress intensity factors and strain energy release rates are given for the DCB specimen-configurations used in this research program. The relationship between the strain energy release rate and the crack length is then used to select a specimen to investigate dynamic crack propagation and crack arrest.

4.1 Stress Intensity Factors from Simple Beam Analysis

The test program employed uniform height DCB specimens (Figure 3) as well as flared DCB specimens of three different dimensions (Figures 4-6). The static strain energy release rate $\mathcal{G}$ for a variable height DCB specimen[8] as obtained from simple beam theory and empirical considerations for a Poisson's ratio of 1/3 is given by the following equation

$$\mathcal{G} = \frac{4P^2}{Ebb_n} \frac{3(a + 0.6h)^2 + h^2}{h^3} \qquad (1)$$

where

P is the applied load

b is the specimen width

b_n is the specimen width along the crack

a is the crack length as measured from the point of loading

h is the beam height at the distance "a"

E is Young's modulus.

The stress intensity factor K_I is then given by

$$K_I = \frac{2P}{\sqrt{bb_n}} \left[\frac{3(a + 0.6h)^2 + h^2}{h^3} \right]^{1/2} \qquad (2)$$

The stress intensity factor for a uniform height DCB specimen with $a/h \geqq 1$, calculated from equation (2) compares within 3 percent with that obtained from a finite element analysis.[9] This approximate expression was used to calculate stress intensity factors for the flared DCB specimens. For ease of calculations, strain energy release rate was normalized as follows.

$$\frac{\mathcal{G} E bb_n}{4P^2} = \frac{K^2 bb_n}{4P^2} = \frac{3(a + 0.6h)^2 + h^2}{h^3} \qquad (3)$$

The expression of equation (3) is graphically represented in Figure 8 for various values of crack length "a" for the flared DCB specimen of Figure 6.

4.2 Stress Intensity Factors from Finite Element Analysis

Finite element analysis was used to calculate the stress intensity factor for the flared DCB specimen shown in Figure 4 and the results were compared with those determined from equation (2) which is based on simple beam theory. The finite element idealization for the specimen with crack lengths of 1.00 and 1.05 inches is shown in Figure 9. A standard computer program for plane stress structures[10] was slightly modified to calculate the strain energy. The computer program, being specially written for plan stress or plane strain structures,

is much more efficient than a general purpose computer code such as Boeing's ASTRA (Advanced STRuctural Analyzer). A load of 1000 lb was applied at a point (0.375, 0.350) instead of the center of loading pin (0.375, 0.375). As expected and as supported by another analysis where the load was applied at a point (0.375, 0.400), the point of load application had no effect on the strain energy release rate and thus on the stress intensity factor. Finite element analyses were conducted for crack lengths of 1.00 and 1.05 inches and crack width and specimen width of 1.00 inch. For each crack length, the strain energy and strain energy release rate were calculated from internal stresses assuming plane stress and plane strain conditions. It is known that the expression for the stress intensity factor is the same for plane stress or plane strain conditions for a simply connected body containing a crack. Stress intensity factors for both conditions were calculated to check numerical accuracy. The strain energies for plane stress and plane strain conditions are given by the following equations.

$$V\Big|_{\text{plane stress}} = \sum_{i=1}^{420} \left\{ \frac{A_i}{2E} \left[\sigma_x^2 + \sigma_y^2 - 2\nu\sigma_x\sigma_y + 2\,(1+\nu)\,\tau_{xy}^2 \right]_i \right\} \qquad (4)$$

$$V\Big|_{\text{plane strain}} = \sum_{i=1}^{420} \left\{ \frac{A_i}{2E} \left[(1-\nu^2)(\sigma_x^2 + \sigma_y^2 - \frac{2\nu}{1-\nu}\,\sigma_x\sigma_y) + 2(1+\nu)\tau_{xy}^2 \right]_i \right\} \qquad (5)$$

where ν is the Poisson's ratio, A_i is the area of element i, and the subscript i stands for values pertaining to element number i. The strain energy release

rate was also calculated from the change in external work with crack extension. The stress intensity factor was also calculated from the crack opening displacement. The stress intensity factor thus calculated is not expected to be as accurate as the one from the strain energy release rate calculations.

The calculated stress intensity factor for a 1000 lb load for 1.0 inch thick flared DCB specimen (Figure 4) having 1.025 inch long crack is 7.939 ksi $\sqrt{in}$ based on plane stress conditions, 7.941 ksi $\sqrt{in}$ based on plane strain conditions, and 8.044 ksi $\sqrt{in}$ based on the strain energy relase rate obtained from the external work. The stress intensity factor calculated from the strain energy release rate obtained from the external work is only 1.25 percent higher than that calculated from the strain energy release rate obtained from stresses. The method based on external work, however, requires minimal calculations. The stress intensity factor calculated from crack opening displacement (first node away from the crack tip) is 7.53 ksi $\sqrt{in}$ which is 5.0 percent lower than that obtained from the strain energy release rate. The stress intensity factor calculated from equation (2) for the same crack length is 8.17 ksi $\sqrt{in}$ which is only 3 percent higher than that of the finite element analysis. For various crack lengths up to 6.0 inches, stress intensity factors were calculated with a finite element analysis by Bartholomew[11] and they compared quite well with those calculated from equation (2).

A finite element analysis was also carried out for the flared DCB specimen of Figure 5. The idealization for the crack lengths of 1.00 and 1.05 in. is shown in Figure 10. The stress intensity factor was calculated from the strain

energy release rate based on internal stresses as well as external work. They agreed within 1 percent. The stress intensity factor, K, calculated from crack opening displacement of the first node was 8.5 percent lower than K from strain energy release rate. The K calculated from equation (2) was approximately 5 percent higher than that calculated from the finite element analysis.

For the specimen in Figure 6, stress intensity factors were calculated with equation (2). The stress intensity factors, thus calculated, are expected to be correct within 10 percent.

4.3 Selection of a Specimen for Rapid Crack Propagation and Arrest

As mentioned in Section 2, a number of different specimens were considered for generating data on the effects of crack velocity and material parameters on the arrest conditions. The specimen required must initiate a propagating crack, accelerate it to terminal crack velocity and finally arrest it within the specimen length. For a number of different reasons, the other specimens examined in Section 2 were not suitable for fast crack propagation and arrest. From static considerations, a radially flaring DCB specimen, such as the ones shown in Figures 4 to 6, under constant applied load, was found to have numerous desirable characteristics for studying the conditions required for dynamic crack arrest. Like any DCB specimen, it offers an efficient specimen design which can be varied to increase and decrease the static stress intensity factor with relative ease. In addition it is a relatively simple configuration for analyzing the static and possibly the dynamic states of stress, strain, and stress intensity factors. An approximate normalized static strain energy release rate versus

crack length calibration for the flared DCB specimen of Figure 6 is given in Figure 8. As seen from Figure 8, static strain energy release rate, $\mathcal{G}$, for a constant load P increases with increasing crack length up to a crack length of 3.5 in. For crack lengths greater than 3.5 in. and for a constant load, $\mathcal{G}$ rapidly decreases with increasing crack length. As seen from Figure 8, $\mathcal{G}$ for an 8.0 in. long crack is only 40 percent of $\mathcal{G}$ for a 1.0 in. long crack for the same load. Hence, if a fracture is initiated from a 2.0 in. long initial crack, under a constant load, the crack would propagate to a length of 5 in. or more before arresting if the arrest K is the same as or lower than the initiation K. Thus, the crack, in this case, would propagate an additional length of at least 3.0 in. and it would have a chance to accelerate to a substantial velocity. By varying the initial crack length, the material, and the specimen thickness, it was then concluded that the effects of crack velocity and material parameters on dynamic crack propagation and arrest could be studied conveniently with this flared DCB specimen under constant load conditions.

5.0 DESCRIPTION AND ANALYSIS OF RESULTS

The data from all the tests conducted during the program are presented in this section. Section 5.1 presents the results of the mechanical property tests. Section 5.2 describes the results of the DCB specimens tested using a conventional loading machine. Section 5.3 presents the results of the DCB specimens tested using a flexible loading system designed to maintain constant load during crack propagation when quasistatic conditions are considered. Section 5.4 describes the results of the 7075-T6 SEN specimen and the two 4340 steel DCB specimens tested with an instrumentation system designed to measure crack velocities over a very wide range.

5.1 Mechanical Property Test Results

The mechanical properties for the 9Ni-4Co-0.2C steel, the 6Al-4V beta-annealed titanium and the 2219-T851 aluminum at room temperature are given in Table II. Along with the mechanical properties, values of the critical stress intensity factors K_{cr}, at which slow tearing type crack propagation starts, are given for particular thicknesses. The values of K_{cr} were determined from uniform height DCB specimens, as shown in Figure 3.

5.2 DCB Specimen Tests Using a Conventional Loading Machine

All the DCB specimens discussed in this section were tested with a conventional stiff test machine (Baldwin Universal machine). The purpose of these tests was to explore whether fast running cracks could be started in the test materials using a standard stiff test machine and DCB specimens containing sharp cracks or notches of moderate root radius. The results of these tests

on five flared and four uniform height DCB specimens are briefly summarized in Table III and are discussed in more detail in the following paragraphs.

Initially two half-inch thick flared DCB specimens (S5X1 and S5X2) were fabricated from 9Ni-4Co-0.2C steel per Figure 4 to determine the minimum side groove requirements to restrict crack propagation to the original plane of the crack. Specimen S5X1 had one 0.05 in. deep (ten percent of specimen thickness) V-groove and a 1.55 in. long crack. At the ungrooved side of the specimen, the crack started to turn away from the plane of the original crack at a load of 5,000 lb. Specimen S5X2 had 0.05 in. deep V-grooves on both sides of the specimen and a 1.50 in. long crack. At a load of 4,700 lb, the crack propagated slowly for a distance in the plane of the fatigue crack and then turned away from the plane of the original crack. All the DCB specimens tested thereafter, and listed in Tables III and IV, had 10 percent deep side grooves on both sides of the specimens.

A flared DCB specimen of 9Ni-4Co-0.2C steel, S7-1 (Figure 5), containing an initial crack length of 2.38 in. was loaded at a rate of 12.5 kip/min. At a load of 15,500 lb, rapid crack propagation started and the specimen was severed into two pieces. Prior to rapid crack propagation, slow crack growth of approximately 0.20 inch took place. After the slow crack growth, symmetric shear lips started to form and grew to occupy 100 percent of the fracture face after approximately 1.0 inch of additional crack extension. The stress intensity factor at the onset of rapid crack propagation (a = 2.60 in) was 235 ksi $\sqrt{\text{in.}}$ If it is assumed that the load remained constant at the maximum value (instantaneous load record was not obtained on Visicorder chart paper

over 13,500 lb), the minimum value that the stress intensity factor reached in the specimen would be 162 ksi $\sqrt{in}$ for a 6.0 in. long crack. Had the arrest value of the stress intensity factor for the particular specimen loading conditions been higher than 162 ksi $\sqrt{in}$, the crack would have arrested.

Since it was not possible to arrest the crack in the previous test, the specimen was redesigned to the configuration shown in Figure 6. The approximate normalized strain energy release rate for this specimen is shown in Figure 8. As seen from Figure 8, a normalized strain energy release rate ($Ebb_n/4P^2$) as low as 1.5 can be obtained with this configuration as compared to the normalized strain energy release rate of 5 for the specimen configuration of Figure 5. All flared DCB specimens mentioned hereafter were fabricated according to Figure 6. A steel specimen S14-1 containing an initial crack length of 2.50 in. was loaded at 40 kip/min. Slow tearing crack growth started at 11,000 lb (K = 162 ksi $\sqrt{in}$), as seen from load-crack opening displacement record in Figure 11. The loading was continued up to 19,500 lb during which time the crack tore slowly an additional 1.50 in. The test was terminated at this load (K = 300 ksi $\sqrt{in}$) since the crack velocity was quite low (velocity <1 in/sec). The fracture faces were identical to the previous specimen. However, the apparent anomaly in the crack propagation behavior between these two specimens is unexplained.

A 2219-T851 aluminum flared DCB specimen A14-1 containing an initial crack length of 2.50 in. was loaded at 10 kip/min. This specimen, as well as all the specimens tested hereafter, were instrumented with a clip gage to measure crack opening displacement. As seen from the load displacement record for the

specimen (Figure 12), slow tearing crack growth started at 2,600 lb, i.e., at K = 38.5 ksi $\sqrt{in}$. The load was increased to 4,340 lb during which time the crack propagated very slowly to a crack length of 4.0 in. At the load of 4,340 lb (K = 76 ksi $\sqrt{in}$), the test was terminated. The crack velocity was less than 1.0 in/sec. The fracture faces of this specimen as well as all other 2219-T851 aluminum specimens described hereafter were quite similar to those for the steel specimen previously described.

A second flared DCB specimen of 2219-T851 aluminum, A14-2 containing a notch of length 2.50 in. and a root radius of 0.0020 in. was loaded at 20 kip/min. The notched specimen required a higher load than the cracked specimen to initiate crack propagation, and thus the higher stored energy in the notched specimen forced the crack to run faster. Figure 12 shows the load-crack opening displacement record. At a load of 2960 lb, slow tearing crack growth started taking place. Treating the notch as a sharp crack, the apparent K is 43.3 ksi $\sqrt{in}$. The notched specimen required approximately 13 percent higher load than the previous specimen with a sharp crack. The loading was continued until load of 4,180 lb during which time the crack slowly grew an additional length of 2.2 in. The crack velocity was less than 1 in/sec.

A flared DCB specimen of 7075-T6 aluminum, A14-3, was tested to eliminate the mixed mode (plane stress - plane strain fracture) and shear lip problems experienced in the 9Ni-4Co-0.2C and 2219-T851 tests. The specimen had a 2.40 in. long crack and was loaded at 10,000 lb per minute. Load-time, displacement-time, and load displacement records are shown in Figures 13, 14, and 15, respectively. A series of 27 pop-ins took place within a period of 8 seconds and the

crack extended approximately 2 in. The fracture faces were flat with no indications of shear lips. The first pop-in occurred at load of 1,930 lb and at the stress intensity factor K_{Ic} of 27.7 ksi $\sqrt{in}$. From visual observation the crack length at the last pop-in was approximately 4.0 to 4.5 in. long. Based on these crack lengths and the final load of 3,160 lb, the stress intensity factor K for last crack propagation is 46-48 ksi $\sqrt{in}$. Each time crack propagation (pop-in) occurred, the load dropped and restricted the crack propagation to a very small distance (less than 0.1 in.). This indicates that, using a conventional test machine, it is not possible to initiate a fast running crack in a DCB specimen.

The slow crack growth behavior of tough materials (aluminum 2219-T87 and steel) can be explained using crack growth resistance curves. Resistance curves characterize the resistance of materials to fracture during incremental slow crack growth extension. Figures 16 and 17 show schematic crack growth resistance curves for load and displacement controlled tests of DCB specimens made from tough materials. The loading conditions for the tests described before are somewhere in between those for Figures 16 and 17. Figures 16 and 17 show that substantial crack growth takes place prior to reaching crack instability. They also show that crack growth resistance increases sharply with increasing crack propagation. From these figures, the crack instability occurs when the rate of increase of applied K due to loading is greater than the rate of increase of crack growth resistance.

A uniform height steel DCB specimen S3-1 containing a 1.45 in. long crack was tested to obtain a crack growth resistance curve. The load-crack opening displacement record is shown in Figure 18 and crack growth resistance curve is

shown in Figure 19. An experimental calibration curve for compliance vs. crack length was not obtained. Hence, this curve was developed from the approximate solution for a DCB specimen[8] and was used to calculate the crack length, a, and Δa and K in Figure 19. The calculated stress intensity factors in Figures 19, 21 and 23 and in the following discussion for specimens S3-1, T3-1, and A3-2 are not corrected for the side grooves. This correction would increase the stress intensity factors by about 12 percent. For specimen S3-1 slow tearing crack growth started at K = 145 ksi $\sqrt{in}$. The crack started propagating at a slow speed (crack velocity less than 10 in/sec) at K = 200 ksi $\sqrt{in}$. At the maximum load, the specimen fractured. As seen from Figures 18 and 19, the load dropped when the crack propagated.

The load-crack opening displacement relationship for the uniform height titanium DCB specimen T3-1 is shown in Figure 20. Figure 21 shows the corresponding crack growth resistance curve. Slow tearing crack growth started at around K = 100 ksi $\sqrt{in}$. Crack propagation started at a load of 10,400 lb (K = 115 ksi $\sqrt{in}$) and arrest occurred at a load of 5,900 lb. The crack length at arrest was 3.20 in. and the static stress intensity factor at arrest was 98 ksi $\sqrt{in}$. The crack velocity was less than one in/sec. Figure 22 is a photograph of the fractured specimen showing the initial crack length before propagation and the crack length at arrest. Had the load remained constant, the crack would have propagated faster and the specimen would have fractured.

Figure 23 shows the load-displacement relationship for the 2219-T851 aluminum, uniform height DCB specimen A3-2 which had a notch length of 1.53 in. and root radius of 0.01 in. Figure 24 shows the crack growth resistance curve for

this specimen. If the specimen had contained a crack instead of a notch, the crack growth resistance curve would have resembled the one shown by the dotted lines. Crack propagation started at the maximum load of 4,770 lb. Assuming the presence of a crack equal in length to the notch, the apparent stress intensity factor would be 49.5 ksi $\sqrt{in.}$ The load required to initiate crack propagation in a specimen with a notch of 0.01 root radius is about 44 percent higher than that for a sharp crack having the same length. Crack arrest occurred at the load of 2,550 lb and crack length of 2.94 in. It took 0.8 second for the notch to propagate 1.41 in. The static stress intensity factor at arrest was 40 ksi $\sqrt{in.}$ A photograph of the fractured specimen (Figure 25) shows the initial notch length, the crack length at arrest, and the crack length after marking cycles.

From the above experiments, it can be concluded that fast running cracks cannot be developed using DCB specimens and conventional loading methods. It was also found that fast running cracks cannot be started in 2219-T851 notched DCB specimens with a notch root radius as blunt as 0.01 in.

5.3 DCB Specimen Tests Using a Flexible Loading System

The series of tests, to be described in this section, were conducted with a Baldwin universal test machine which was modified with flexible springs as shown in Figure 26. The stiffness of each of the springs, shown in Figure 26, is 150 lb/in. The spring is 36 in. long and has an external diameter of 2.5 in. and internal diameter of 2.0 in. The load capacity of each spring is 1800 lb, thus, permitting a maximum extension of 12 in. The spring attachment system in Figure 26 is designed such that up to fourteen springs can be attached. The

flexibility of the springs in the loading system was chosen so that at peak load the extension of springs is many times greater (100 to 300 times) than the opening of specimens due to load. Because of the softness of the loading system, the increase in compliance of the specimen due to crack propagation will have a very small effect (less than 2 percent for one inch of crack propagation) on the applied load when quasi-static conditions are considered. For example, an aluminum DCB specimen (Figure 3) with an initial crack length of 2 in. is subjected to a peak load of 3,000 lb when the crack extends an additional one inch. As a result, the compliance of the specimen increases over 100 percent while the deflection of the springs for quasi-static conditions changes only 0.05 in. If two springs are attached in parallel to the test machine, the load change, for the quasi-static conditions, will be less than one percent of the maximum load.

It is known that for a DCB specimen subjected to the fixed grip loading condition the energy available is not sufficient to generate large amounts of crack propagation. Unless additional energy is fed from a source such as the spring system described above, crack propagation would be followed immediately by crack arrest. However, this energy is not available instantaneously to accelerate the crack. The time required for the stress waves to propagate between the energy source and crack tip will govern the maximum velocity of a crack. Consequently, as long as the crack velocity is slow compared to the stress wave velocity in the spring system, the loading system shown in Figure 26 can maintain constant load. The stress wave velocity in the spring system, however, is quite low (less than 200 ft/sec). The following

tests were conducted to study the effect of the spring system on crack velocity and to evaluate conditions required to arrest a slowly propagating crack.

The results of the tests conducted under this flexible loading system on four flared and four uniform height DCB specimens are briefly summarized in Table IV and are discussed in more detail in the following paragraphs.

A uniform height DCB specimen (A3-3) of 7075-T6 aluminum containing a crack 1.75 in. long was loaded at 3000 lb/min with two springs attached in the system. The loading rate for all the specimens tested under the loading system of Figure 26 was 10 in. of test machine loading head motion per minute. No slow crack growth took place during loading and a rapid flat fracture occurred at 2,680 lb. The fracture toughness, K_{Ic} for the specimen was 28.2 ksi $\sqrt{in}$. From the visicorder records, the time required for the crack to propagate through the length of specimen was less than 0.04 second indicating the crack velocity was higher than 100 in/sec.

A flared DCB specimen of 7075-T6 aluminum, A14-4, with an initial crack length of 2.25 in. was loaded in the same setup at the same rate as the previous specimen. No slow crack growth took place during loading and at a load of 2,115 lb, fast crack propagation started. The crack arrested at a length of 4.55 in. The crack length at arrest was determined by marking the crack under a low load, high frequency fatigue loading and then loading the specimen to failure. Figure 27 shows the load-time and crack opening displacement-time records obtained for the specimen. Figure 28 shows the load-crack opening displacement record. Figure 29 is a photograph of the fractured specimen showing the initial crack length (crack length of the onset of propagation).

crack length at arrest and crack length after marking cycles. The fracture face was perfectly flat indicating plane strain conditions prevailed. From this test, a fracture toughness (K_{Ic}) of 28.9 ksi $\sqrt{in}$ was obtained. This is almost the same as that obtained from the previous specimen. From Figures 27 and 28, it can be inferred that arrest occurred at a load of 2,290 lb. The stress intensity factor at arrest, based on static conditions, is 32.9 ksi $\sqrt{in}$ which is 14 percent higher than K_{Ic}. However, the stress intensity factor solution used to determine the arrest K is an approximate solution based on simple beam theory. Also, during the fast crack propagation, the crack front became considerably rougher than the intial fatigue crack and thus, may have resulted in a higher K at arrest than K_{Ic}. The average crack velocity was approximately 200 in/sec. As seen from Figure 27, the load variation was never more than 8 percent during the entire phase of fast crack propagation.

A 2219-T851 aluminum, 1.50 in. thick uniform height DCB specimen, A3-4, having a 1.75 in. long crack was tested with eight springs attached in the loading system. The load-crack opening displacement record for the specimen is shown in Figure 30. Slow crack growth atarted to occur at a load of 10,000 lb (K_Q = 39.1 ksi $\sqrt{in}$). At 11,200 lb (K = 43.8 ksi $\sqrt{in}$), continuous slow tearing crack propagation started. It took approximately 16 seconds for crack to propagate 4 in. at which time the test was terminated. The fracture faces were similar to those described previously for steel specimens.

A 2219-T851 aluminum, 1.50 in. thick flared DCB specimen, A14-5, with a 1.73 in. long crack was loaded in the same setup as the previous specimen.

The load vs. crack opening displacement record for the specimen is shown in Figure 31. The crack propagation behavior was very similar to that of the uniform height DCB specimen A3-4. Slow crack growth started at 10,000 lb (K_Q = 39 ksi $\sqrt{in}$) and continuous slow crack propagation started at 11,300 lb (K = 44.1 ksi $\sqrt{in}$). The crack propagated to a length of 3.61 in. (a = 1.88 in) in approximately 10 seconds with load remaining essentially constant. The test was then terminated.

A 2219-T851 aluminum, 1.0 in. thick flared DCB specimen (A14-6) containing a notch of length 1.82 inch and root radius of 0.007 in. was tested. This and the next three specimens were tested in the loading machine with 10 springs attached. The load vs. time and crack opening displacement vs. time records are shown in Figure 32. As seen from Figure 32, crack propagation started at a load of 7,420 lb. The crack arrested at a load of 7,320 lb. The crack length at arrest was 4.35 in. The photograph of the fractured specimen in Figure 33 shows the initial notch length, the crack length at arrest, and the crack length after marking cycles. The crack ran 2.53 in. in 0.26 second resulting in an average crack velocity of 10 in/sec. Treating the notch as a crack, the stress intensity factor at the onset of crack propagation was 44.6 ksi $\sqrt{in}$ and K at arrest was 54.5 ksi $\sqrt{in}$.

A 0.55 in. thick uniform height DCB specimen of titanium (T3-2) was tested to investigate the velocity that can be obtained using the spring loading system. Initial crack length was 1.45 in. The resulting load vs. crack opening displacement record is shown in Figure 34. As revealed by Figure 34, considerable slow crack growth occurred. Crack propagation started at load of 8,900 lb,

when K = 99 ksi $\sqrt{in}$. The crack velocity was less than 20 in/sec.

Figure 35 shows the load vs. crack opening displacement record for a 0.53 in. thick uniform height DCB specimen of steel, S3-2. The initial crack length was 2.37 in. At a load of 9,940 lb (K_{cr} = 132 ksi $\sqrt{in}$), slow tearing crack propagation started as is seen from Figure 35.

Figure 36 shows the load vs. crack opening displacement record for a half inch thick flared DCB specimen of steel (S14-2). The initial crack length was 2.46 in. Slow crack growth started at 9,500 lb (K_{cr} = 138 ksi $\sqrt{in}$). The slow crack propagation continued until the test was terminated at a crack length of 4.43 in. and a load of 11,500 lb. The crack velocity was less than one in/sec.

5.4 Tests Using a Sensitive Instrumentation System

The crack propagation velocity of the tests described so far was measured from the plots of crack opening displacement and load versus time on Visicorder chart paper. As mentioned before, the fastest speed of the Visicorder chart paper was 25 in/sec. Thus, if the velocity of the crack propagation was quite large and if the event occurred in less than a millisecond, the Visicorder would not be able to record it properly on the chart paper. For this reason, the subsequent tests were conducted with a sensitive instrumentation system that can record events happening in as short a time as 5 μsec and can, thus, measure crack velocities as great as several thousands of feet per second.

As described in previous sections, with the cracked or notched (notch root radius equal to or less than 0.01 in.) DCB specimens of 2219-T851 aluminum,

6Al-4V β titanium, and 9Ni-4Co-0.2C steel alloys, it is not possible to start rapidly running cracks. It was the intent to determine if a fast running crack can be developed in a cracked panel of a brittle material such as 7075-T6 aluminum. Also, it was the intent to investigate if a fast running crack can be developed and arrested in a bluntly notched DCB specimen of a brittle material such as high strength 4340 steel alloy. For these purposes, a single edge cracked panel of 7075-T6 aluminum and bluntly notched DCB specimen of 4340 steel were tested. It was also the intent to show that a rapidly running crack cannot be started even in a brittle material such as high strength 4340 steel with a cracked DCB specimen under static loading conditions. For this purpose, a flared DCB specimen of 4340 steel containing a crack was tested in a flexible loading system with a sensitive instrumentation system.

In this section, an instrumentation system used for the subsequent tests is described with which: 1) crack velocities over a wide range--from almost zero to terminal crack velocities--can be measured, and 2) instantaneous crack opening displacement, load, and strain readings at chosen locations can be recorded and correlated with time. Then the two tests, outlined below and conducted with this instrumentation system, are described.

1) An edge-cracked panel of 7075-T6 aluminum tested to measure crack velocity.

2) A 4340 steel-flared DCB specimen containing a sharp crack and a 4340 steel uniform height DCB specimen containing a blunt notch tested to measure unstable fracture resistance, crack velocity and arrest conditions.

5.4.1 Instrumentation System

The instrumentation system and hook-up for the tests are shown in Figure 37. Signals from the strain gages, the crack propagation displacement gage and the load cell were fed into signal conditioners and then to AC or DC amplifiers and were then recorded on different channels of a fourteen channel high speed tape recorder in direct or FM recording mode. The tape speed at recording was 120 in/sec and the recording ranges of the tape recorder in the direct and the FM modes were from 400 Hz to 1.5 MHz and from DC to 200 kHz, respectively. The signals from the strain gages and the crack propagation gages were fed through the AC amplifiers and were recorded in direct mode when a high crack velocity (over 1000 ft/sec) was anticipated. The output range of the AC amplifiers was from 10 Hz to 1 MHz. Thus, the instrumentation system was able to respond to step signals 5 μsec apart, thereby permitting the measurement of crack velocities as great as several thousands of feet per second. Signals from the crack propagation gages and some of the strain gages were also fed through the DC amplifiers and were recorded in the FM mode to determine the crack velocity if it was less than a thousand feet per second. Signals from the crack opening displacement gage and load cell were recorded in the FM mode. Along with an IRIG-B time code, a 10 kHz sine wave was also recorded so that a time-span of 50 μsec could be easily read off on oscillograph records. Channel 14 of the tape was used for voice annotation on test.

A calibration with a known reference voltage from the oscillator for each of the different gages was recorded on the respective channel prior to recording the test data. Prior to being fed into the amplifiers, signals from the signal conditioners were taped into a switch panel for checking purposes and monitoring on an oscilloscope during the tests. The signals

from the amplifiers were treated in the same manner before being fed into the tape recorder. The recorded data on the original tape was transferred onto another tape by reducing the original tape speed from 120 in/sec to 15 in/sec and recording onto a tape that was running at 60 in/sec. This tape was then run at a reduced speed and the data on a few channels (with time code) at a time was recorded on oscillograph paper running at a high speed. Where the crack velocity was high, the tape was run a 1-7/8 in/sec (256 to 1 speed reduction from original tape) and the oscillograph paper was run at 160 in/sec to determine the behavior with time varying in micro-seconds.

5.4.2 Edge Cracked Panel Test

A half-inch thick single edge cracked panel of 7075-T6 aluminum, as shown in Figure 7, was tested with the instrumentation system to measure the crack velocity. The specimen was cycled under low stress tension fatigue until the crack was 1.0 in. long. Seven strain gages (FAE-12-12513) were affixed in the line of the crack at various distances from the crack tip on one side of the specimen, as shown in Figure 38. On the other side of the specimen, a crack propagation gage (TK-090CPC03-003) was installed. The crack propagation gage consisted of 20 resistor strands connected in parallel. The distance between the centerlines of consecutive strands was 0.08 in. The progression of the crack caused the successive strands to break and produced an increase in the total resistance.

The panel was loaded in a MTS test machine at a loading rate of 100 kip/min. At a load of 65,000 lb (K_I = 27.3 ksi $\sqrt{in}$), the first pop-in took place. A

series of pop-ins then occurred prior to rapid crack propagation. The record of load versus crack opening displacement is shown in Figure 39. The load remained relatively constant at 98 kip (within ±3 percent) while the crack length increased from 1.45 in. to 2.41 in. The load dropped to 90 kip when the crack length had increased to 3.35 in. At the crack length of 4.35 in., the load was 88 kip.

Figure 40 shows a plot of crack velocity versus crack length (initial crack length = 1.00 in.). As seen from the plot, the crack velocity was almost zero for the initial 0.75 in. increase of crack length. Then the crack started propagating fast and developed a velocity of over 1,000 ft/sec (approximately 9 percent of the shear wave velocity). When the crack length was close to 4.0 in., the time elapsed between the fracture of the last strain gage and the specimen (the time when load dropped to zero) was 606 μsec indicating the average crack velocity was greater than 780 ft/sec.

Strain gage #4, located at a distance of 2.10 in. from the edge of the specimen, was the only gage recorded in FM mode. Thus, it was the only gage recording strains as the crack was moving. Figure 41 shows a plot of strain versus crack length. Locations of the crack tip for strain readings were determined from the data of the crack propagation gage. As seen from Figure 41, the strain was 0.002 in/in at a crack length of 1.4 in. The strain was approximately proportional to crack length until the crack tip was slightly ahead of the strain gage. The strain started to increase very rapidly when the crack length was greater than 2.2 in. and the gage broke when crack length was 2.42 in.

Comparisons of data from strain gages and crack propagation gages for this

test as well as tests to be described in Section 5.4.3 revealed that the strand of the crack propagation gage located at the same distance as the strain gage was breaking before the strain gage broke. Thus, the strain gage was breaking after the crack had gone through the location of the strain gage and had moved ahead a certain distance. This was due to the stretchy backing of the strain gage and the considerably higher strain (4 to 5 percent) required for the strain gage to break than that (1.5 percent) for the crack propagation gage.

5.4.3 4340 Steel DCB Specimen Tests

A flared DCB specimen and a uniform height DCB specimen of 4340 steel, as shown in Figures 6 and 42 respectively, were tested to measure the unstable fracture resistance, crack velocity and arrest conditions. These tests are described in detail in the following paragraphs.

A flared DCB specimen of 4340 steel containing a sharp crack of length 1.45 in. was loaded in the flexible loading system described in Section 5.3. The locations of strain gages and the crack propagation gages are shown in Figure 43. Signals from all the strain gages, crack propagation gages, crack opening displacement gage and the load cell were recorded in the FM mode. The specimen was loaded at 15 kip per minute. At a load of 6,300 lbs and stress intensity factor $K = K_{Ic} = 60$ ksi $\sqrt{in}$, the crack started propagating. The crack propagated in its plane for a distance of 1.75 in. from the initial crack tip. The crack then started turning and the specimen arm broke at a distance of 3.95 in. from the edge of the specimen. Figure 44 is a plot of distance from the initial crack tip versus time elapsed. Figure 45 is a plot of the distance from the

initial crack tip versus crack velocity obtained from Figure 44. In Section 5.3, it was inferred that the time required for the stress waves to propagate between the energy source (spring system) and the crack tip would govern the maximum velocity of crack and consequently, the crack velocity would have to be considerably slower than the stress wave velocity in the spring system. This is also borne out by the test results shown in Figure 44. However, the instrumentation (Visicorder) used previously in Section 5.3 to measure crack velocities was not sensitive enough to measure rapid crack velocities if they occurred over a short period of time--micro-seconds. With the instrumentation system described here, it is clear that rapid crack velocities cannot be developed in precracked DCB specimens with the static loading even in a brittle material. Hence, a DCB specimen containing a blunt notch, similar to one described in Reference 12 was tested. The blunt notch allows the specimen to sustain a much higher load prior to the onset of notch extension than that for a sharp crack of the same length. Thus, in a blunt notched specimen, a significant amount of excess energy can be stored which is available instantaneously to drive the crack at high speeds as soon as the notch propagates and becomes a sharp crack.

DCB specimen (Figure 42) containing a notch of length 2.13 in. and root radius of 0.047 in. was loaded with a wedge having an included angle of 11°, as shown in Figure 46. Locations of strain gages and crack propagation gages are shown in Figure 47. Signals from the strain gages (1 to 3) were recorded both in the direct and the FM modes. Signals from the crack propagation gages, the crack opening displacement gage and the load cell were recorded in the FM mode. The specimen was loaded by driving the wedge slowly into the specimen in

the Bladwin universal test machine. The wedge and the loading procedures were similar to those described in Reference 12. As shown in Figure 42, the crack opening displacement was measured at a distance of 0.05 in. away from the edge of the specimen. When the crack opening displacement reached 0.110 in. (the load applied at the time was 31,500 lb), unstable fast fracture started and the crack propagated almost an additional 5.0 in. under essentially constant displacement. When the crack length was 7.00 in. the measured opening displacement was 0.112 in. Without any side grooves to restrain the crack path, the crack ran straight for approximately 4.75 in. from the notch tip under the wedge loading due to the compressive stress parallel to the crack plane introduced by the loading. The crack then started turning (crack length equal to approximately 7.0 in.) and the specimen arm broke at a distance of 8.5 in. from the edge of the specimen.

Kanninen's beam on elastic foundation analysis [13,14] and the measured crack opening displacements were used to calculate stress intensity factors. The displacement δ measured at the end of the specimen at a distance e (0.58 in.) from the centerline of loading pins was transformed into the displacement δ measured at the centerline of loading pins by the following relation

$$\delta' = \delta \left[1 + \frac{3e}{2a} \left(\frac{1}{1 + 0.64\ h/a} \right) \right] \qquad (6)$$

where h is the beam height. The stress intensity factors were calculated from the following relation

$$K_I = \frac{\sqrt{3}}{4} \frac{E\delta h^{3/2}}{a^2(1 + 0.64\ h/a)^2} \qquad (7)$$

Treating the notch as a sharp crack, the apparent stress intensity factor K at the onset of rapid crack propagation was 323 ksi $\sqrt{in}$ which is over five times greater than the fracture toughness K_{Ic} of the material (K_{Ic} = 60 ksi $\sqrt{in}$). The crack did not arrest. However, the crack started turning when crack length was 7.0 in., δ' was 0.112 in., and K was 70 ksi $\sqrt{in}$. Based on this, it can be concluded that the static stress intensity factor at arrest was less than 70 ksi $\sqrt{in}$. Had the crack not turned, the crack probably would have arrested.

The data obtained from the crack propagation gages, strain gages and the time code were reduced from the oscillograph plots. The data is shown in Figure 48 as a plot of distance from the notch tip versus time elapsed. As seen in the plot, emphasis is put on the data from the crack propagation gage. The reason for this is obvious from the earlier discussion on strain gages and crack propagation gages. Figure 49 shows a plot of distance from the notch tip versus crack velocity obtained from Figure 48. The plot shows that the crack velocity reached over 2,100 ft/sec (approximately 21 percent of the shear wave velocity) and the crack velocity was nearly constant for distances between 0.5 in. and 2.25 in. from the notch tip. Figures 48 and 49 show that the velocity for this notched specimen reached the maximum velocity almost immediately and then it started to decrease rapidly. This behavior of crack propagation becomes obvious from the stored energy considerations.

6.0 CONCLUSIONS AND RECOMMENDATIONS

6.1 Conclusions

From the test results in Section 5, the following conclusions can be drawn:

1. For aircraft structural materials, a cracked DCB specimen of any configuration under a static loading is not suitable for investigating the dynamic growth behavior of rapidly running cracks and crack arrest conditions.

2. In order to develop fast running cracks with static loading, an energy source has to be available which can supply the energy instantaneously to the moving crack. This would require a specimen-loading system combination where either the energy is available in the specimen itself for fast crack propagation or a system in which the energy is stored and the wave particle velocity of the system is many times greater than the crack velocity.

3. For the materials tested, notched DCB specimens with large notch root radii (considerably greater than 0.01 inch) are required to develop fast running cracks.

4. It was demonstrated that an instrumentation system can be devised with which crack velocities from zero to several thousands of feet per second can be measured. Also instantaneous crack opening displacement, load, crack length, and strains at chosen locations can be recorded and correlated with time.

5. For crack velocities less than 20 feet per second, use of the value of stress intensity factor at the initiation of the crack propagation as the arrest criterion is sufficient for the materials considered.

6.2 Recommendations

As mentioned in Section 6.1, fast running cracks can be developed in DCB specimens under static conditions only if an energy source is available which can supply the energy instantaneously to the moving crack. One such specimen is a DCB specimen containing a blunt notch. As mentioned before, the blunt notch allows the specimen to sustain a much higher load prior to the onset of the notch extension than that for a sharp crack of the same length. A significant amount of excess energy is thus stored in the specimen and is available instantaneously to drive the crack at high speeds as soon as the notch propagates and becomes a sharp crack. Rapid crack propagation and crack arrest can be obtained in a wedge loaded DCB specimen such as described in References 12 through 14 and in this report.

For some tough alloys, even with a blunt notch, it may not be possible to initiate a rapidly running crack. For such cases, it may be necessary to construct a specimen by welding a brittle material to the tough material. A rapidly running crack could then be initiated in the brittle material and run into tough material.

Double tension specimens as described in References 4 and 6 may also be used for the study of crack propagation and arrest.

REFERENCES

1. C. F. Tiffany, "*Fracture Control of Metallic Pressure Vessels*", NASA Space Vehicle Design Criteria, NASA-SP-8040, May 1970.

2. J. I. Bluhm, "*Fracture Arrest*", Fracture, An Advanced Treatise, Edited by H. Liebowitz, Vol. 5, 1969, pp. 1-63.

3. R. G. Hoagland, "*On the Use of the Double Cantilever Beam Specimen for Determining the Plane Strain Fracture Toughness of Metals*", J. of Basic Eng., Trans. of ASME, 1967.

4. M. Yoskiki, T. Kanazawa and S. Machida, "*Some Basic Considerations on Crack Arresting Mechanism in Welded Steel Structures*", Faculty of Engineering, Department of Naval Architecture, University of Tokoyo.

5. H. Vlieger, "*Restricted Residual Strength of Cracked Stiffened Panels*", NRL-TR-71004-C, December 1970.

6. T. Kanazawa and S. Machida, "*Fracture Mechanics Analysis of Stiffener-Type Crack Arrester*", Inst. of Welding, Document X-464-68.

7. G. R. Irwin, "*Basic Concepts for Dynamic Fracture Testing*", J. of Basic Engineering, Vol. 91, December 1969.

8. S. Mostovoy, P. B. Crosley and E. J. Ripling, "*Use of Crack-Line Loaded Specimens for Measuring Plane Strain Fracture Toughness*", J. of Materials, Vol. 2, 1967, pp. 661-681.

9. A. S. Kobayaski, D. E. Maiden, B. J. Simon and S. Iida, "*Application of Finite Element Analysis Method to Two Dimensional Problems in Fracture Mechanics*", ASME Paper No. 69-WA/PVP-12.

10. E. L. Wilson, "*Analysis of Plane Stress Structures*", Computer Program, University of California, Berkely, California.

11. Personal communication with R. Bartholomew, AFFDL, Wright-Patterson Air Force Base, Dayton, Ohio.

12. G. T. Hahn, R. G. Hoagland, M. F. Kanninen and A. R. Rosenfield, "*A Preliminary Study of Fast Fracture and Arrest in the DCB-Test Specimen*", Presented at the International Conference on Dynamic Crack Propagation, Lehigh University, Bethlehem, Pennsylvania, July 10-12, 1972.

13. M. F. Kanninen, "*An Augmented Double Cantilever Beam for Studying Crack Propagation and Arrest*", International Journal of Fracture, Vol. 9, March 1973.

14. R. G. Hoagland, A. R. Rosenfield and G. T. Hahn, "*Mechanisms of Fast Fracture and Arrest in Steels*", Metallurgican Transactions, Vol. 3, 1972.

Table I: Chemical Composition Of Materials Tested

Element (% by Weight)	2219–T851 Aluminum Plates Heat No. SE-24528-3		9Ni–4Co–0.2C Steel Plates Heat No. 3811304	4340 Steel Plates Heat No. 51683
	Min.	Max.		
Silicon	---	0.20	0.05	0.25
Copper	5.8	6.8	---	0.16
Manganese	0.20	0.40	0.23	0.72
Magnesium	---	-.02	---	---
Chromium	---	---	0.80	0.81
Zinc	---	0.10	---	---
Vanadium	0.05	0.15	0.09	---
Zirconium	0.10	0.25	---	---
Phosphorous	---	---	0.010	0.010
Sulphur	---	---	0.006	0.011
Nickel	---	---	9.29	1.83
Molybdenum	---	---	0.96	0.22
Cobalt	---	---	4.55	---
Titanium	0.02	0.10	---	---
Carbon	---	---	0.18	0.39
Others	0.05	0.15	---	---
Iron	---	0.30	Balance	Balance
Aluminum	Balance	Balance	---	---

Table II: Mechanical Properties Of Materials At Room Temperature

Material	Gage Thickness In.	Grain Direction	Ultimate Strength F_{tu},Ksi	Yield Strength F_{ty},Ksi	Elongation % in 2-In.	Crack Propagation Direction	Critical Stress Intensity Factor K_{cr},Ksi $\sqrt{In.}$
Steel 9Ni–4Co–0.2C	0.50	L	203.1	186.5	19.5	LT	140–160
	0.50	T	204.9	186.7	15.0	---	
Titanium 6Al–4V β	0.50	L	140.3	131.0	13.5	LT	80–100
	0.50	T	140.1	130.1	15.0	---	
Aluminum 2219–T851	0.50	L	67.2	51.6	11.8	TL	40
	1.50	L	69.8	53.2	9.5	TL	40

Table III: Results Of DCB Specimens Tested Using A Conventional Loading Machine At Room Temperature

SPECIMEN				Notch Root Radius or Crack	Initial Crack or Notch Length a_o (In.)	Slow Crack Growth, Δa_o (In.)	Loading Rate Kip / Min.	Load P at $a_o + \Delta a_o$ (Lbs.)	Stress Intensity K at P Ksi $\sqrt{In.}$	Crack Velocity In./Sec.	REMARKS
Identification	Configuration	Material	Thickness (In.)								
S7-1	Fig. 5	9Ni–4Co–0.2C	0.50	Crack	2.38	0.20	12.5	15,500	235.0	---	Seemed Fast Fracture – Velocity not Measured.
S14-1	Fig. 6	9Ni–4Co–0.2C	0.50	Crack	2.50	1.50	30.0	19,500	300.0	<1.0	Test Terminated Due to Excessive Slow Crack Growth
A14-1	Fig. 6	2219–T851	0.50	Crack	2.50	1.50	10.0	4,340	76.0	<1.0	Test Terminated Due to Excessive Slow Crack Growth
A14-2	Fig. 6	2219–T851	0.50	Notch 0.002	2.50	2.2	20.0	4,180	45.3	<1.0	Test Terminated. Specimen Later Pulled to Failure
A3–1	Fig. 3	2219–T851	0.50	Notch 0.004	1.50	Yes	20.0	4,330	46.7	<6.0	Slow Crack Growth Started at p and Specimen Fractured.
A14-3	Fig. 6	7075–T6	0.50	Crack	2.40	---	10.0	1,930	27.7	---	First Pop-In Occured at P
S3-1	Fig. 3	9Ni–4Co–0.2C	0.50	Crack	1.45	Yes	40.0	---	---	<10.0	See Figures 17 , 18
T3-1	Fig. 3	6Al–4V β	0.50	Crack	1.47	Yes	20.0	---	---	<1.0	Crack Ran and Arrested at a = 3.20 In. and p = 5,990 Lb. K_a = 98 Ksi $\sqrt{In.}$
A3-2	Fig. 3	2219–T851	0.50	Notch 0.01	1.53	---	20.0	4,770	49.5	<2.0	Crack Ran and Arrested at a = 2.94 In. P = 2,550 Lb. K_a = 40 Ksi $\sqrt{In.}$

Table IV: Results of DCB Specimens Tested Using A Flexible Loading System At Room Temperature

SPECIMEN				Notch Root Radius or Crack	Initial Crack or Notch Length. a_o (In.)	Slow Crack Growth, Δa_o (In.)	Loading Rate Kip/Min.	Load P at $a_o + \Delta a_o$ (Lbs.)	Stress Intensity K at P Ksi $\sqrt{In.}$	Crack Velocity In./Sec.	REMARKS
Identification	Configuration	Material	Thickness (In.)								
A3-3	Fig. 3	7075-T6	0.50	Crack	1.75	None	3.0	2,680	28.2	> 100	Rapid Flat Fracture
A14-4	Fig. 6	7075-T6	0.50	Crack	2.25	None	3.0	2,115	28.9	200	Rapid Flat Crack Propagation Crack Arrested at a = 4.55 In. P = 2,290 Lbs. K_a = 32.9 Ksi $\sqrt{In.}$
A3-4	Fig. 3	2219-T851	1.50	Crack	1.75	Yes	12.0	---	---	---	Test Terminated Due to Excessive Slow Crack Growth See Fig. No. 27
A14-5	Fig. 6	2219-T851	1.50	Crack	1.73	Yes	12.0	---	---	---	Test Terminated Due to Excessive Slow Crack Growth See Fig. No. 28
A14-6	Fig. 6	2219-T851	1.0	Notch 0.007	1.82	No	15.0	7,420	44.6	10.0	Crack Propogated at P and Arrested at a = 4.35, in P = 7,320 Lbs. and K_a = 54.4 Ksi $\sqrt{In.}$
T3-2	Fig. 3	6Al-4Vβ	0.55	Crack	1.45	Yes	15.0	---	---	< 20.0	Slow Tearing Crack Growth. See Fig. No. 30
S3-2	Fig. 3	9Ni-4Co-0.2C	0.53	Crack	2.37	Yes	15.0	---	---	< 4.0	Slow Tearing Crack Growth. See. Fig. No. 31
S14-2	Fig. 6	9Ni-4Co-0.2C	0.50	Crack	2.46	Yes	15.0	---	---	---	Slow Tearing Crack Growth. See Fig. No. 32

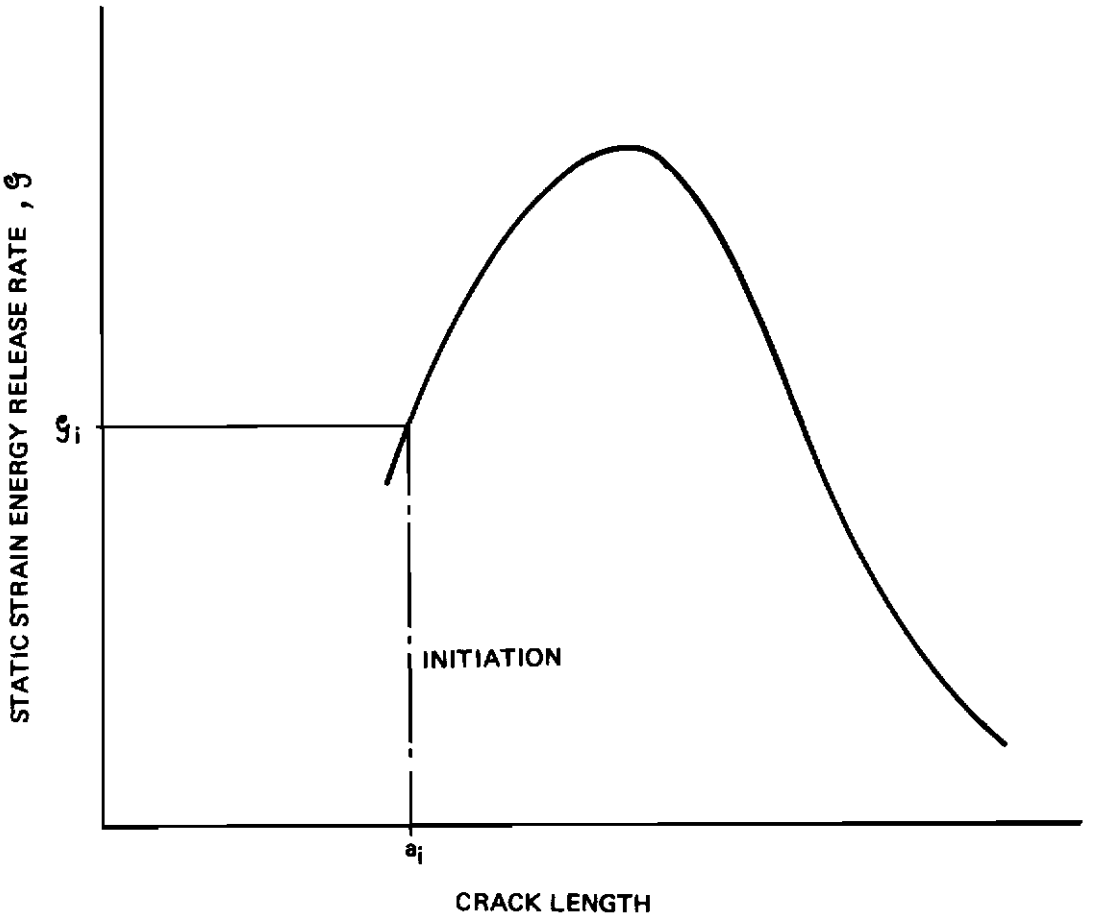

Figure 1: Static Strain Energy Release Rate Versus Crack Length For The Specimen (Schematic)

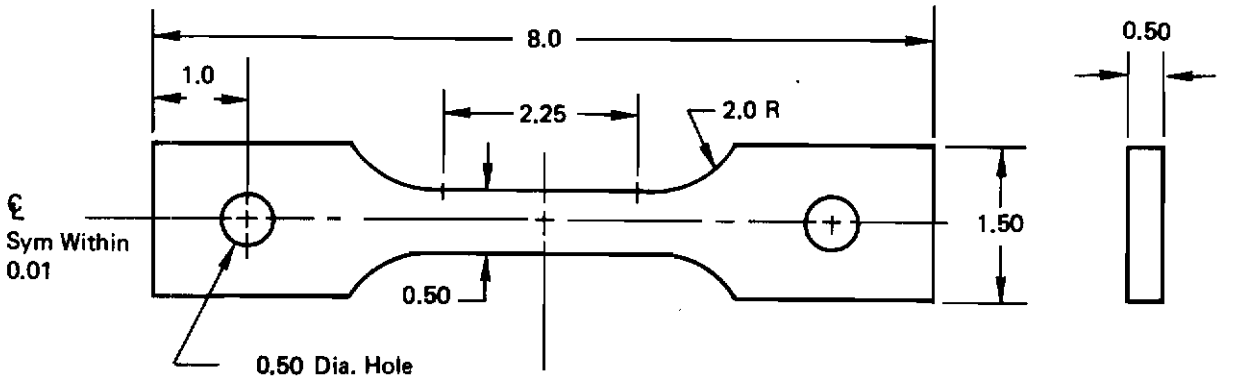

Figure 2: Tensile Specimen For Mechanical Property Measurements

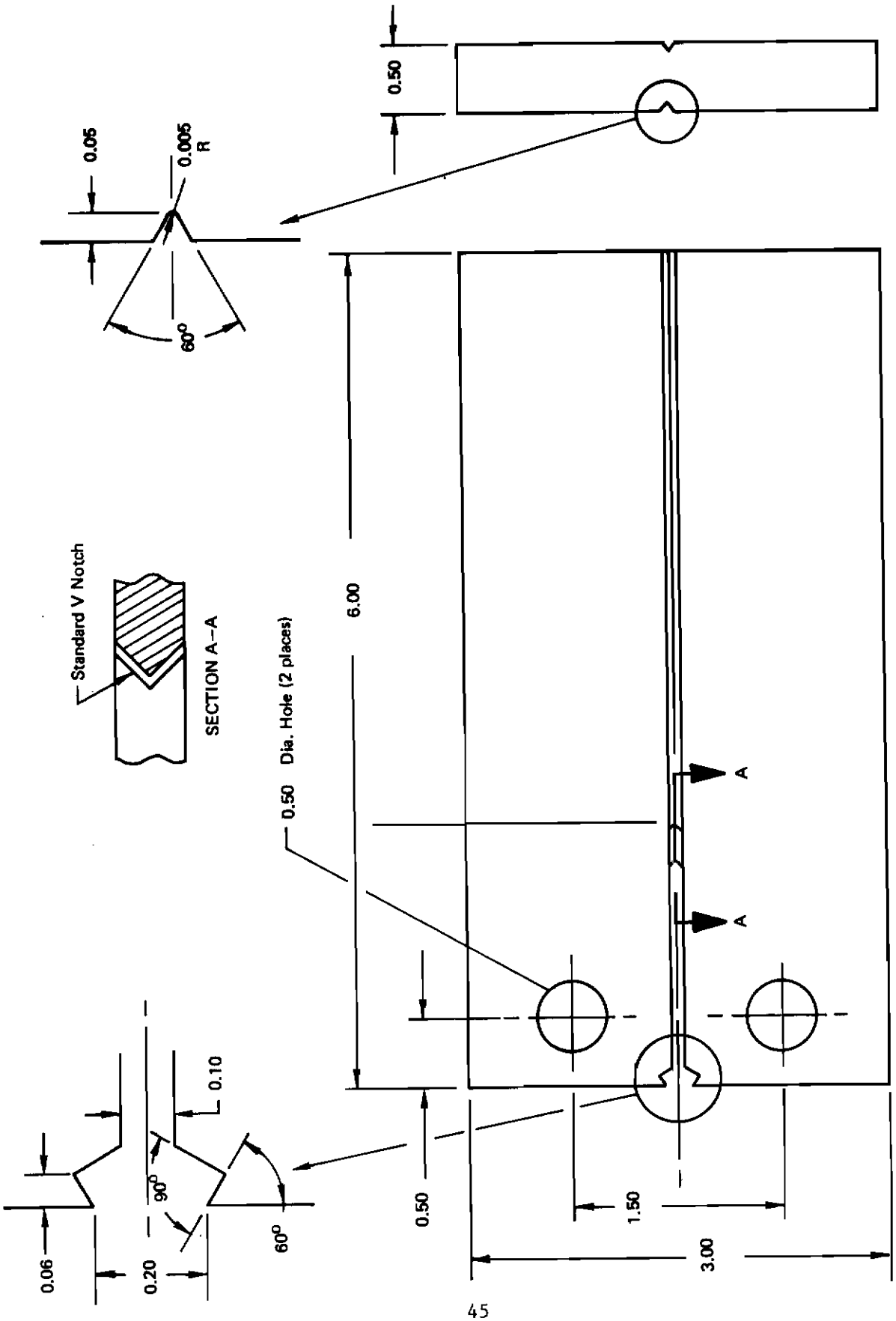

Figure 3: Uniform Height DCB Specimen

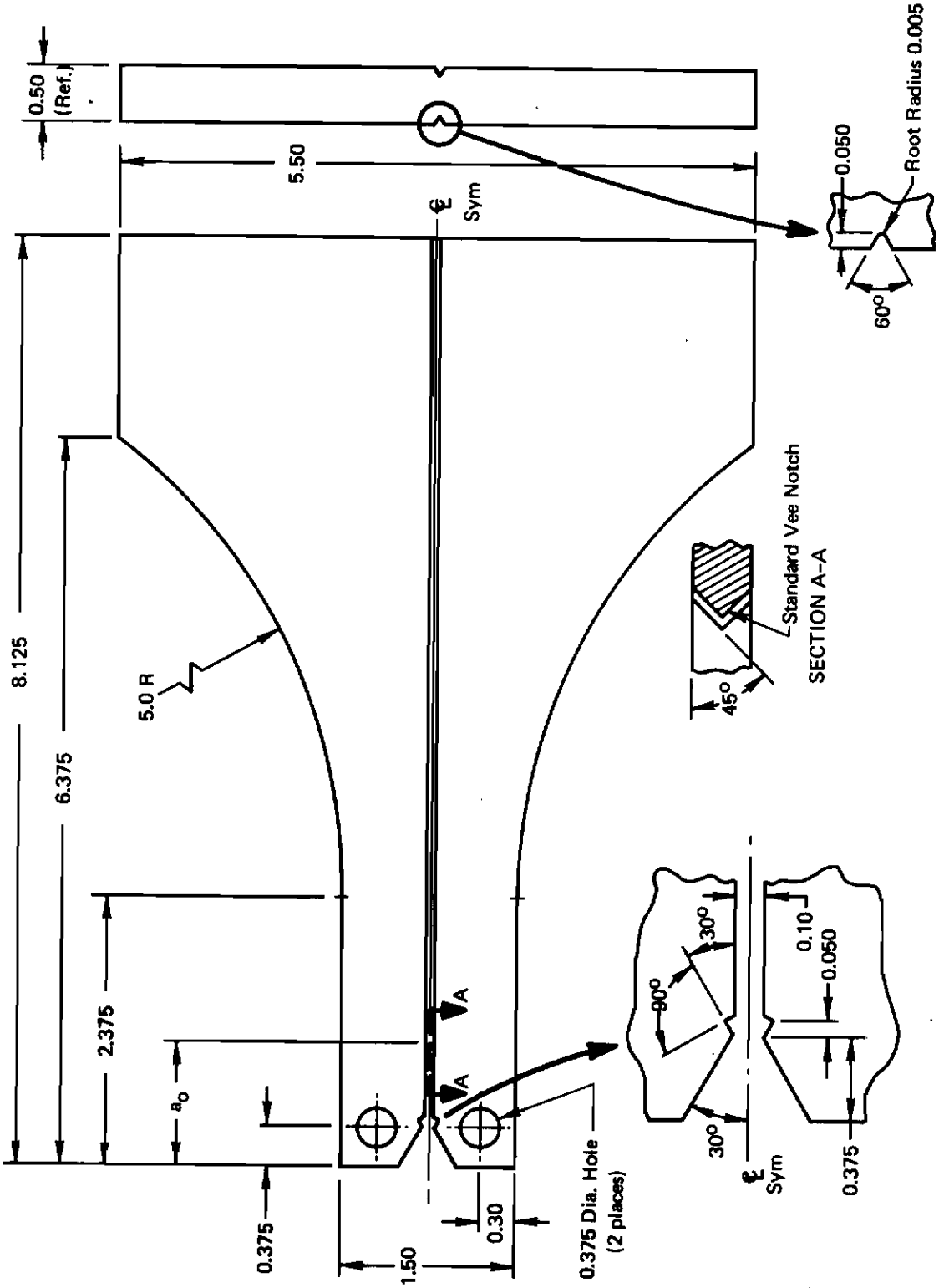

Figure 4: Flared DCB Specimen For Exploratory Tests

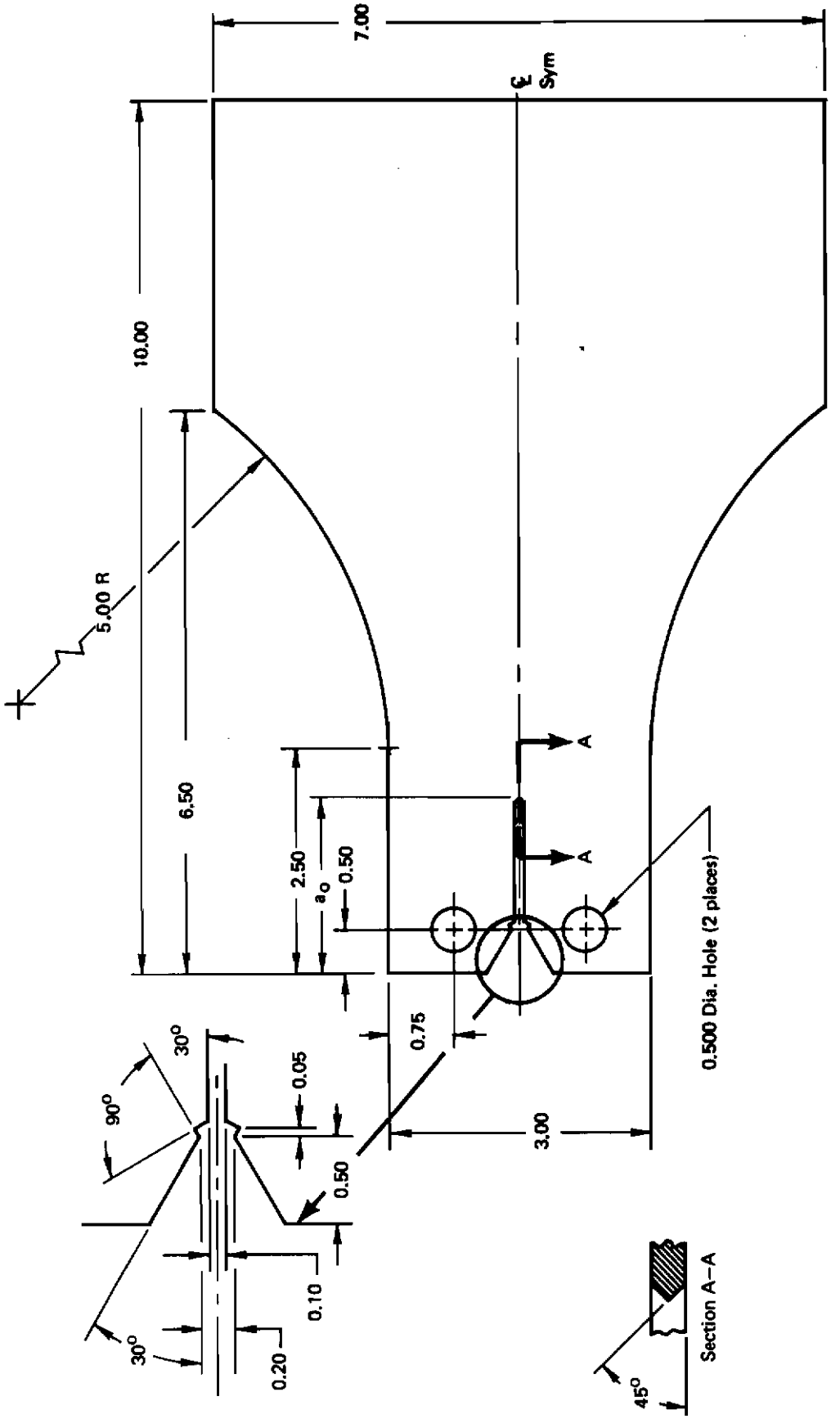

Figure 5: Flared DCB Specimen For Crack Velocity And Arrest Tests

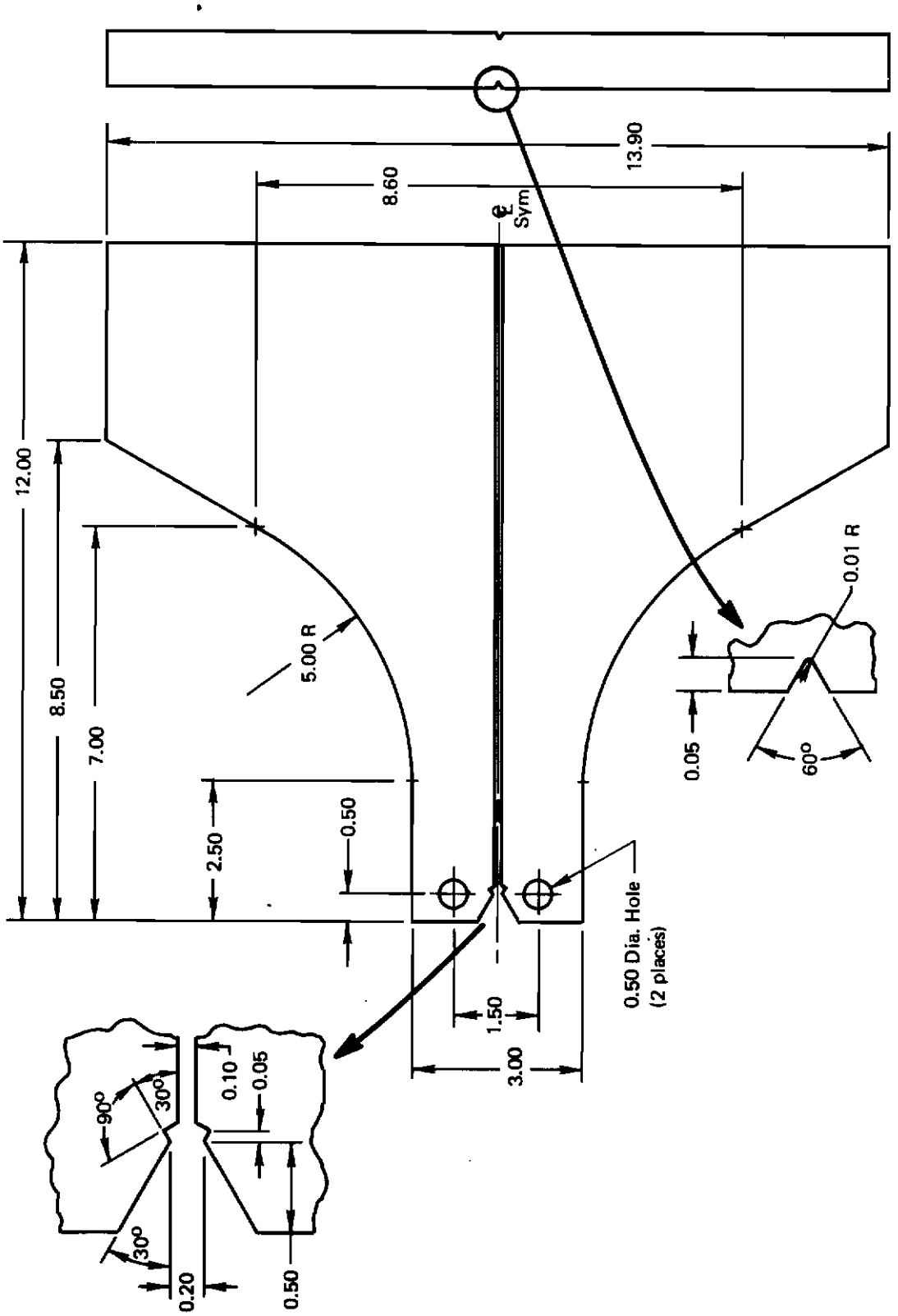

Figure 6: Flared DCB Specimen for Crack Velocity and Arrest Tests

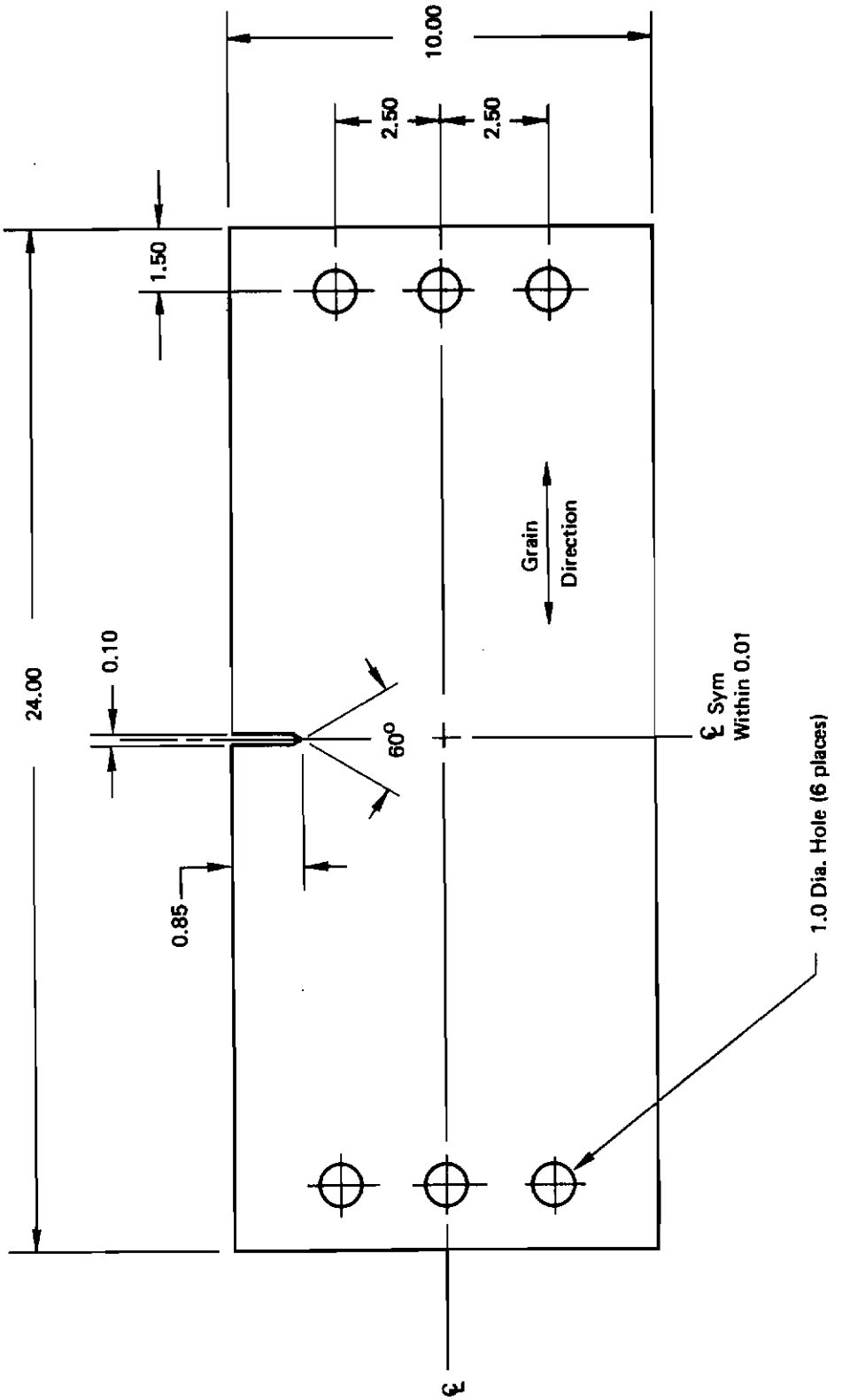

Figure 7: Single Edge Cracked Specimen Of 7075-T6 Aluminum For Crack Velocity Measurement

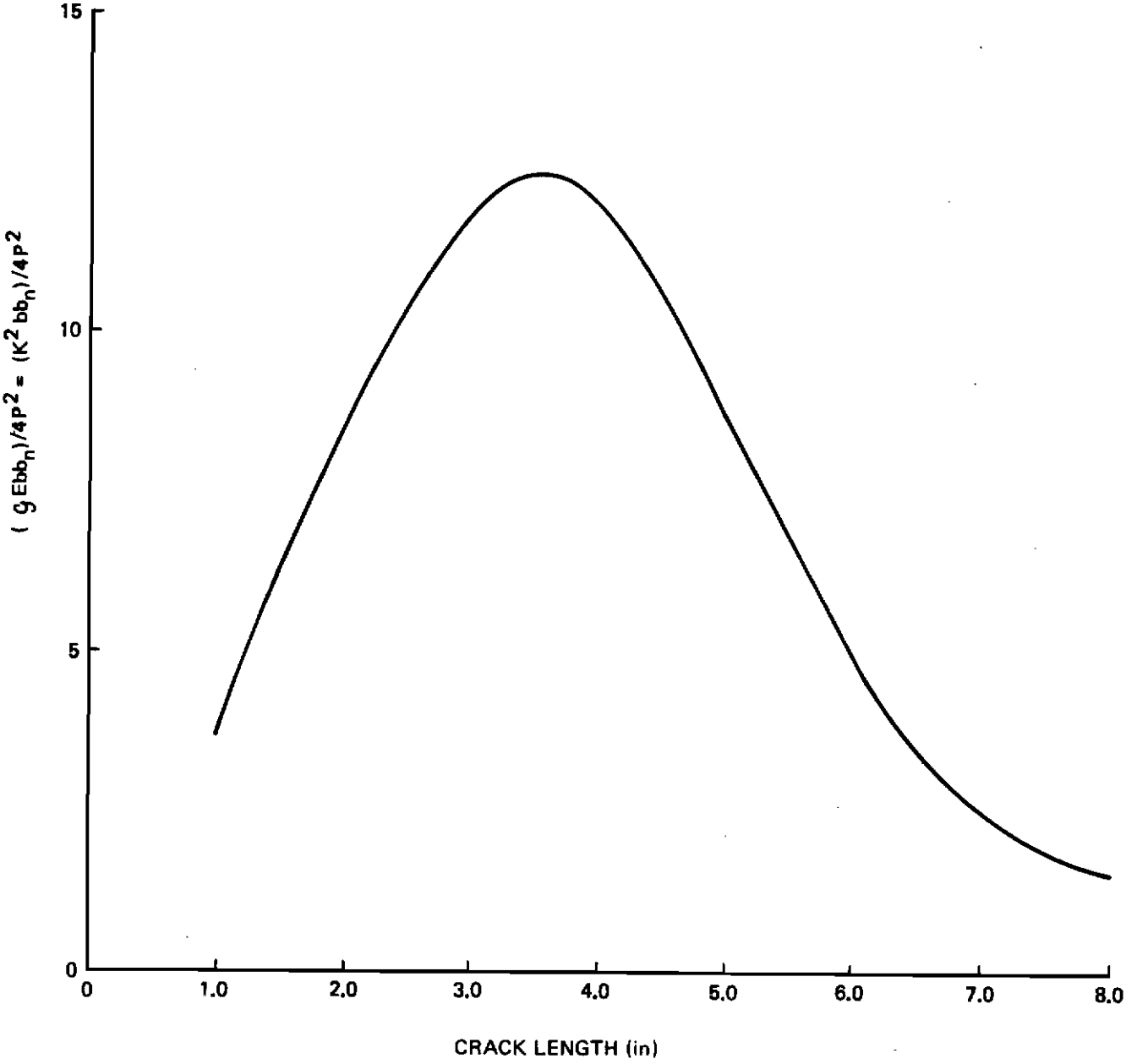

Figure 8: Approximate Normalized Strain Energy Release Rate For The Flared DCB Specimen Of Figure 6

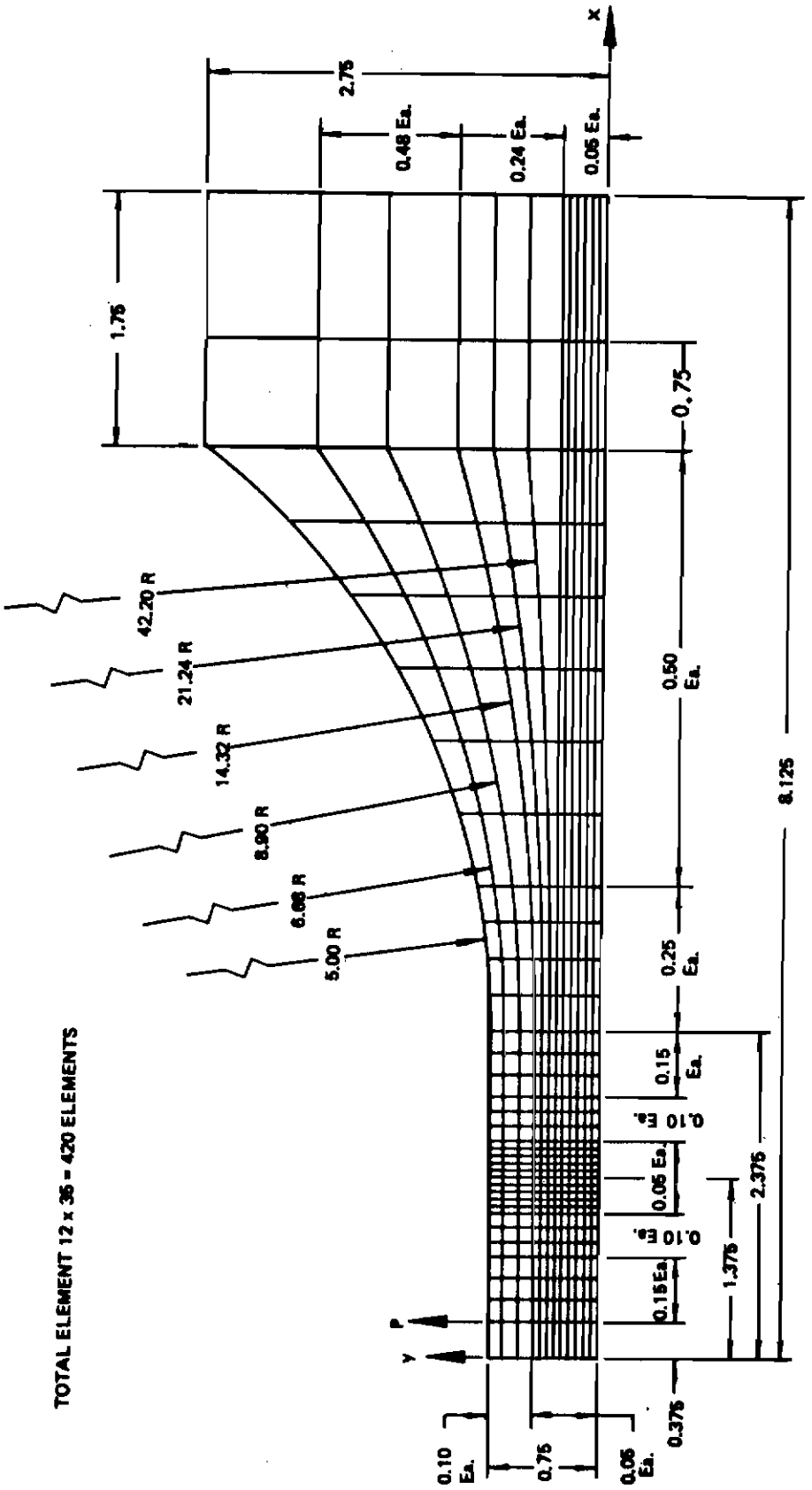

Figure 9: Finite Element Idealization For A Flared DCB Specimen Of Figure 4 With A Crack Length Of 1.0 And 1.05 Inch

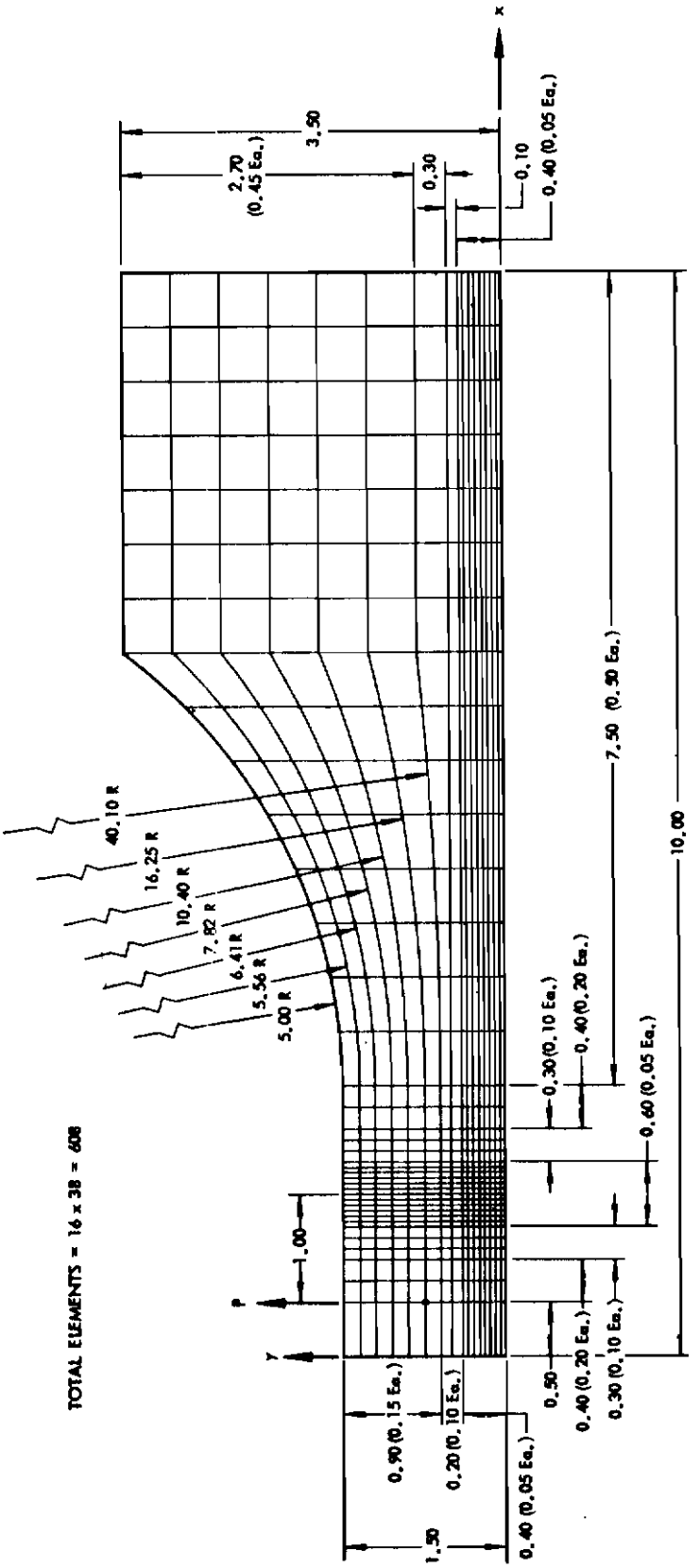

Figure 10: Finite Element Idealization For A Flared DCB Specimen Of Figure 5 With A Crack Length Of 1.00 And 1.05 Inch

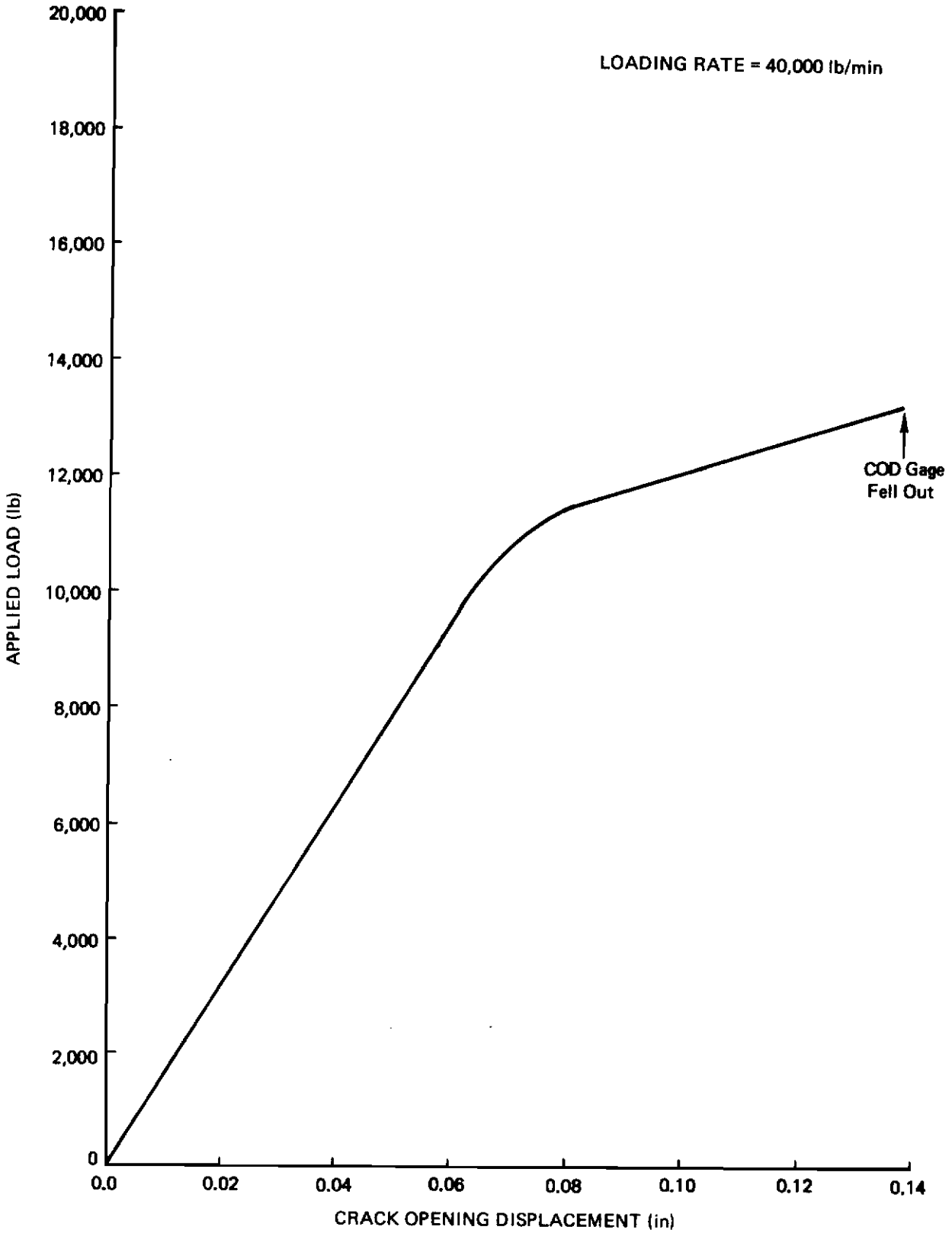

Figure 11: Load–Displacement Diagram For A 9Ni–4Co–0.2C Steel Specimen S14-1

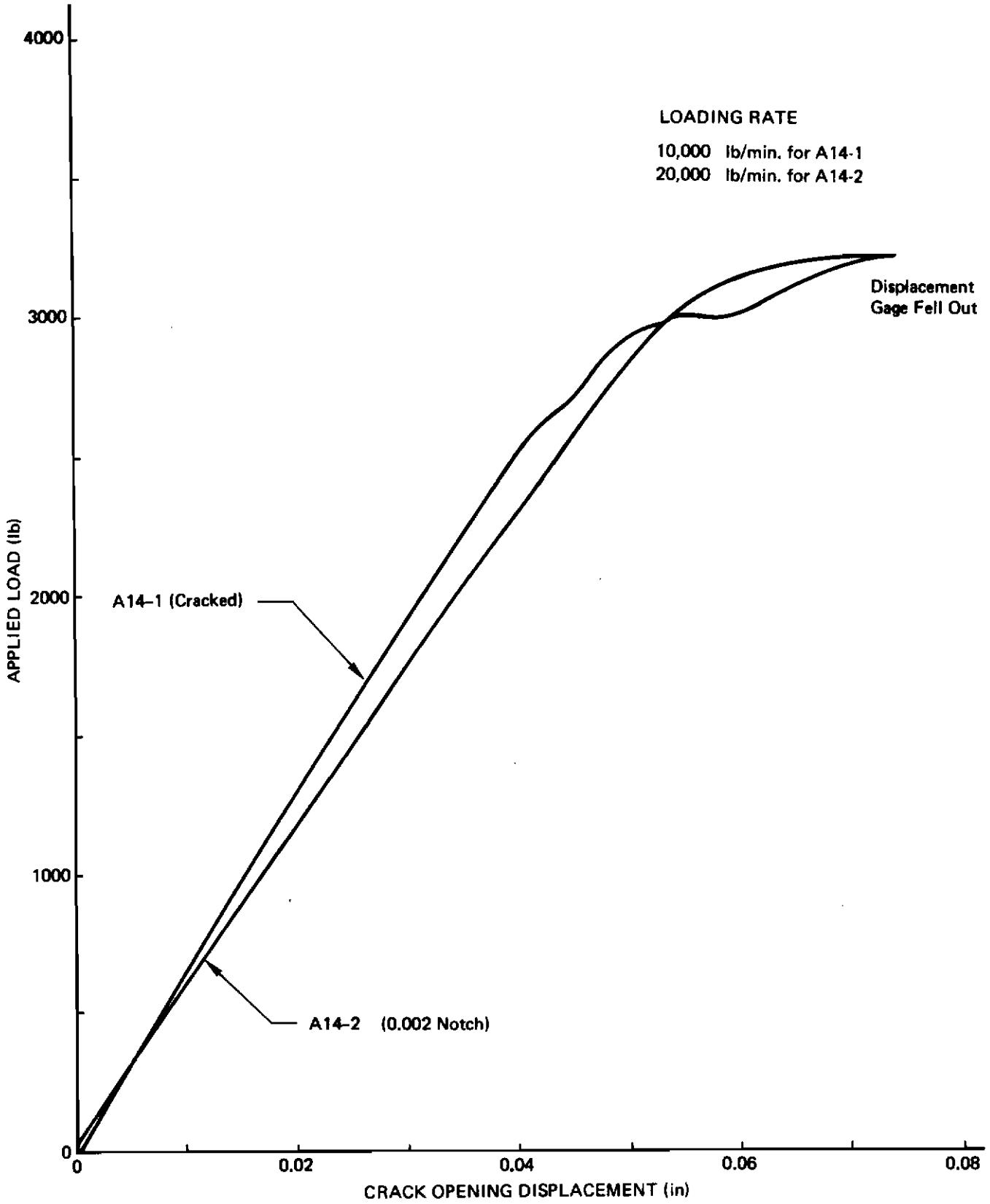

Figure 12: Load–Displacement Record For 2219-T851 Aluminum Flared DCB Specimens A14-1 And A14-2

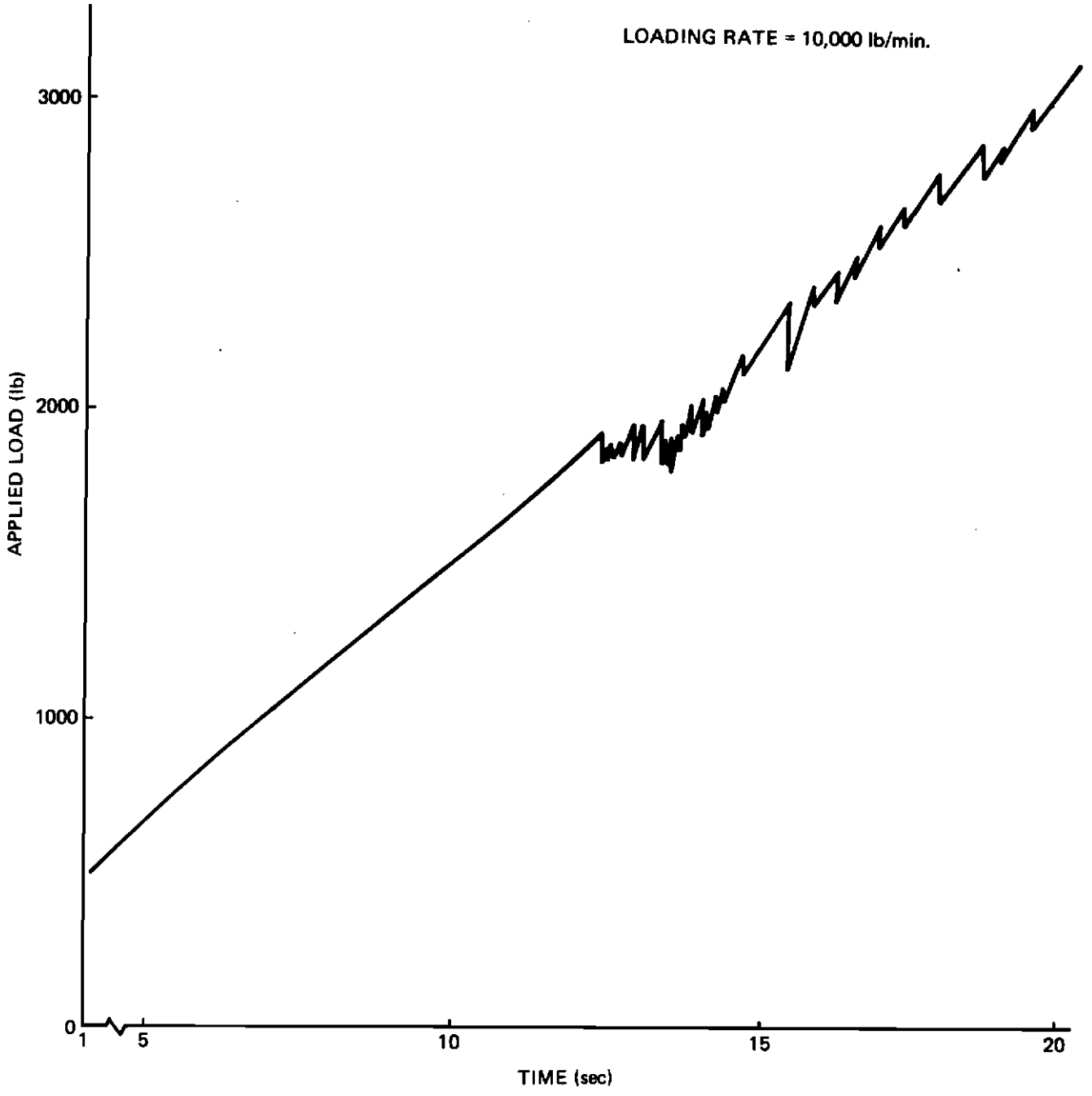

Figure 13: Load–Time Diagram For A 7075-T6 Aluminum Flared DCB Specimen – A14-3

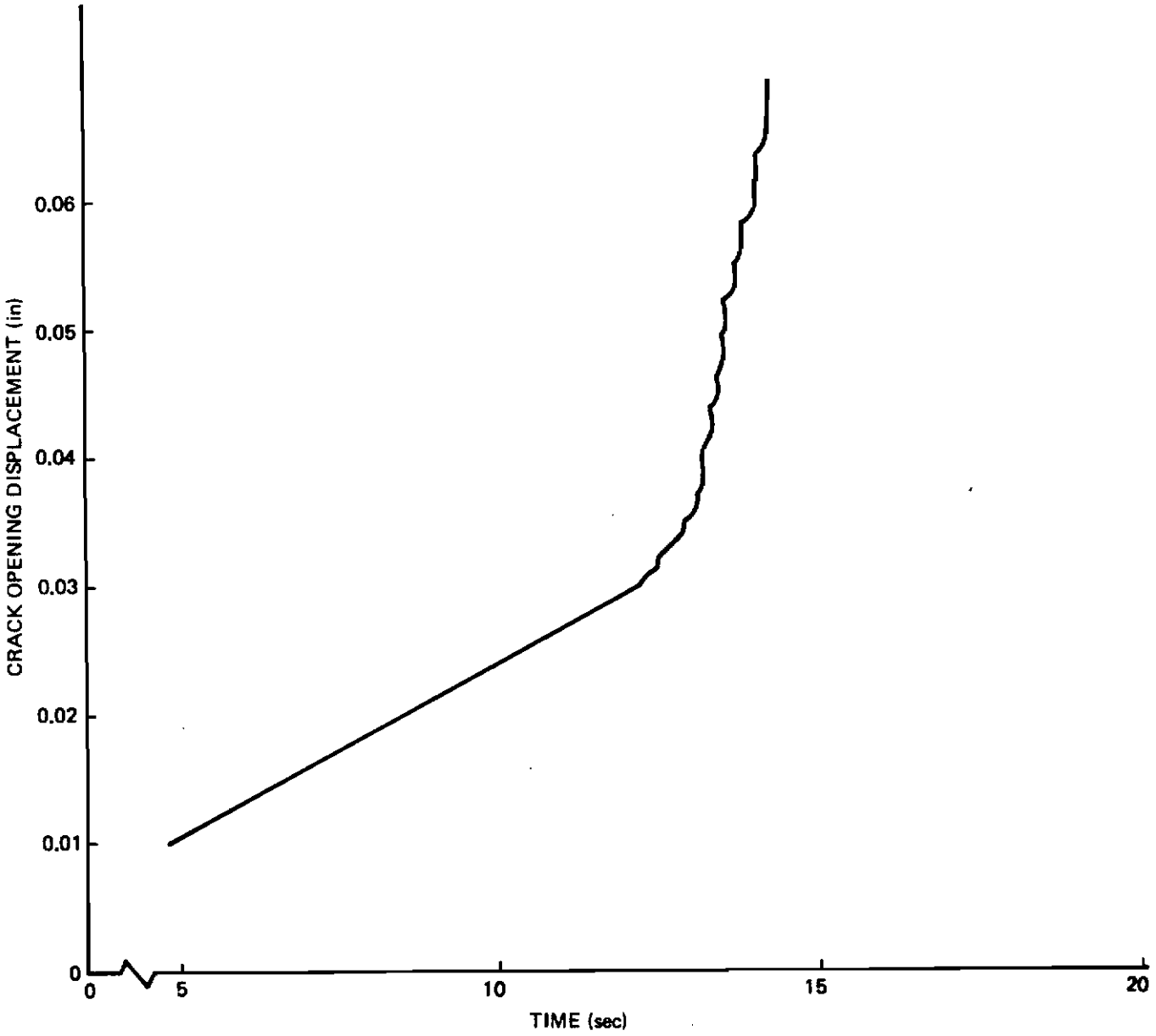

Figure 14: Displacement Time Diagram For A 7075-T6 Aluminum Flared DCB Specimen – A14-3

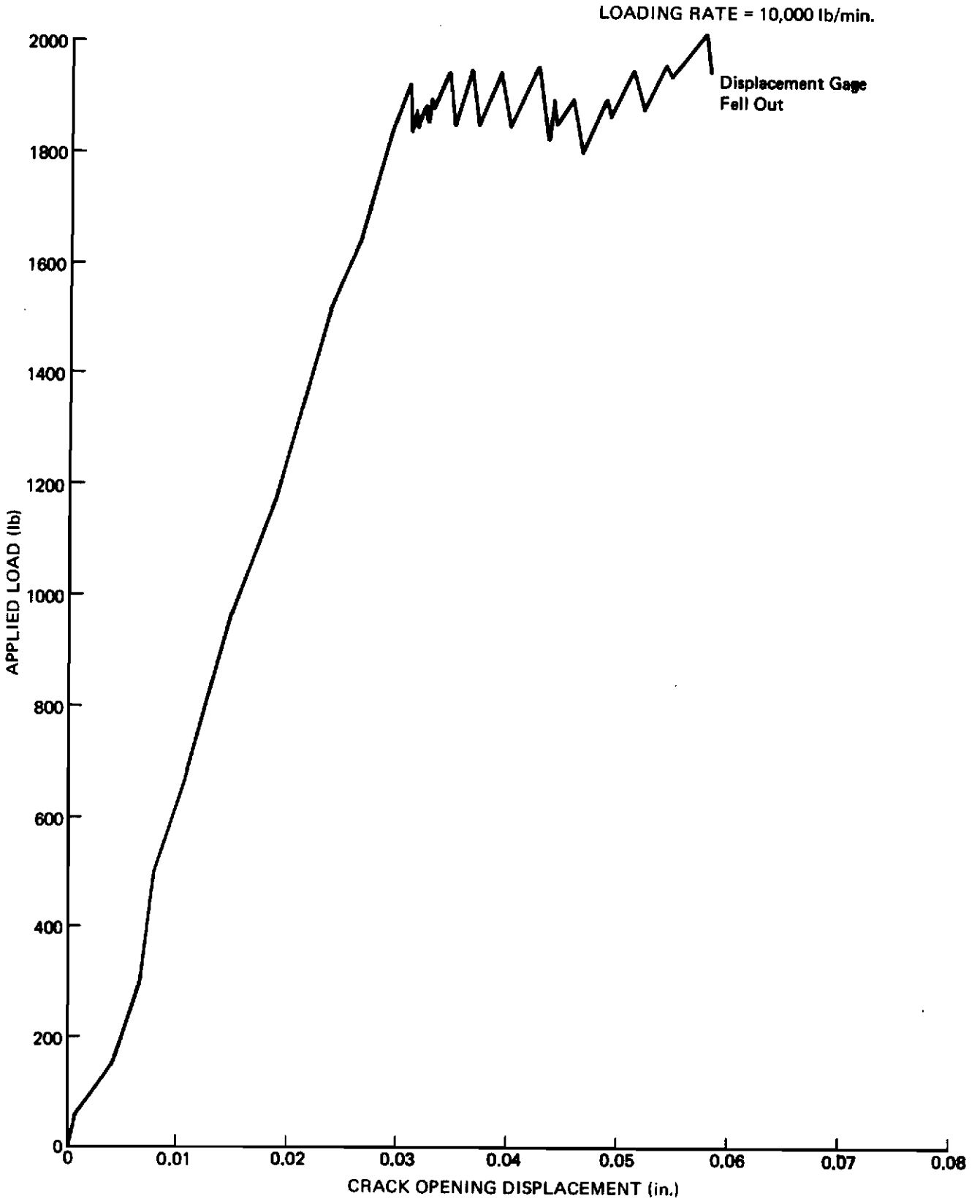

Figure 15: Load–Displacement Diagram For A 7075-T6 Aluminum Flared DCB Specimen – A14-3

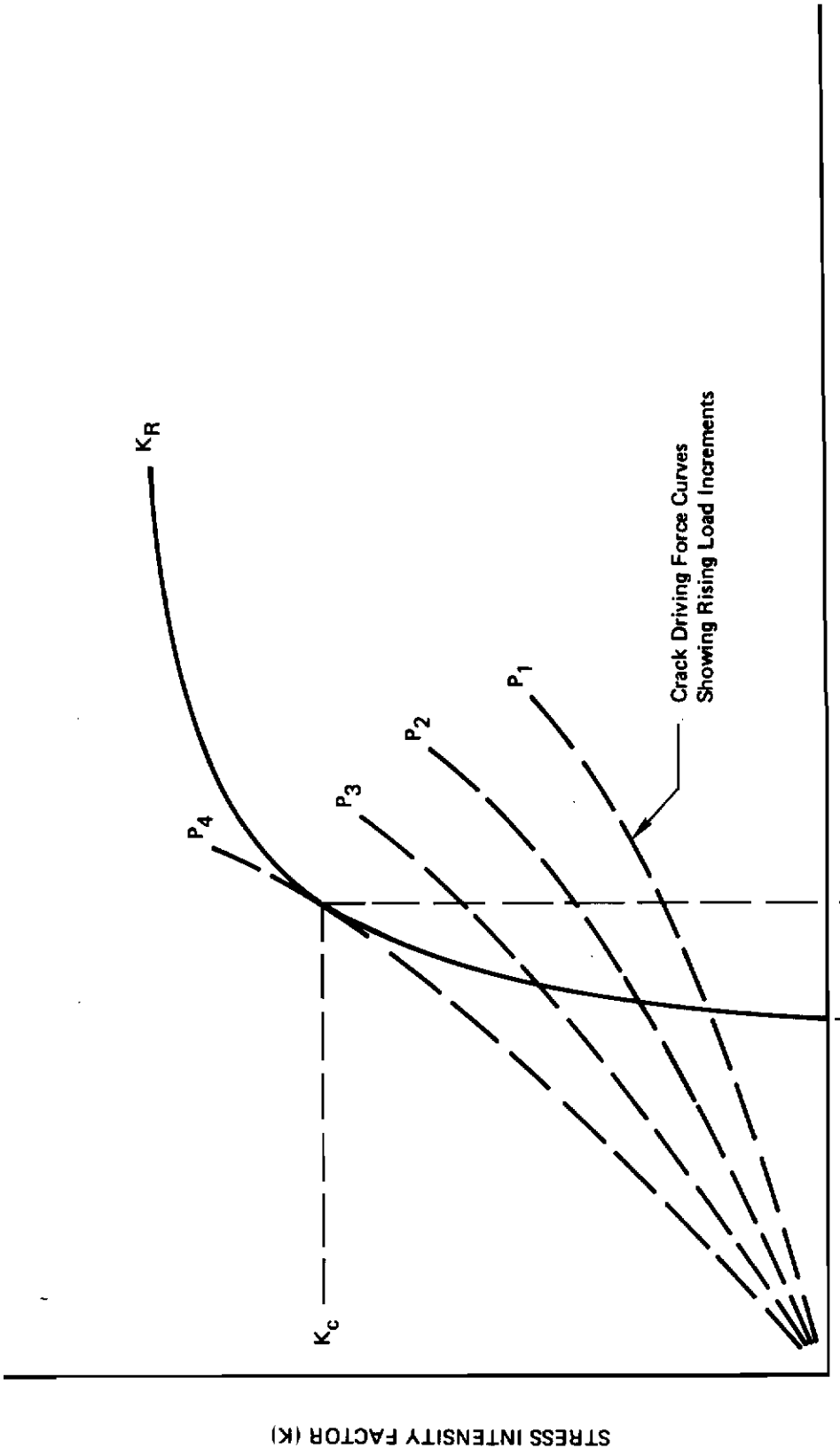

Figure 16: Crack–Growth–Resistance Curve And Crack Driving Force Curves For Load Controlled Test

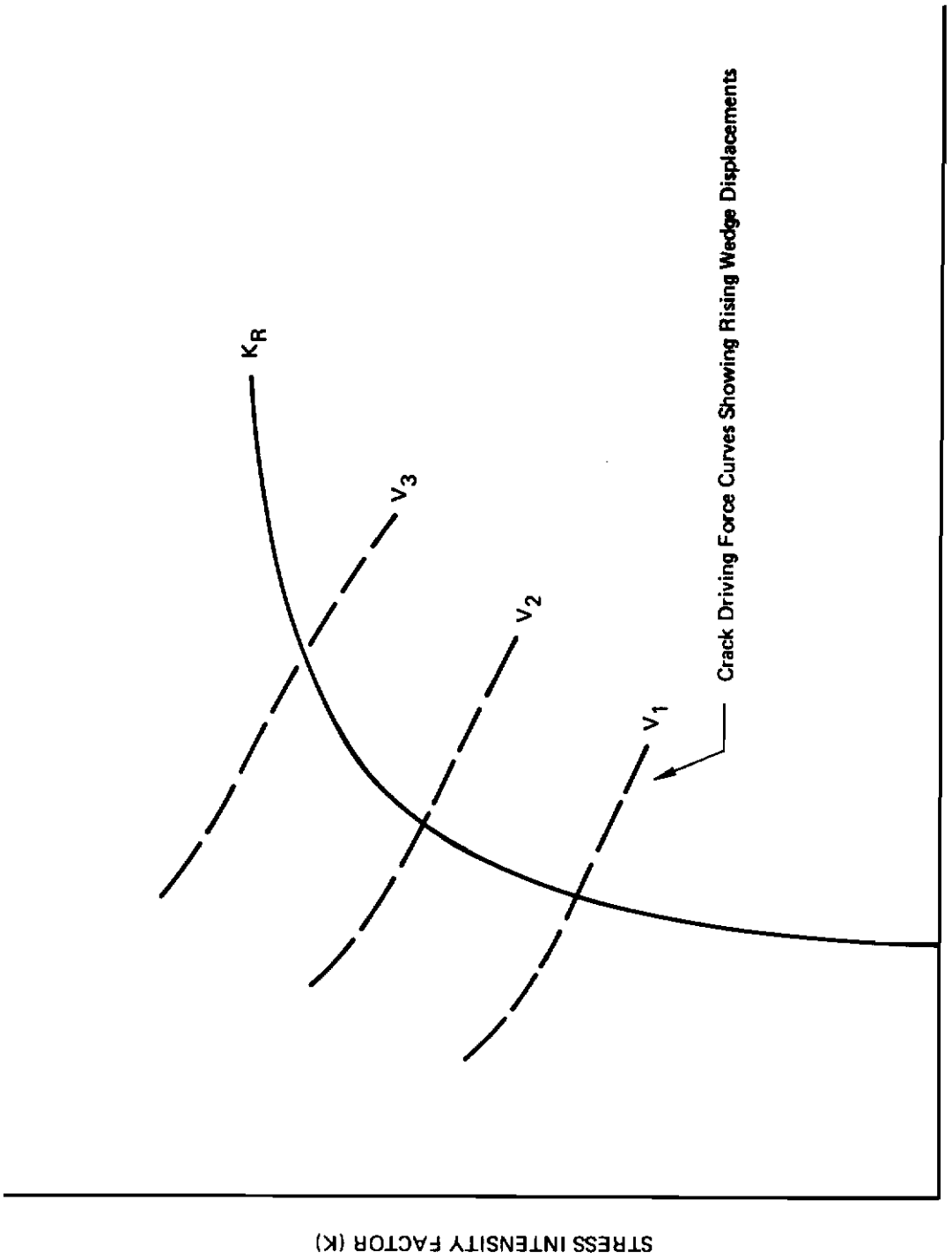

Figure 17: Crack–Growth–Resistance Curve And Crack Driving Force Curves For Displacement Controlled Test

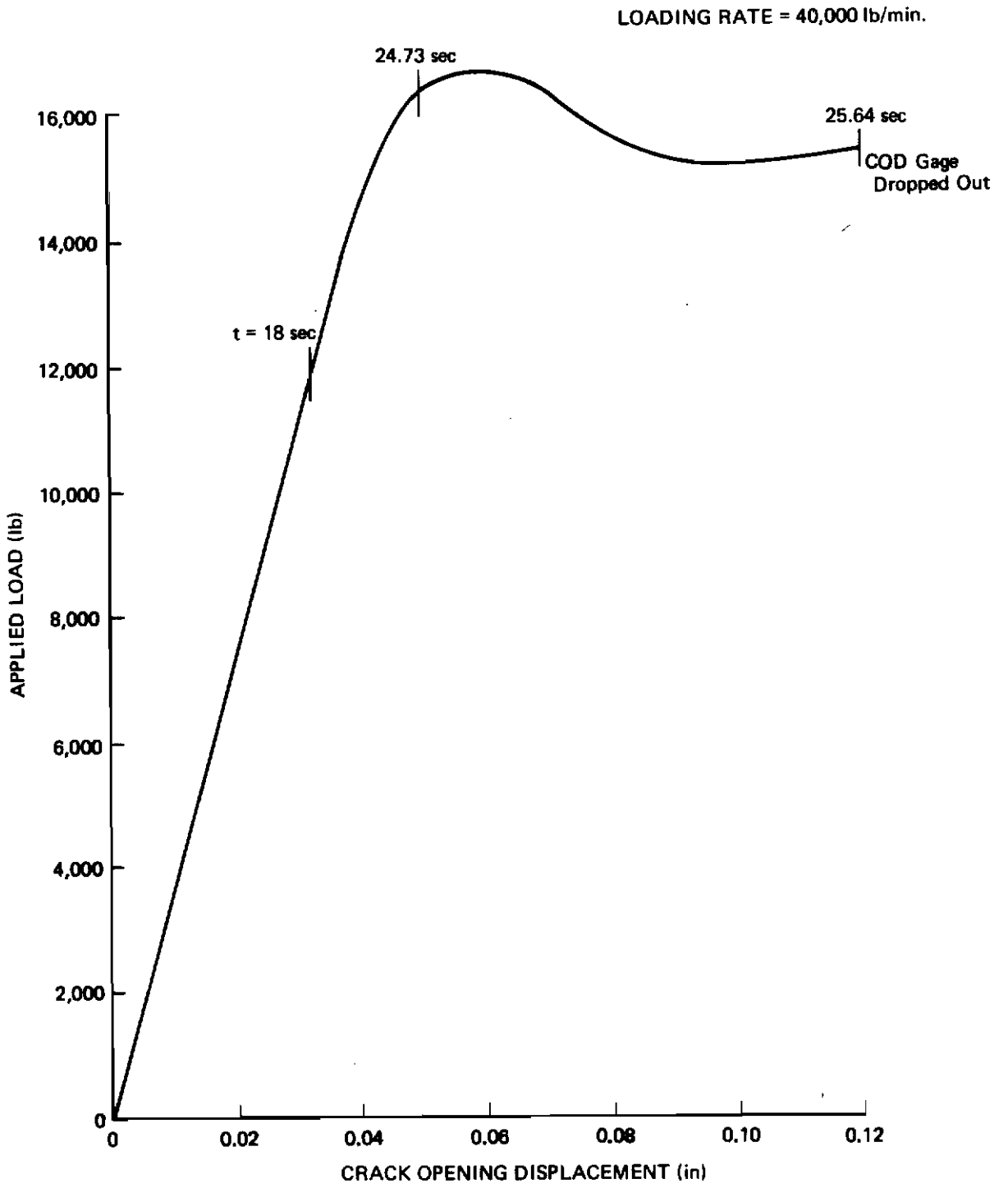

Figure 18: Load–Displacement Diagram For A 9Ni–4Co–0.2C Steel Uniform Height DCB Specimen – S3-1

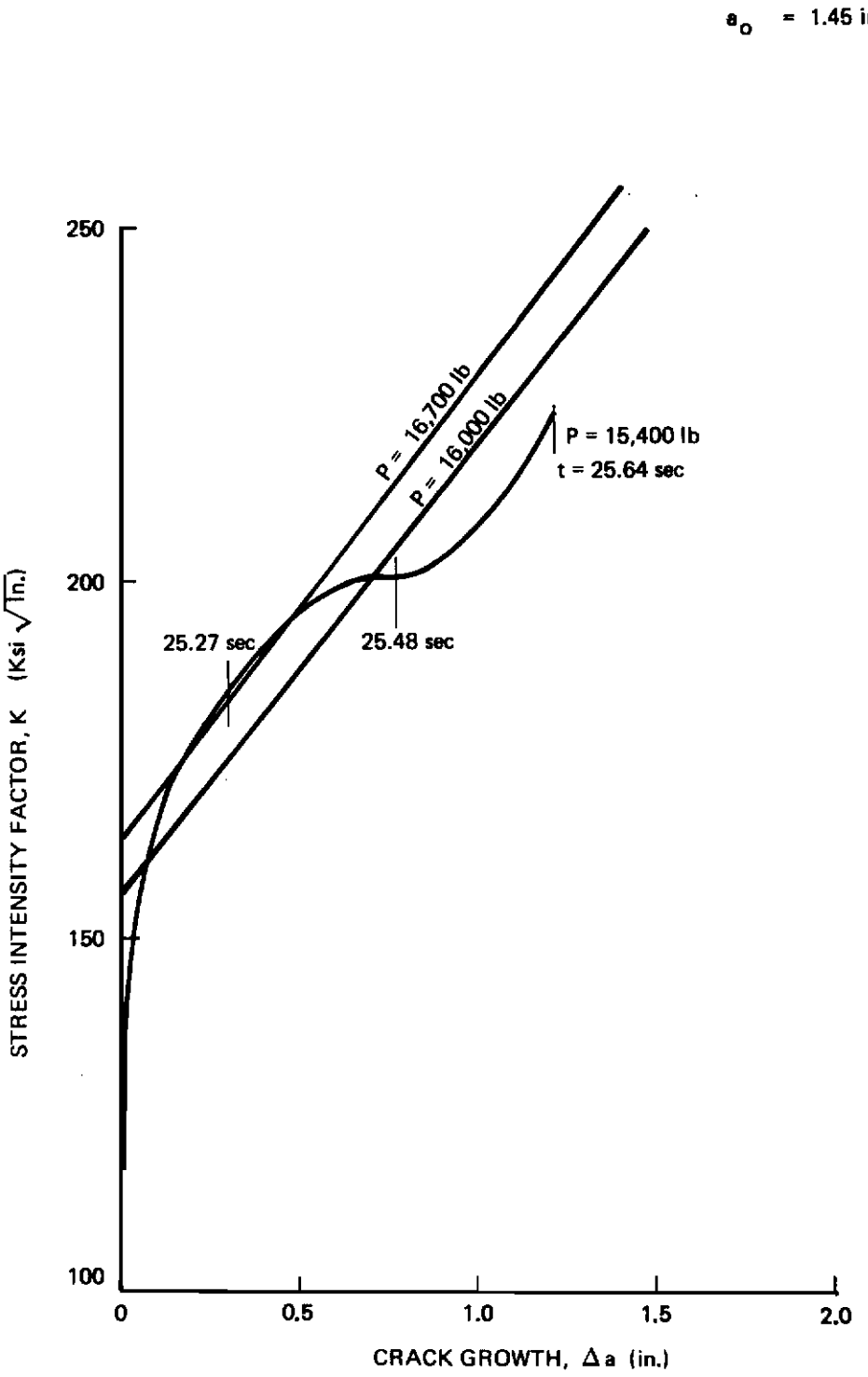

Figure 19: Crack Growth Resistance Curve Obtained From Testing A 9Ni–4Co–0.2C Steel Uniform Height DCB Specimen – S3-1

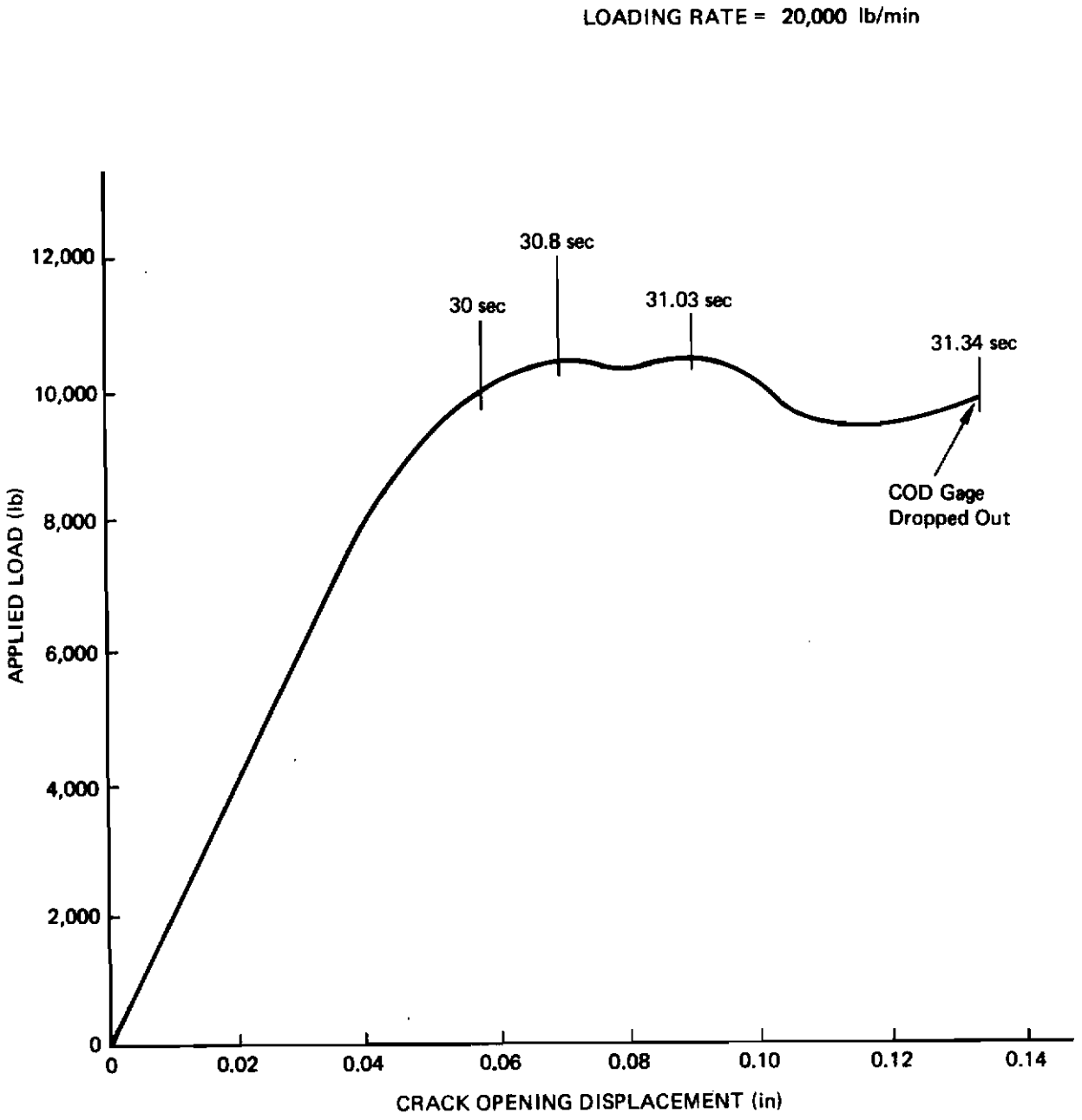

Figure 20: Load–Displacement Diagram For A 6Al–4V β Titanium Uniform Height DCB Specimen – T3-1

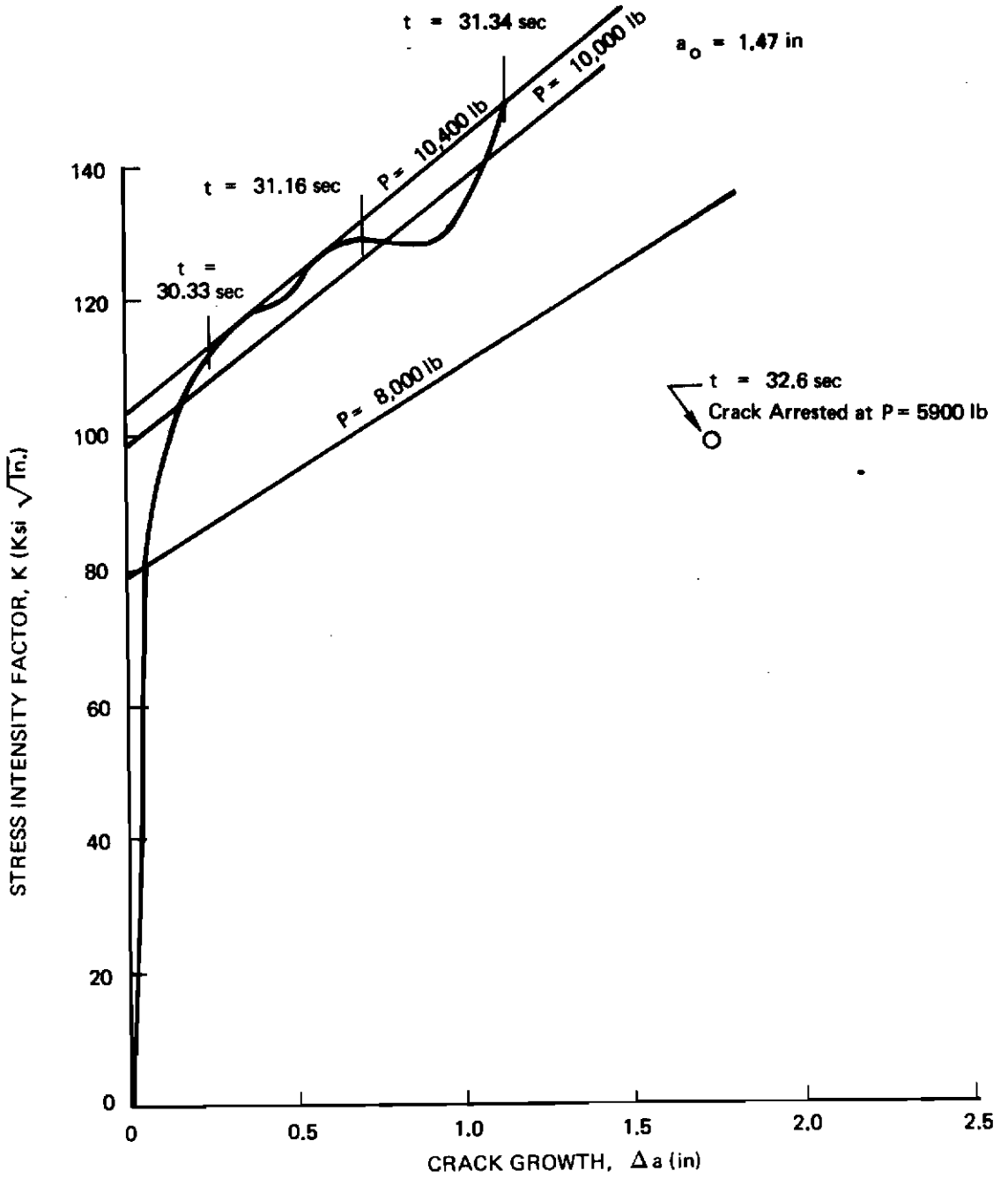

Figure 21: Crack Growth Resistance Curve Obtained From Testing A 6Al–4V β Titanium Uniform Height DCB Specimen – T3-1

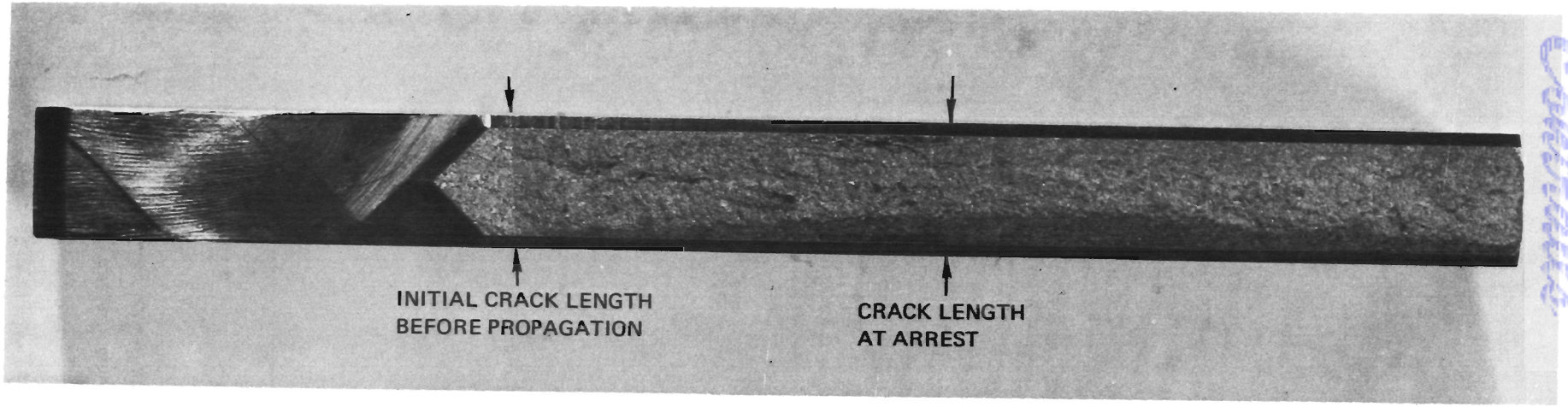

Figure 22: 6Al–4Vβ Titanium Specimen – T3-1 – Showing Crack Lengths Before Propagation And At Arrest

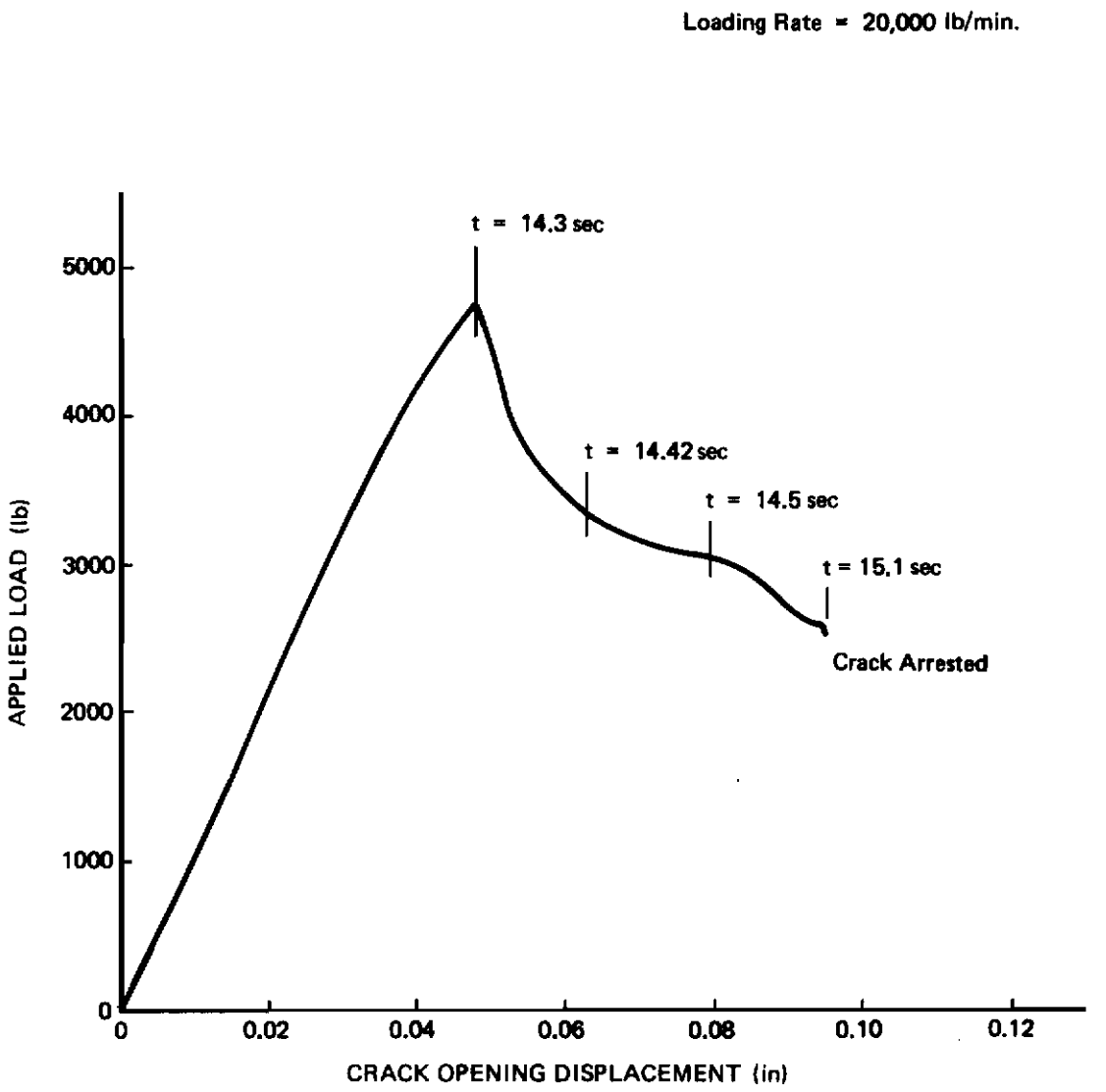

Figure 23: Load-Displacement Diagram For A 2219-T851 Aluminum Uniform Height DCB Specimen A3-2

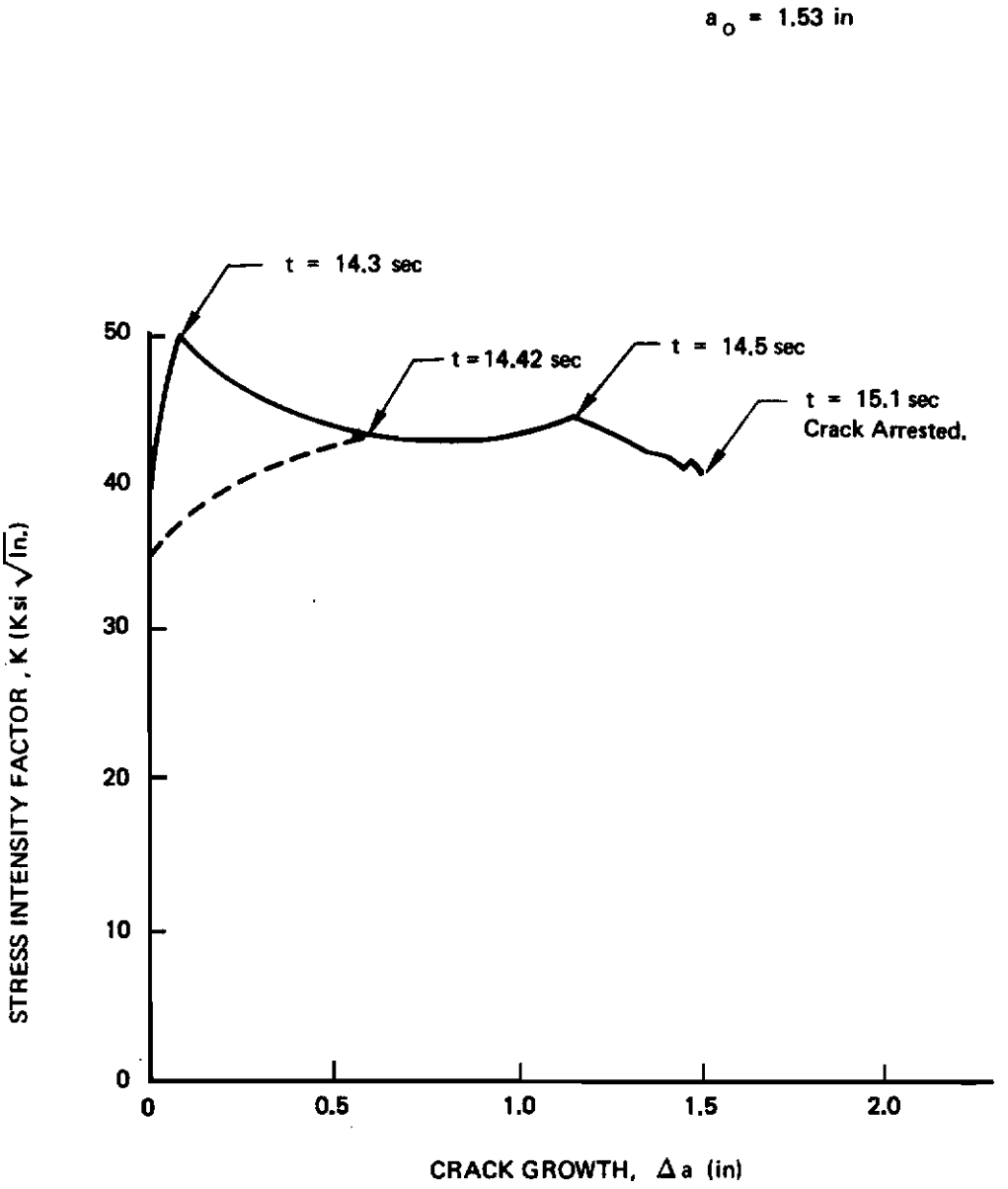

Figure 24: Crack Growth Resistance Curve Obtained From Testing A 2219–T851 Aluminum Uniform Height DCB Specimen A3-2

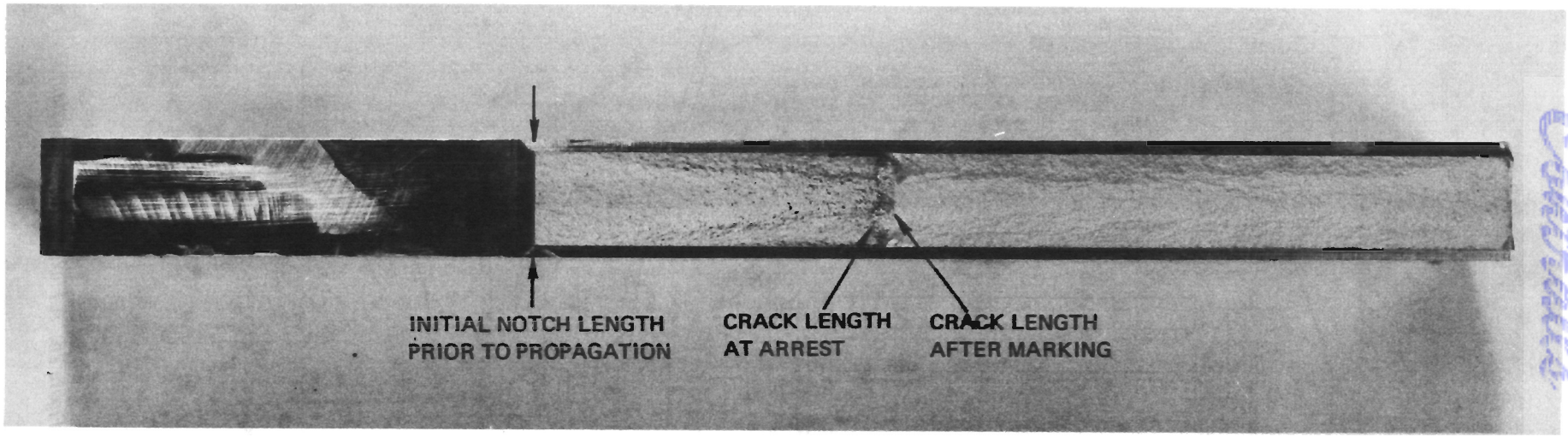

Figure 25: 2219-T851 Aluminum Specimen – A3-2 – Showing Crack Lengths Before Propagation And At Arrest

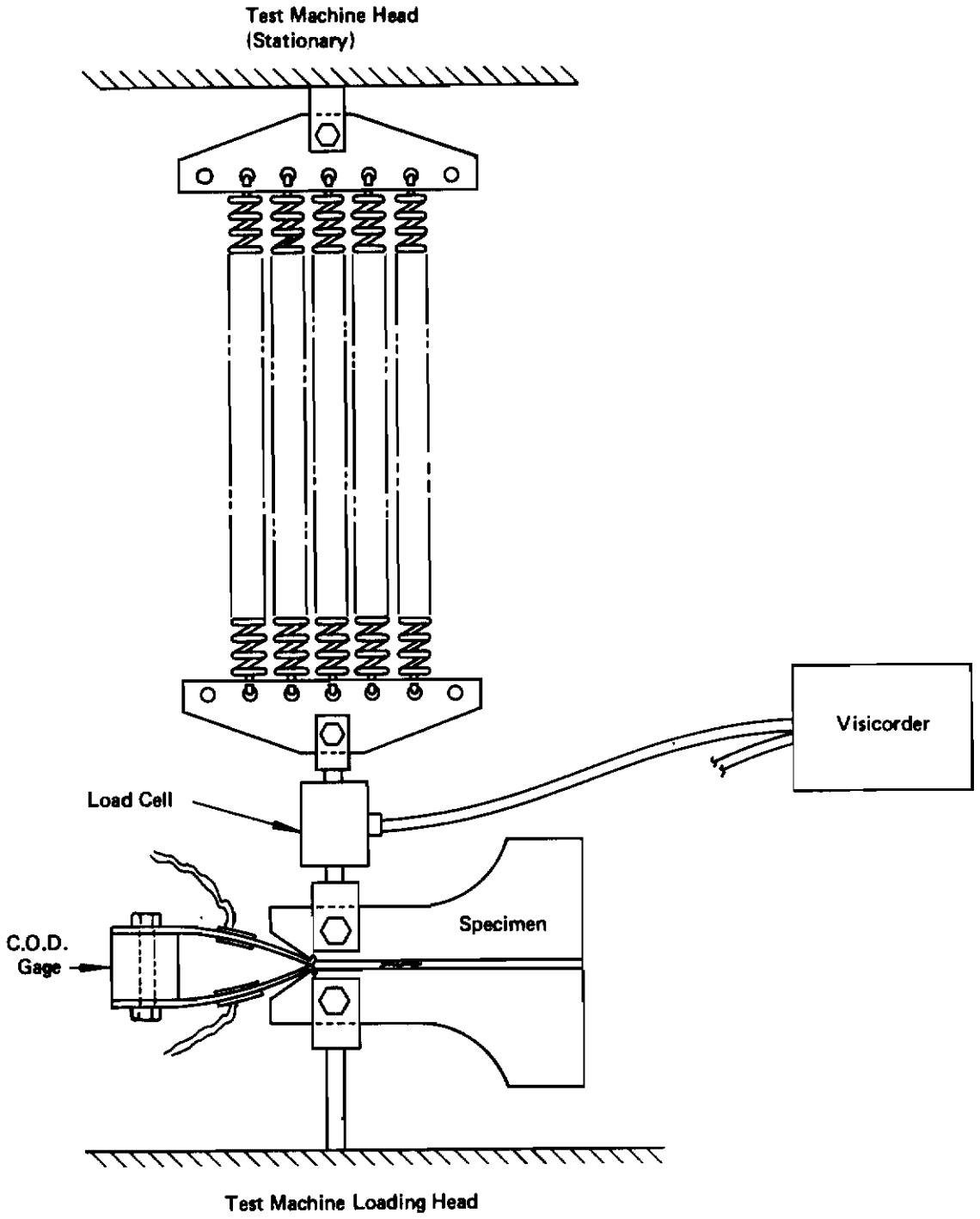

Figure 26: A Flexible Loading System

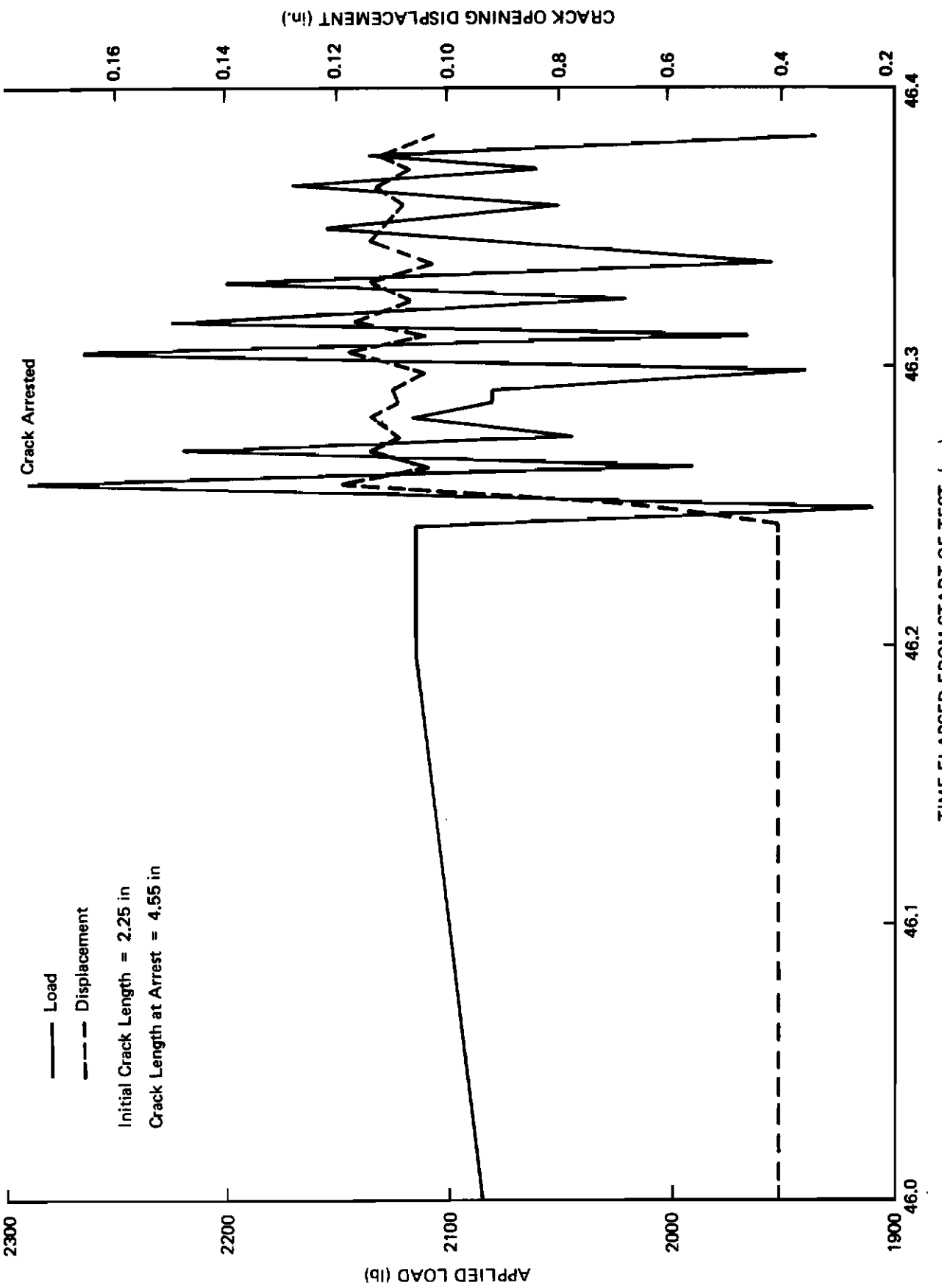

Figure 27: Load–Time And Displacement–Time Records Obtained For A 7075-T6 Aluminum Flared DCB Specimen A144

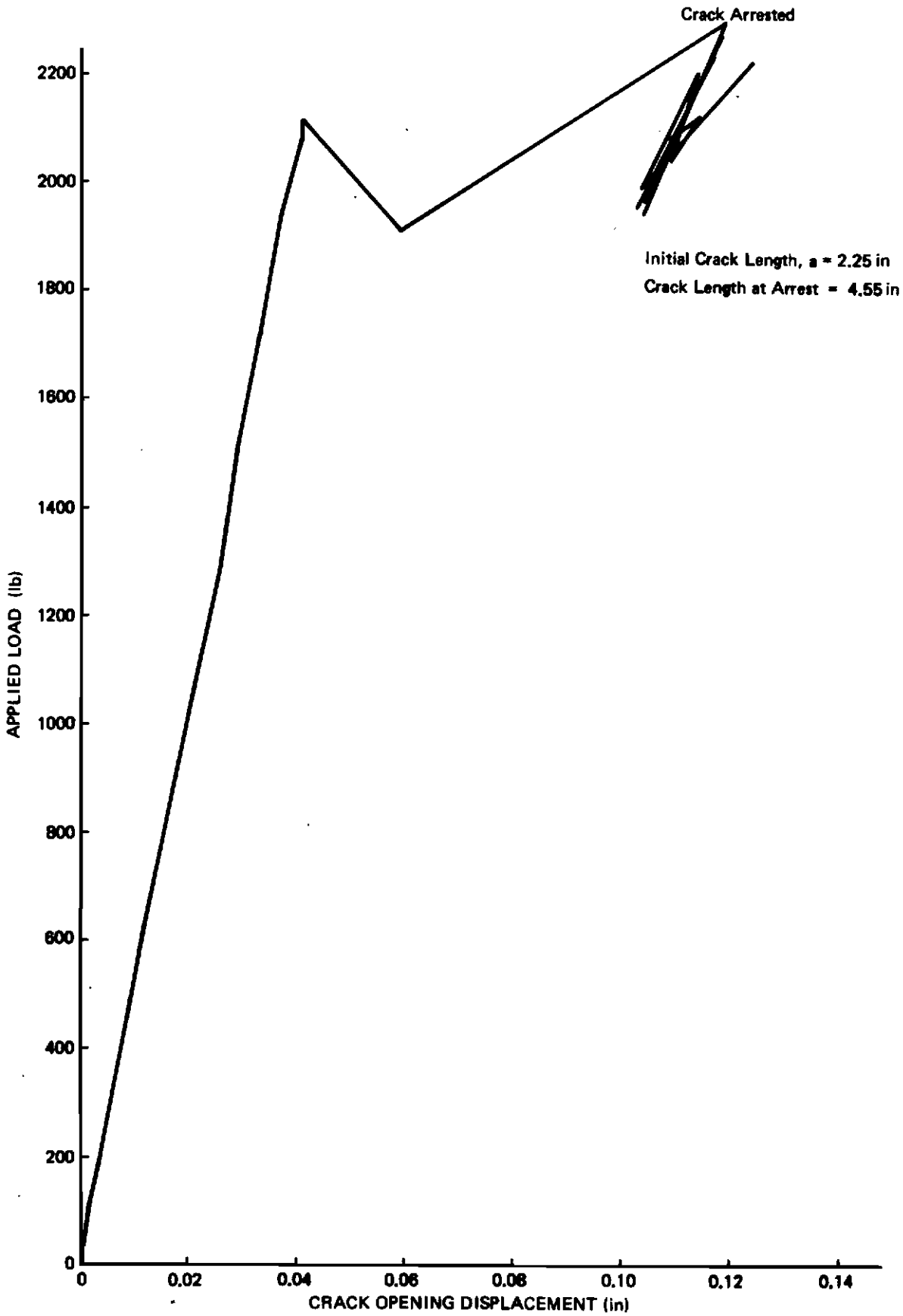

Figure 28: Load–Displacement Record Obtained For A 7075-T6 Aluminum Flared DCB Specimen A14-4

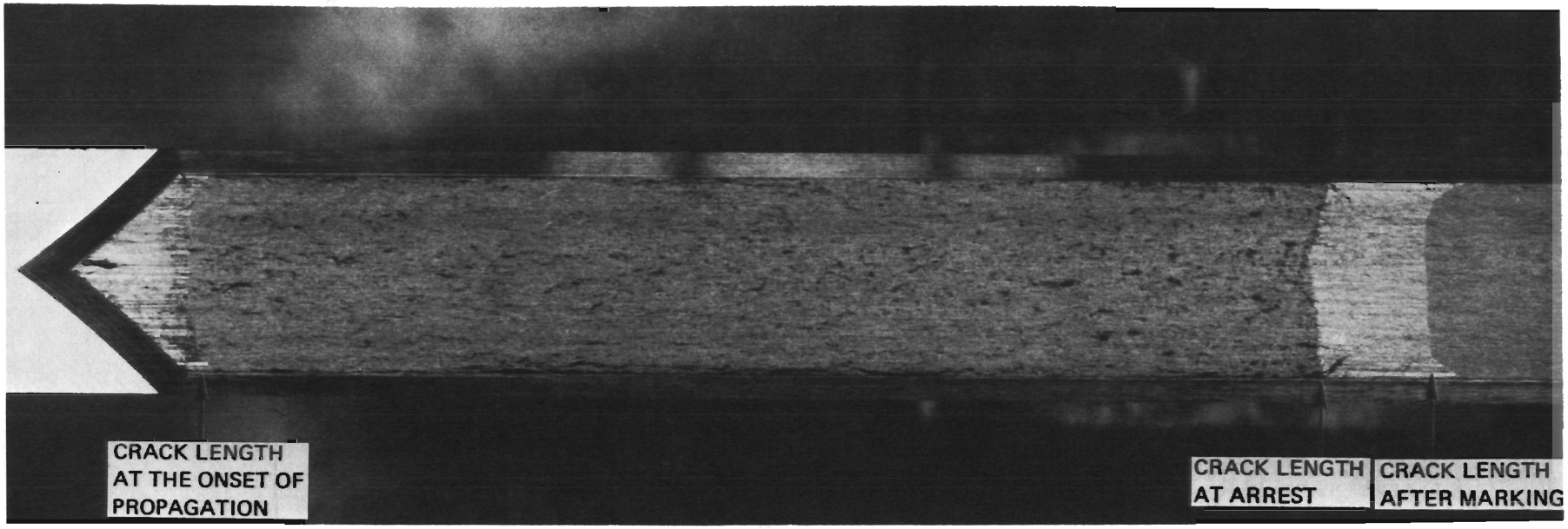

Figure 29: 7075-T6 Aluminum Specimen Showing Crack Lengths Before Propagation And At Arrest

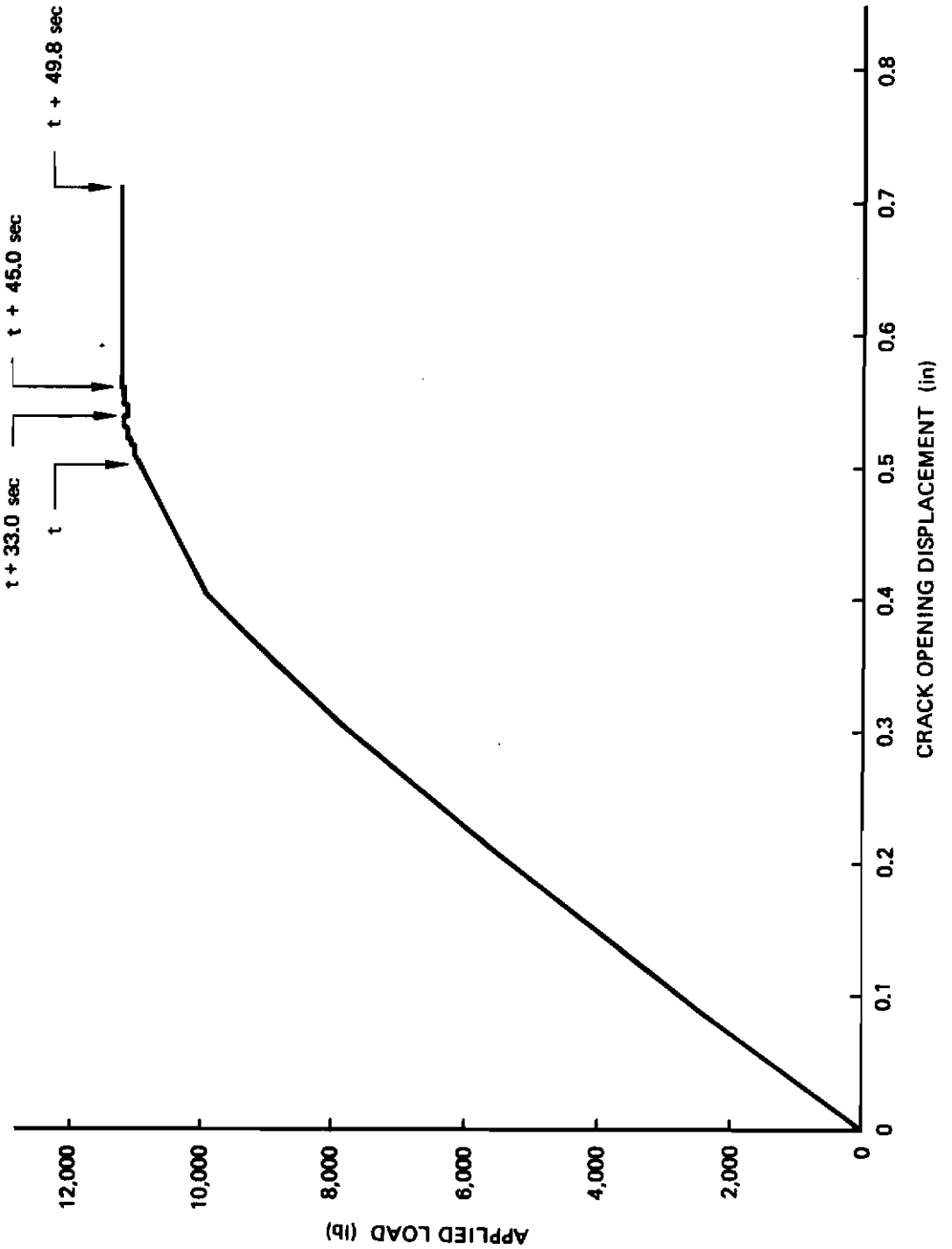

Figure 30: Load–Displacement Record For A 1.50 Inch Thick 2219-T851 Aluminum Uniform Height DCB Specimen A3-4

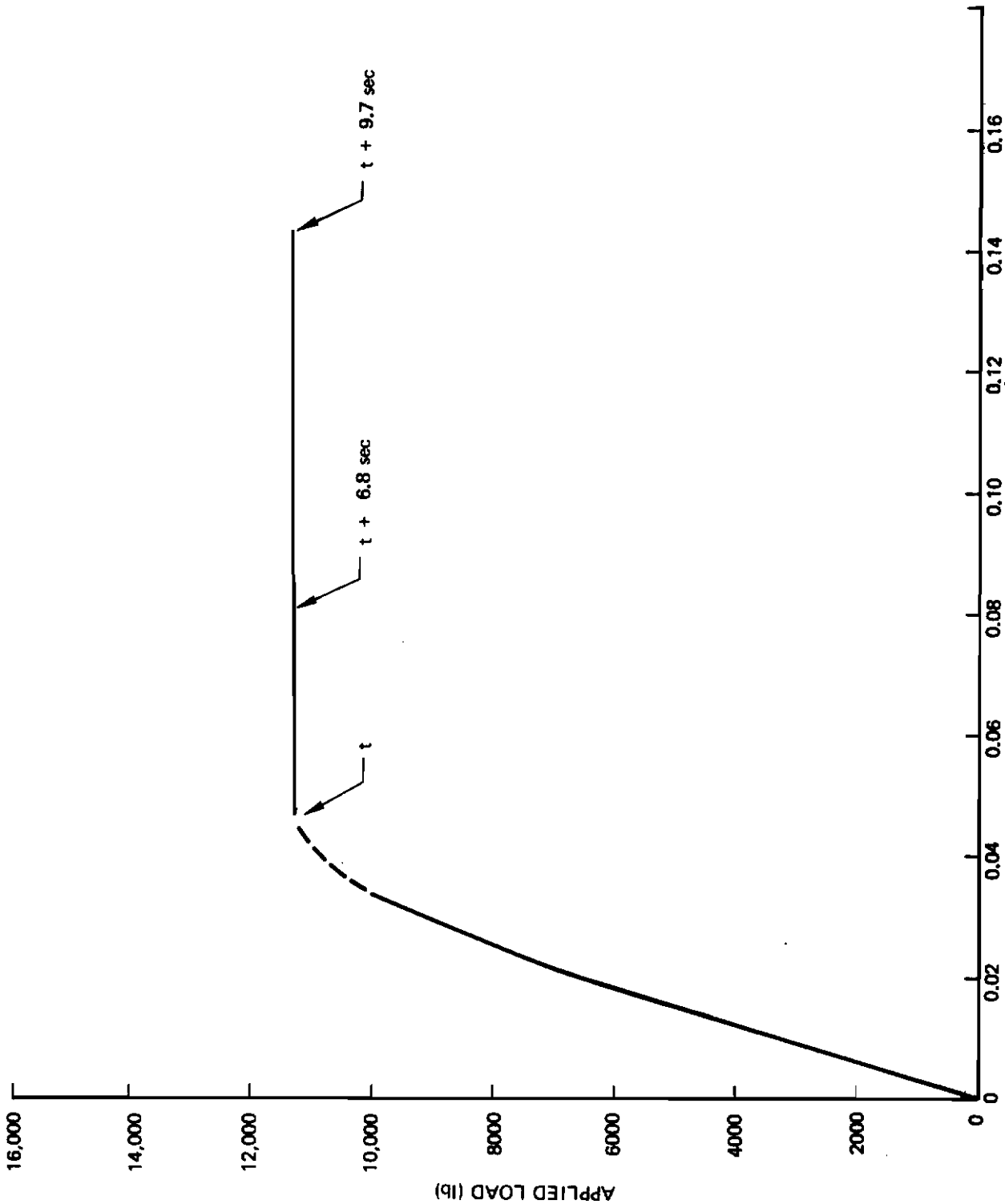

Figure 31: Load–Displacement Record For A 1.50 Inch Thick 2219-T851 Aluminum Flared DCB Specimen A14-5

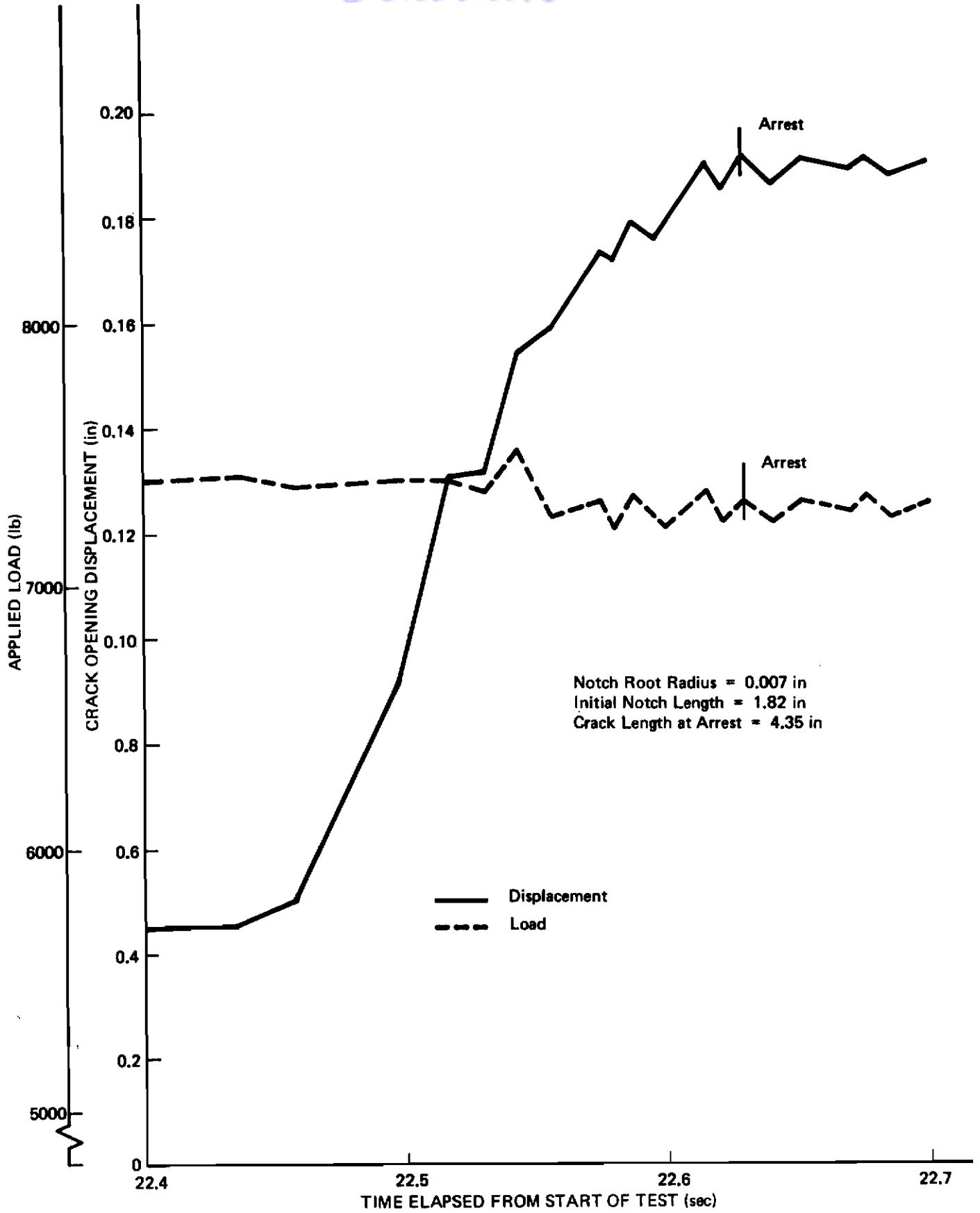

Figure 32: Load–Time And Displacement–Time Records For A 1.0 Inch Thick 2219-T851 Aluminum Flared DCB Specimen A14-6

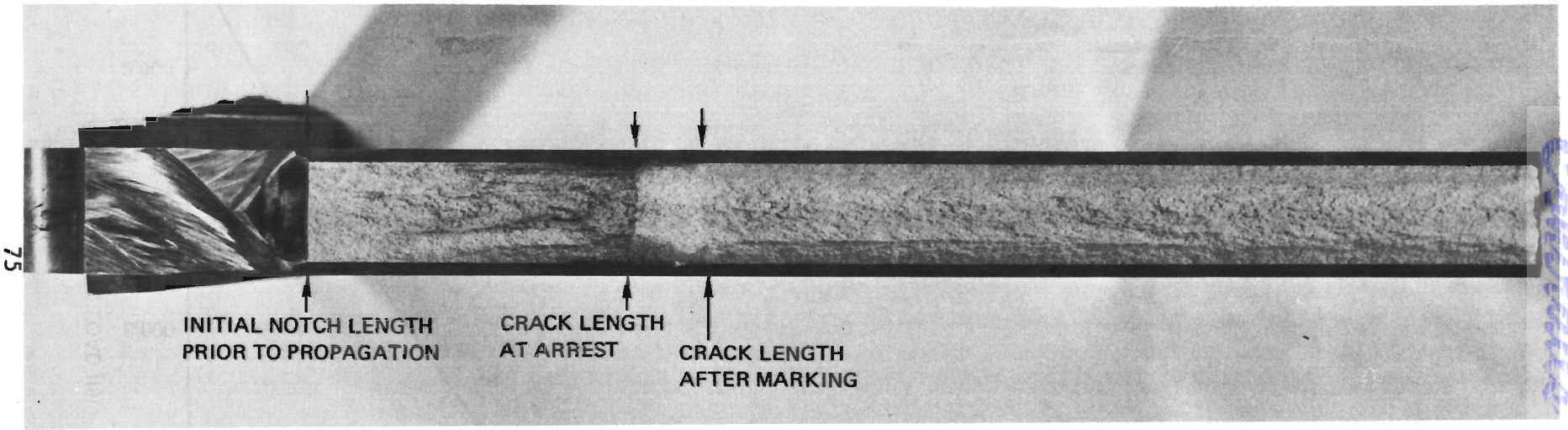

Figure 33: 2219-T851 Aluminum Specimen A14-6 Showing Crack Lengths Before Propagation And At Arrest

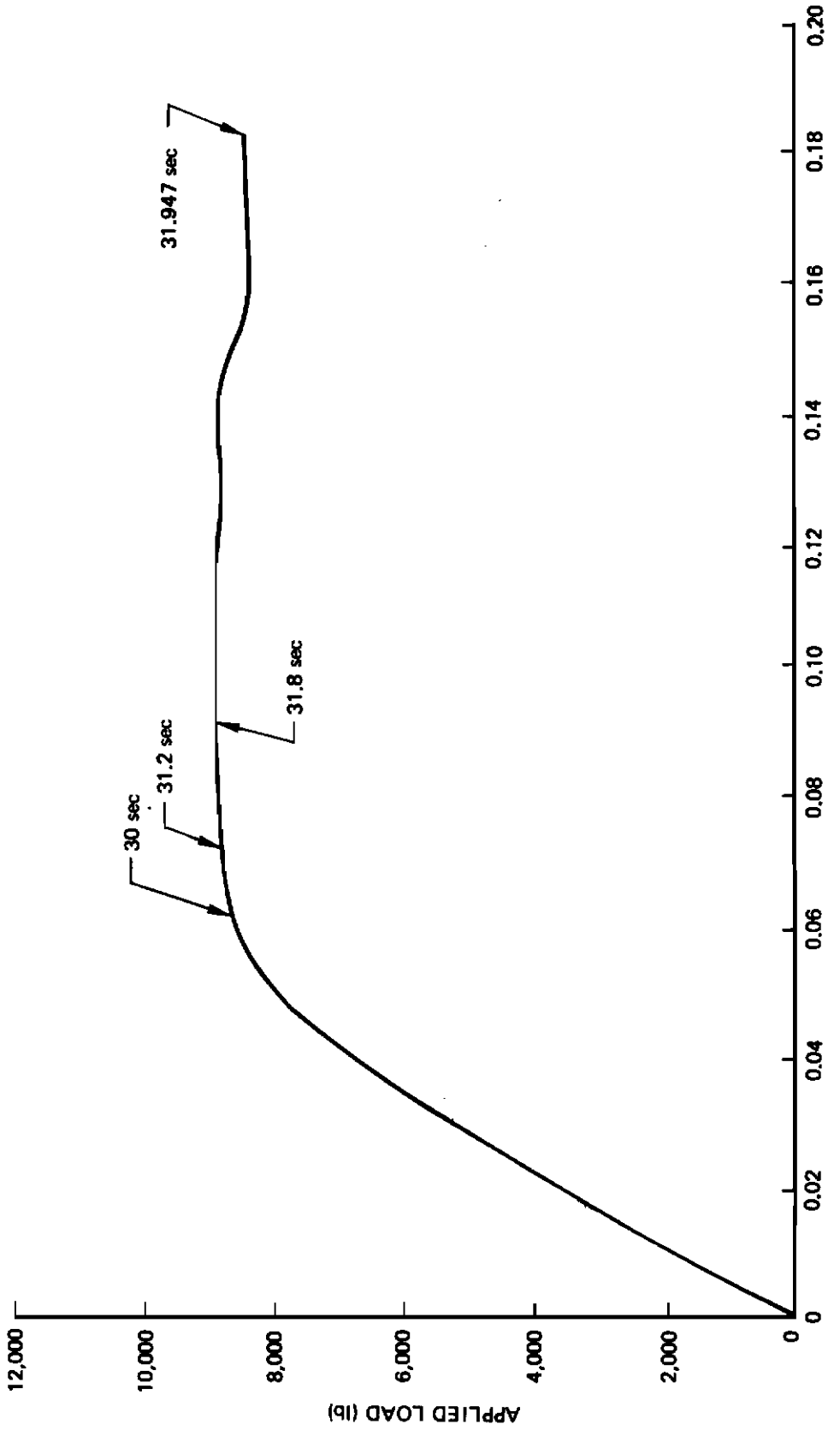

Figure 34: Load–Displacement Record Obtained For A 6Al-4V β Titanium Uniform Height DCB Specimen T3-2

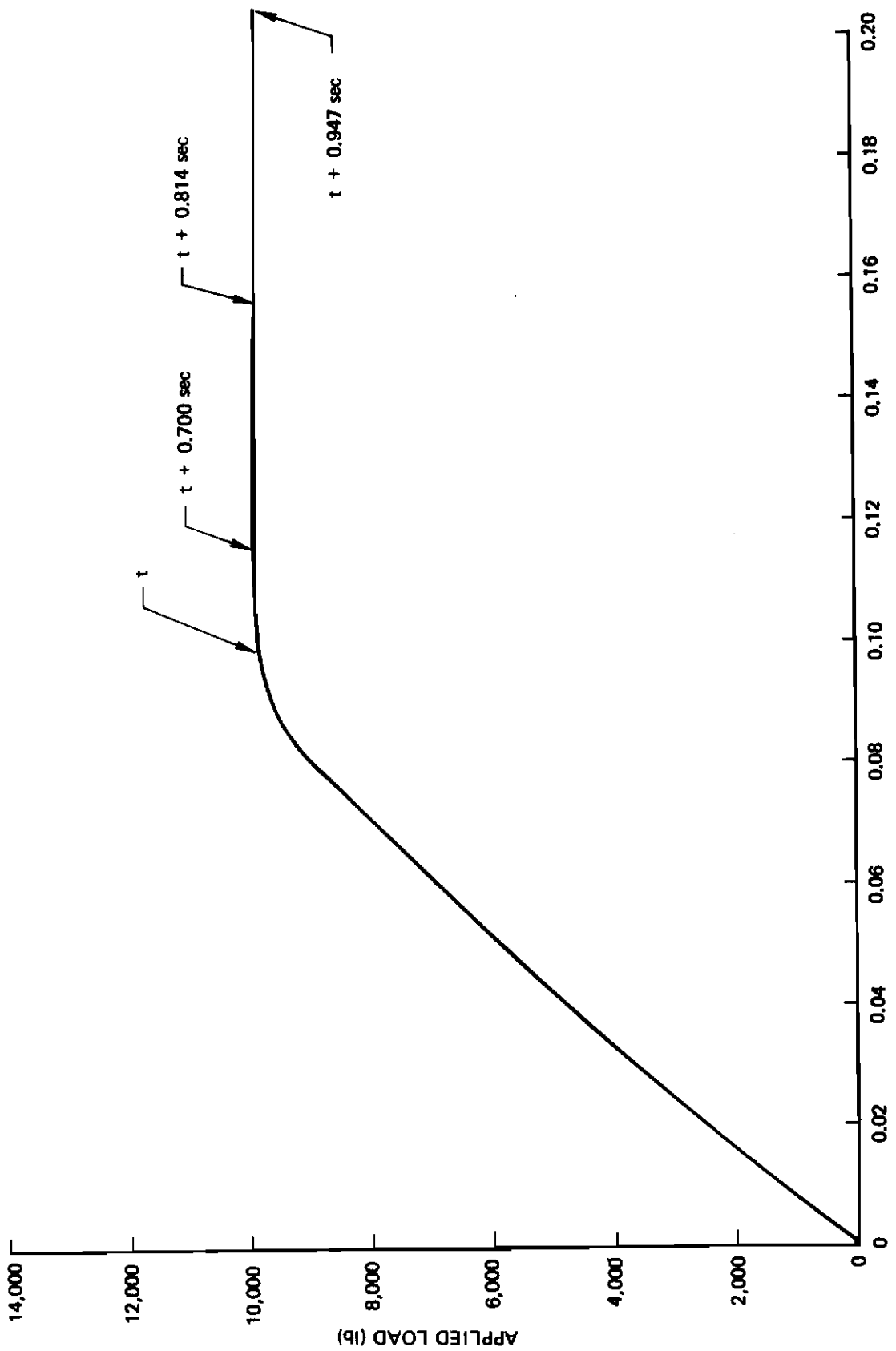

Figure 35: Load–Displacement Record For A 9Ni–4Co–0.2C Steel Uniform Height DCB Specimen S3-2

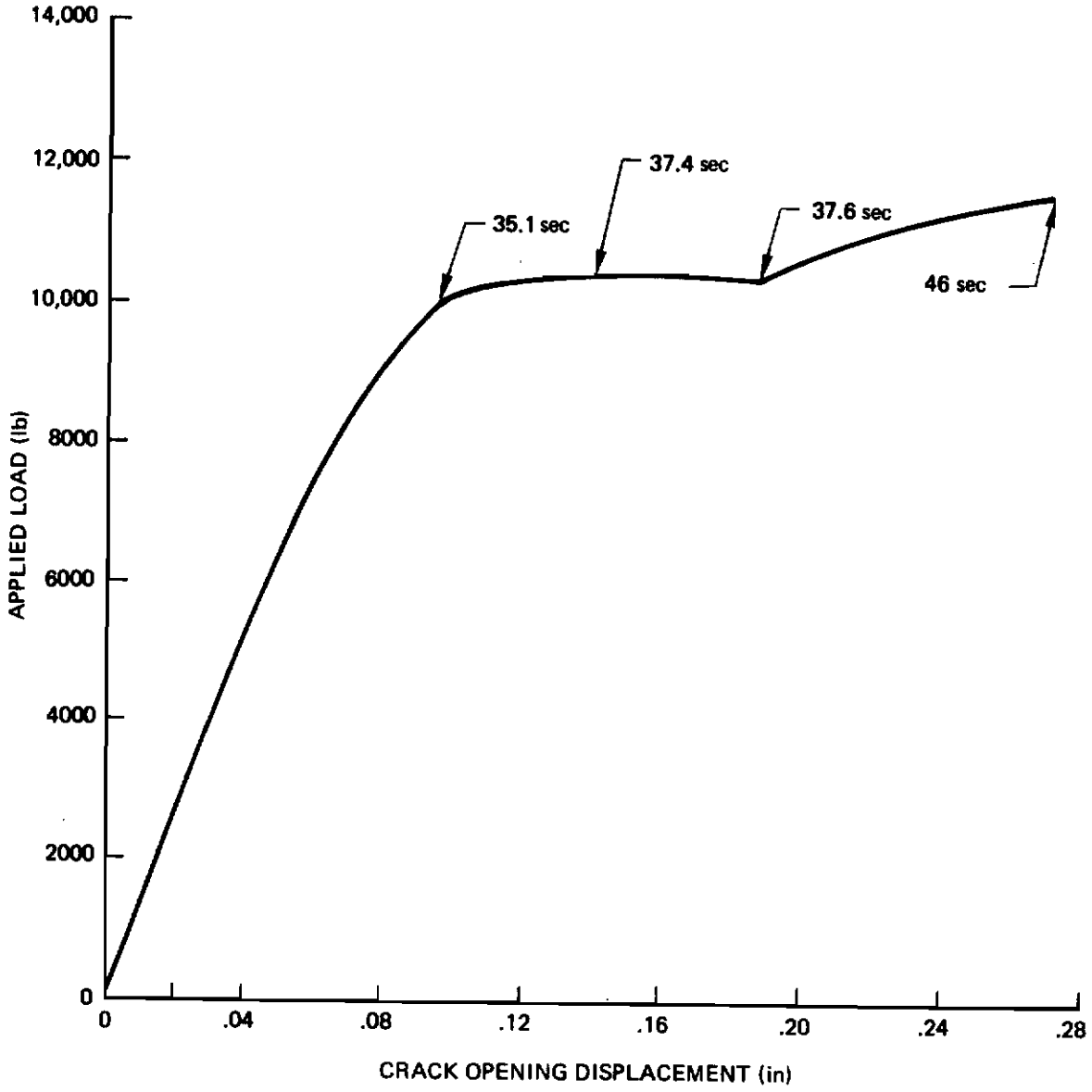

Figure 36: Load Versus Displacement Record For A 9Ni–4Co–0.2C Steel Flared DCB Specimen S14-2

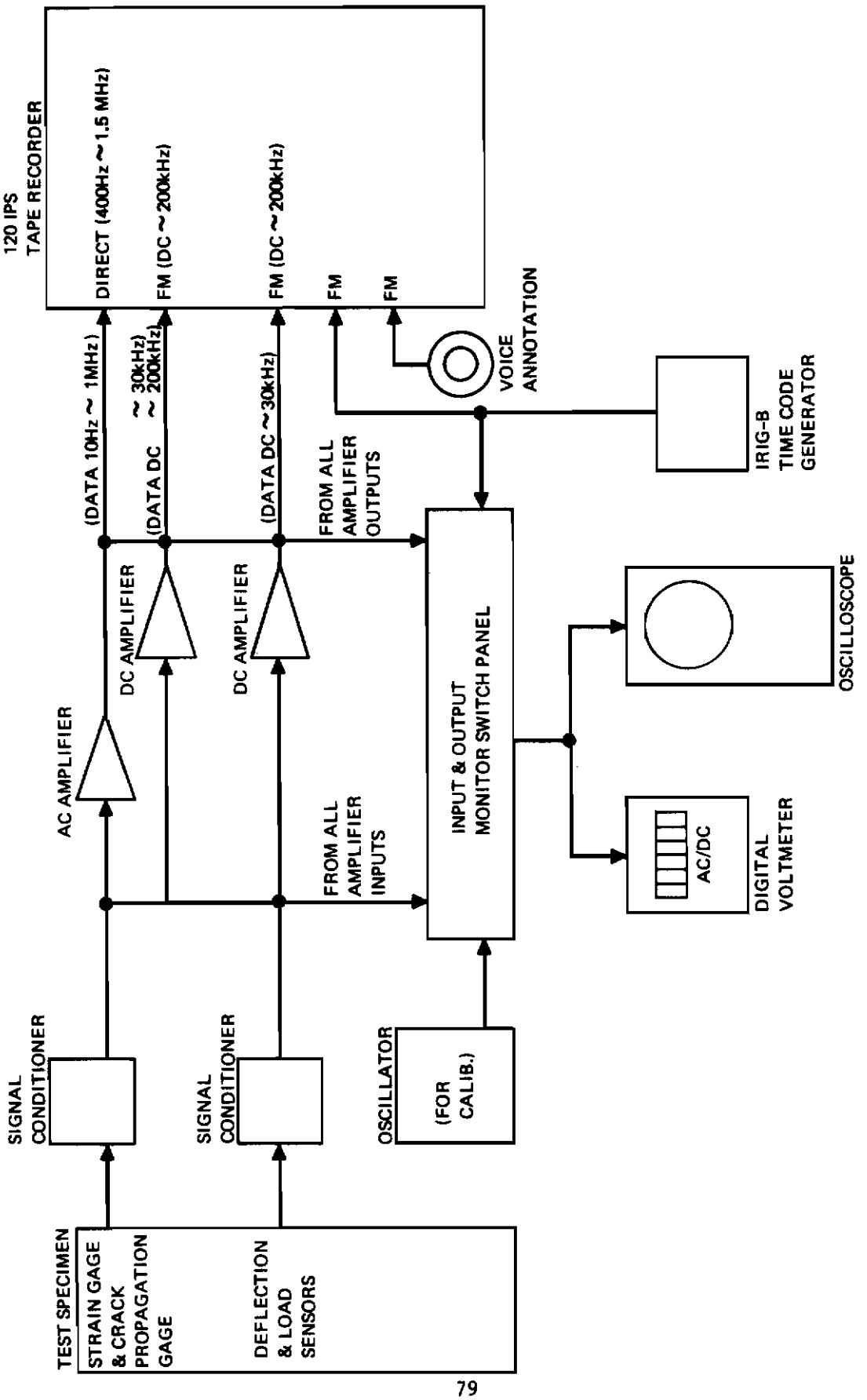

Figure 37: Instrumentation System And Hook-up For Dynamic Crack Velocity And Arrest Tests

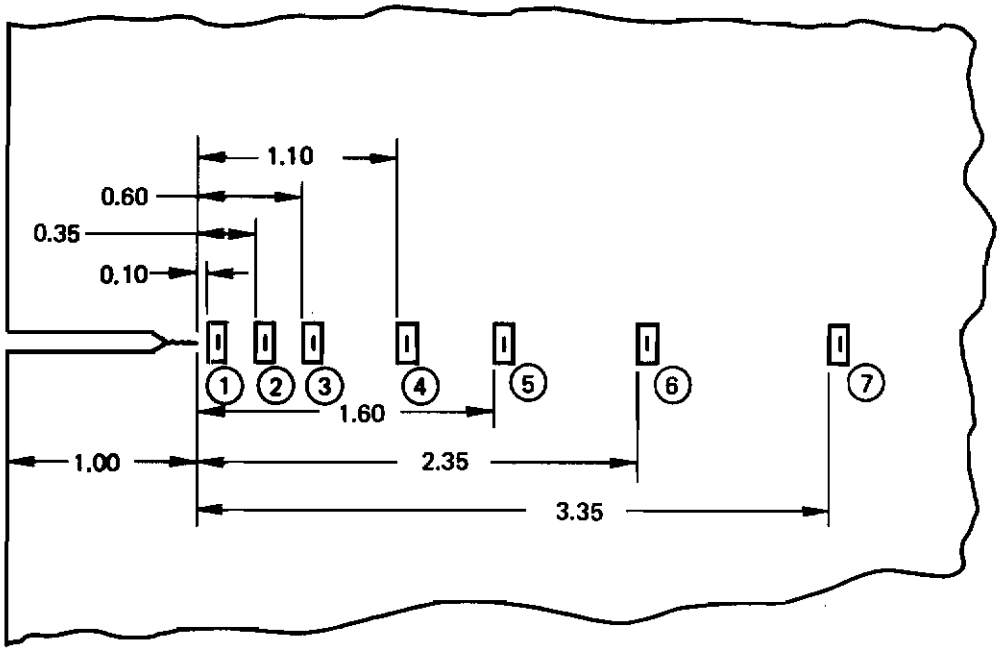

SIDE ONE

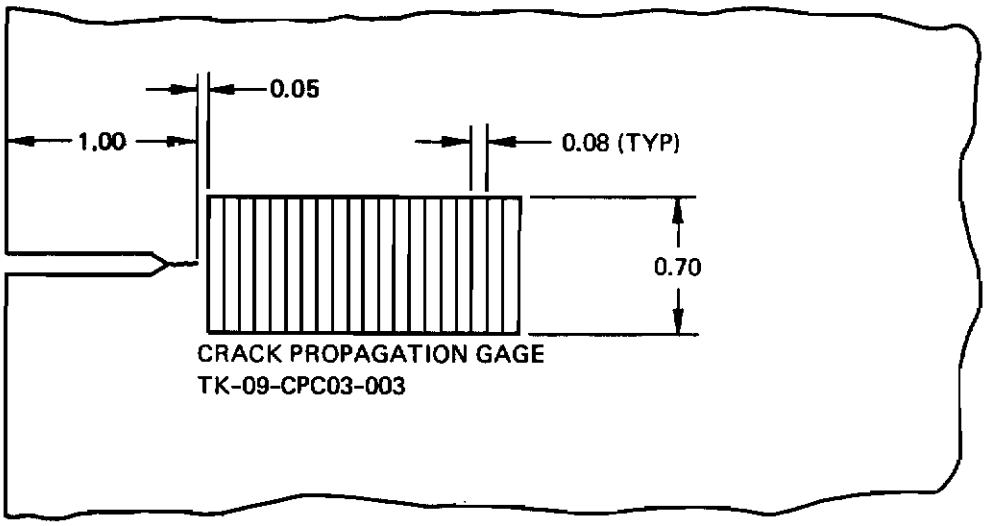

OTHER SIDE

Figure 38: Strain Gage And Crack Propagation Gage Locations For The Single Edge Cracked Panel Of 7075-T6 Aluminum

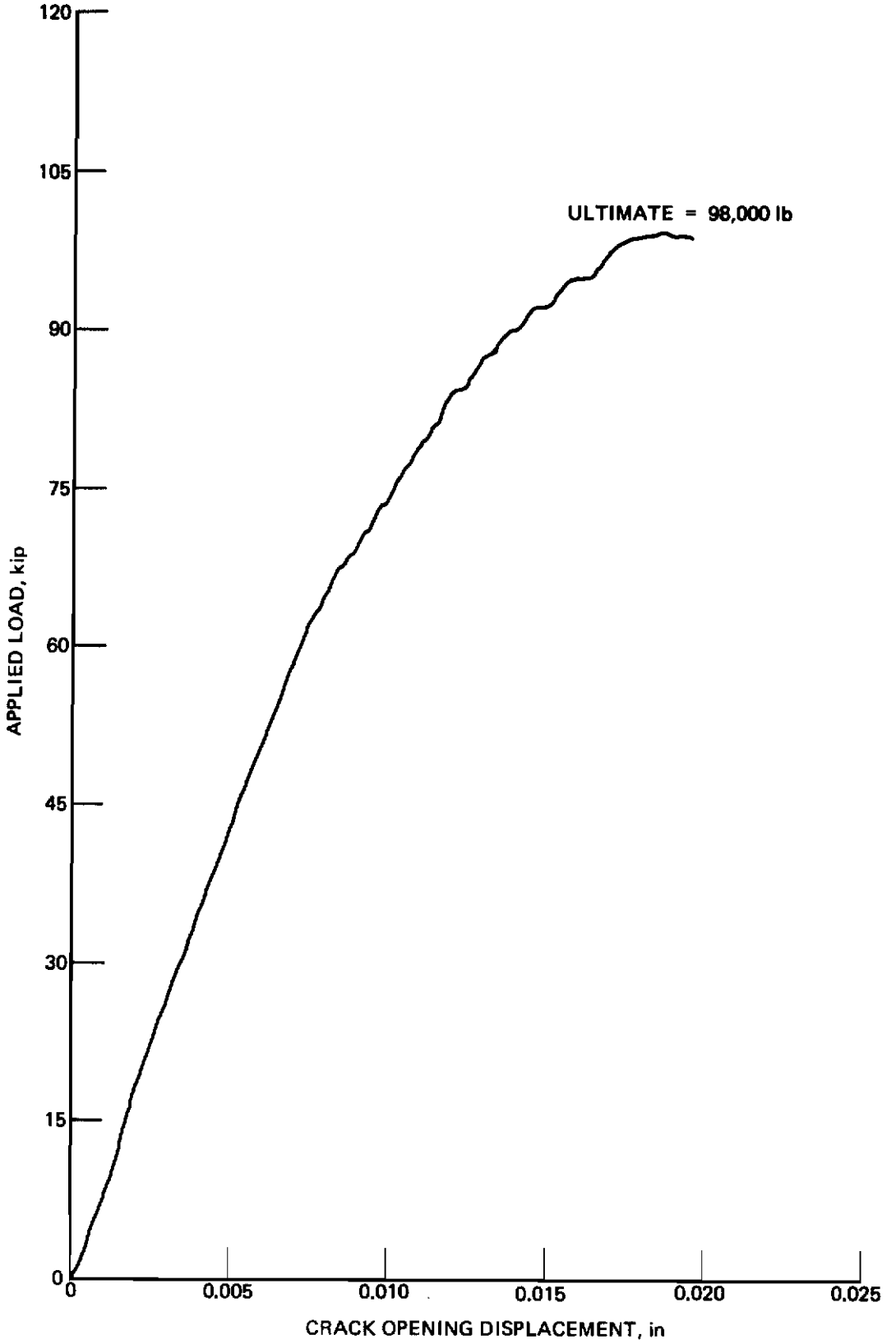

Figure 39: *Load Vs. Crack Opening Displacement Record for the 7075-T6 Aluminum Single Edge Cracked Panel*

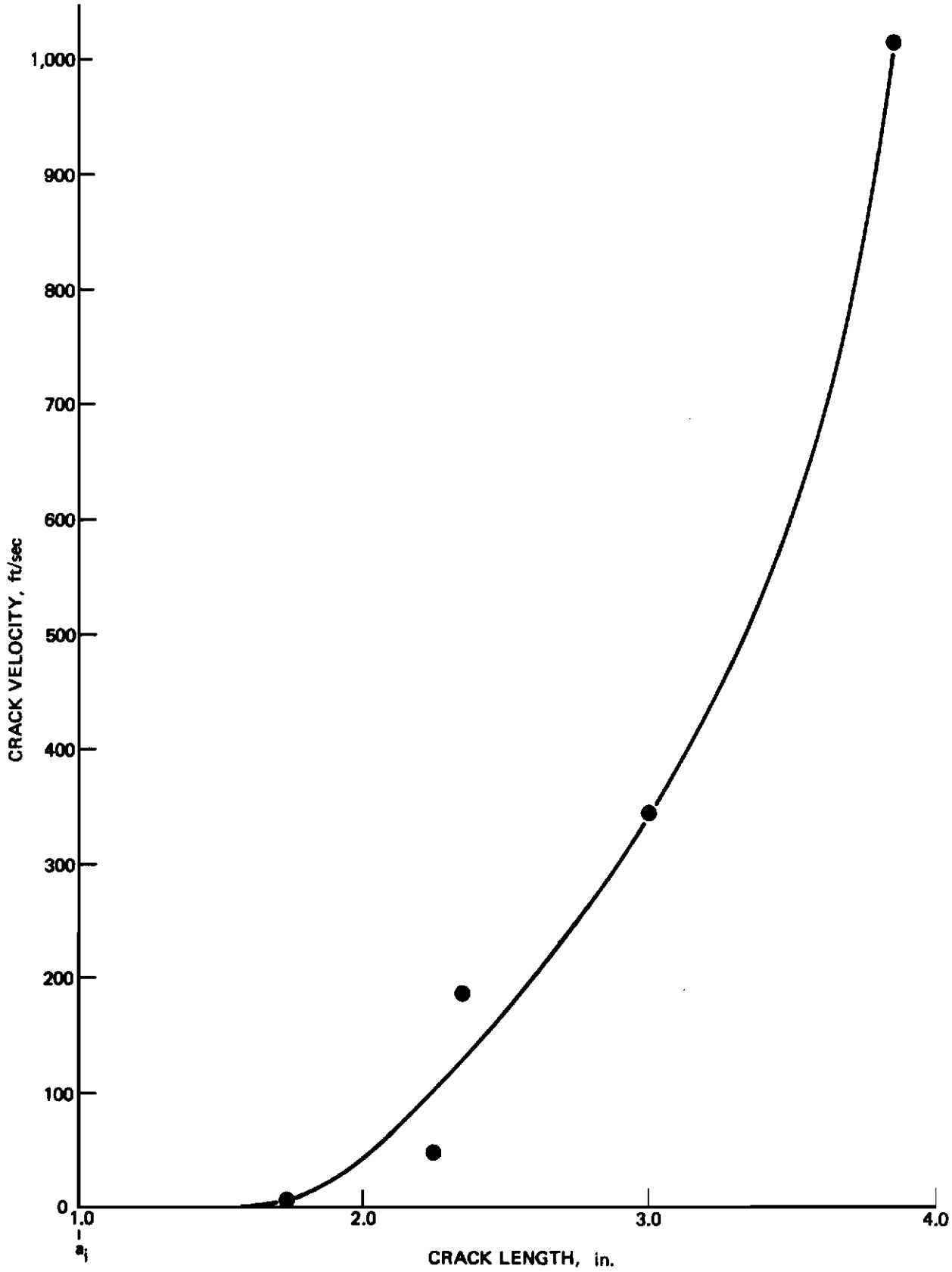

Figure 40: Crack Velocity As A Function Of Crack Length For The 7075-T6 Aluminum Single Edge Cracked Panel

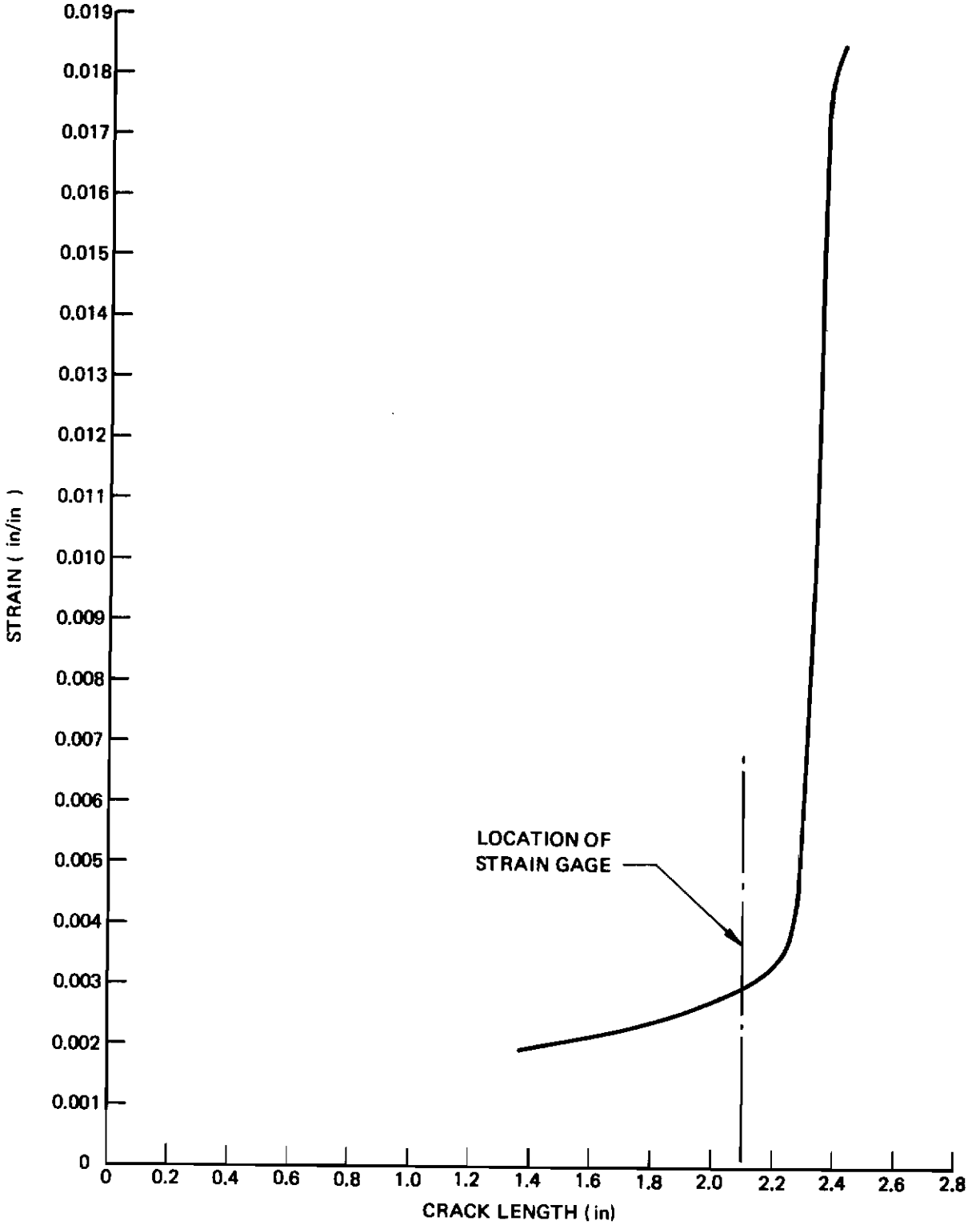

Figure 41: Strain Versus Crack Length For A Strain Gage Located At 2.10 Inch Away From The Edge Of A Single Edge Cracked Panel Of 7075-T6 Aluminum

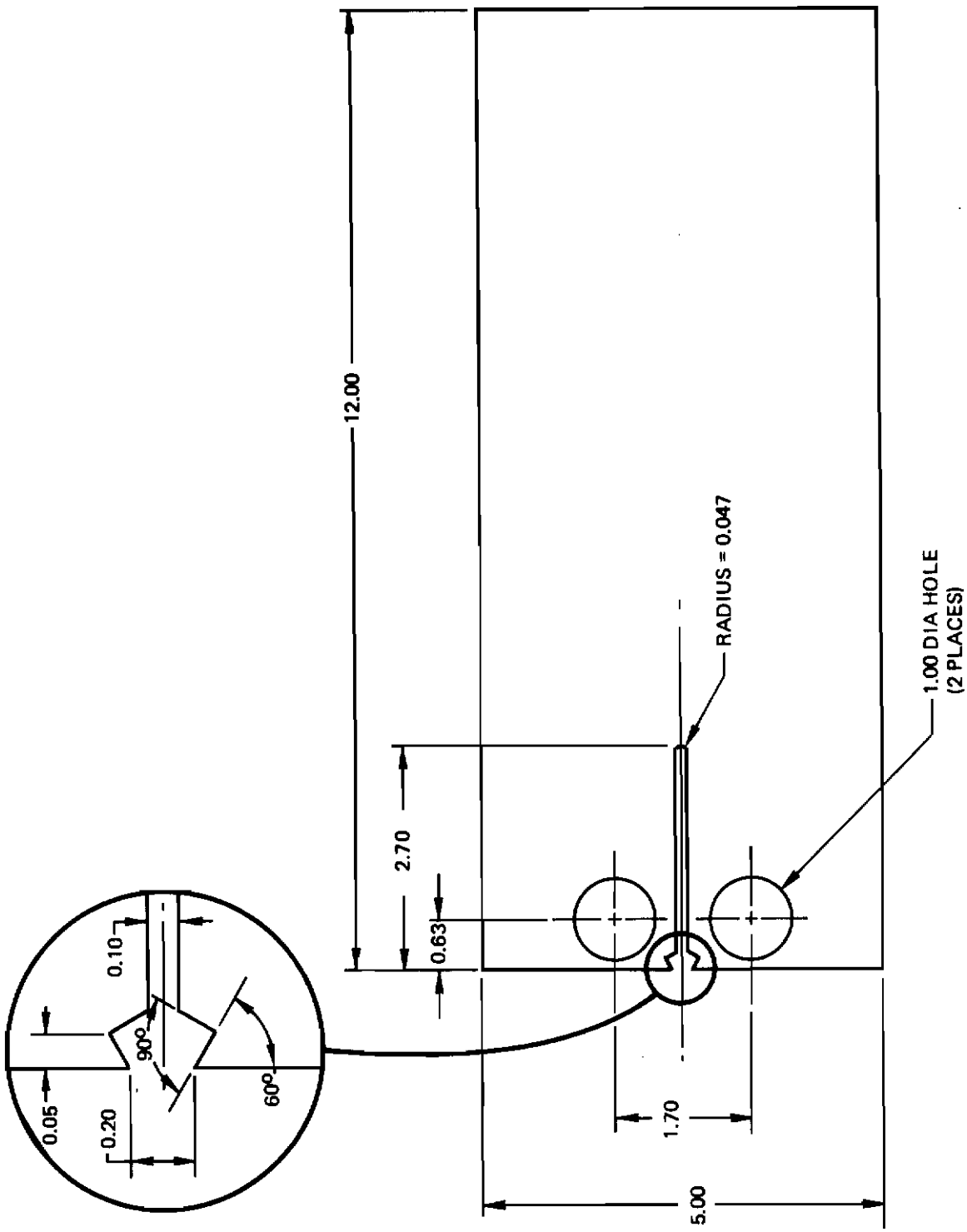

Figure 42: A 4340 Steel DCB Specimen Containing A Blunt Notch

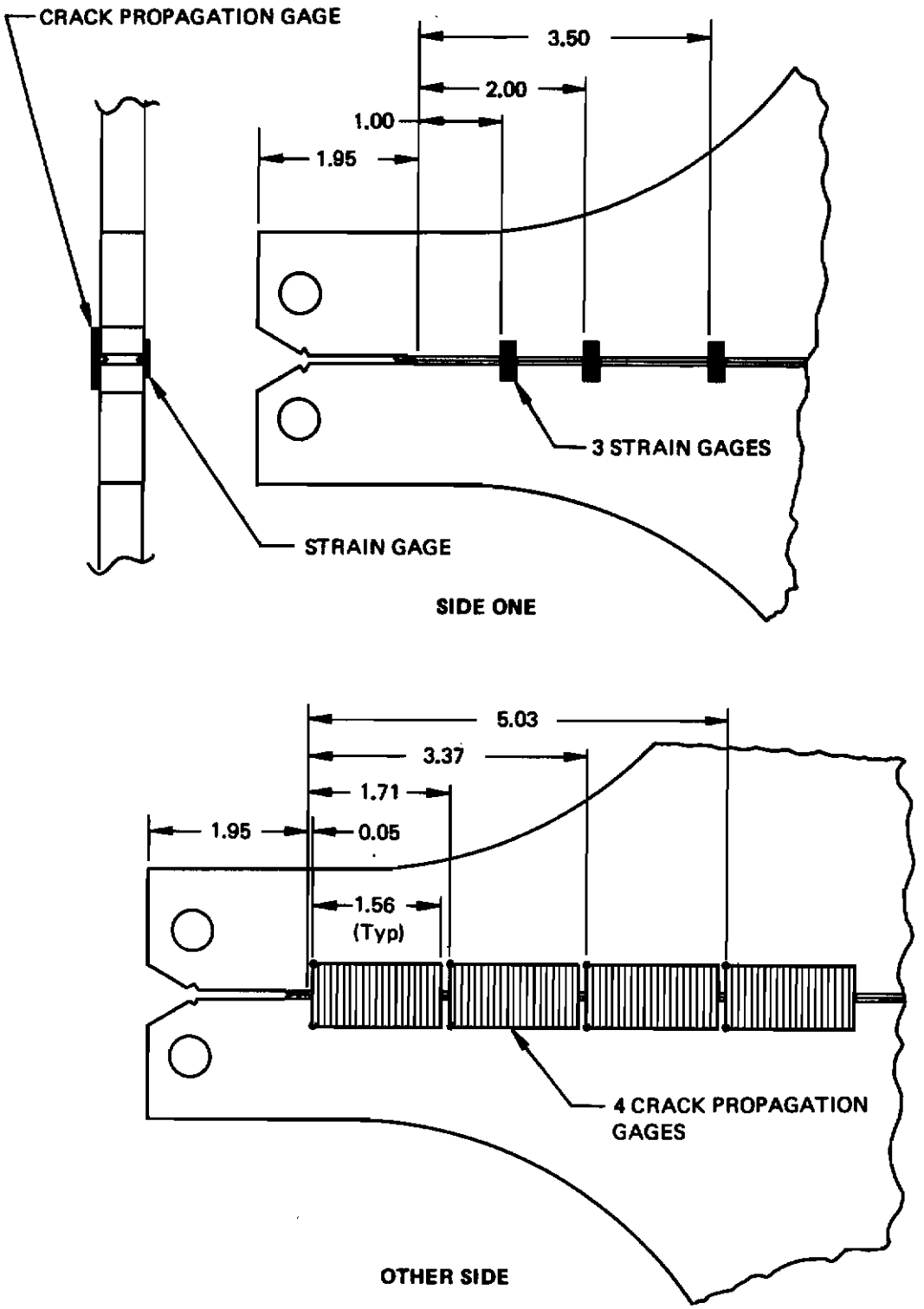

Figure 43: Strain Gage and Crack Propagation Gage Locations for the Flared DCB Specimen of 4340 Steel

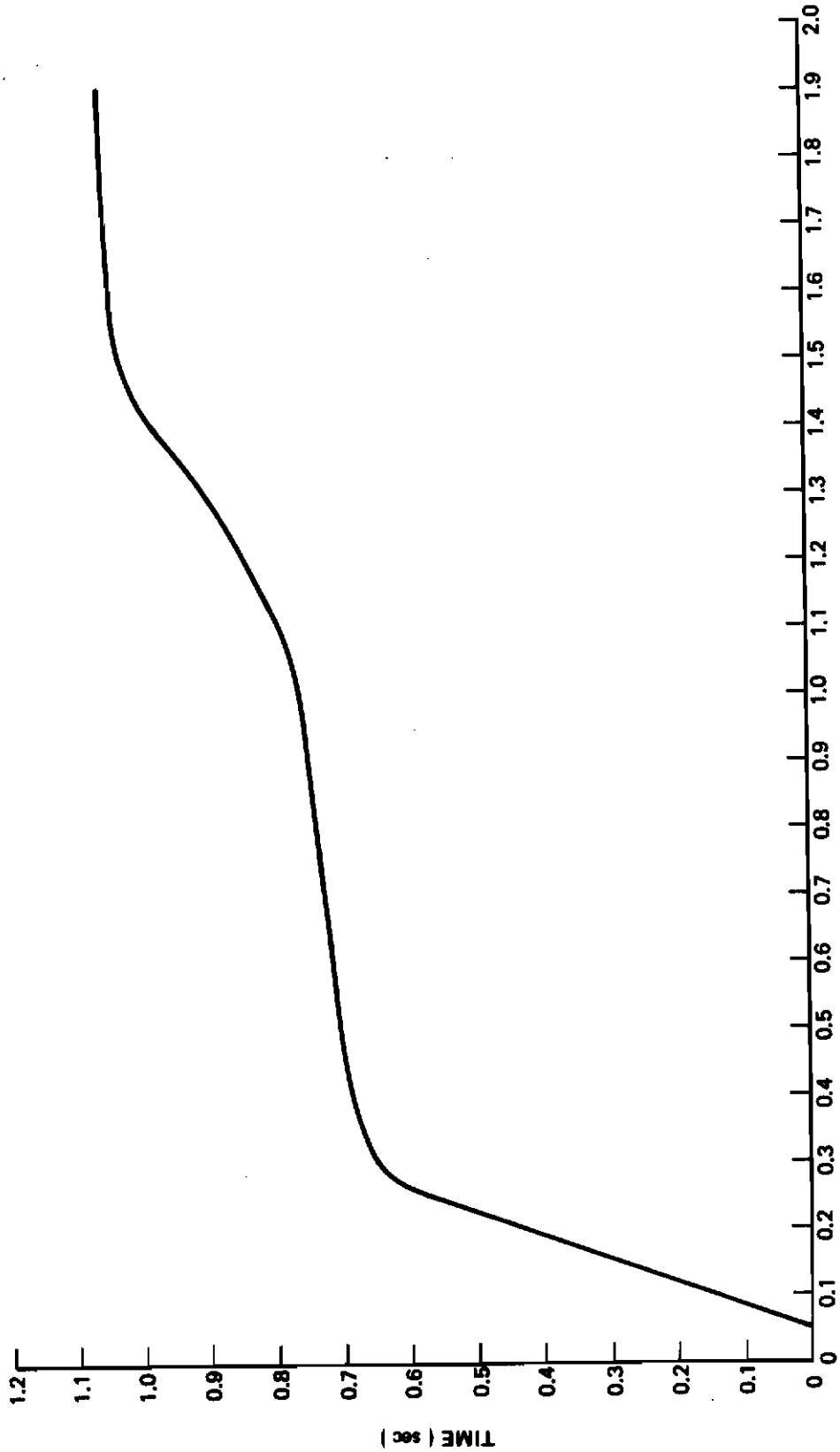

Figure 44: Increase In Crack Length Versus Time For The Flared DCB Specimen of 4340 Steel

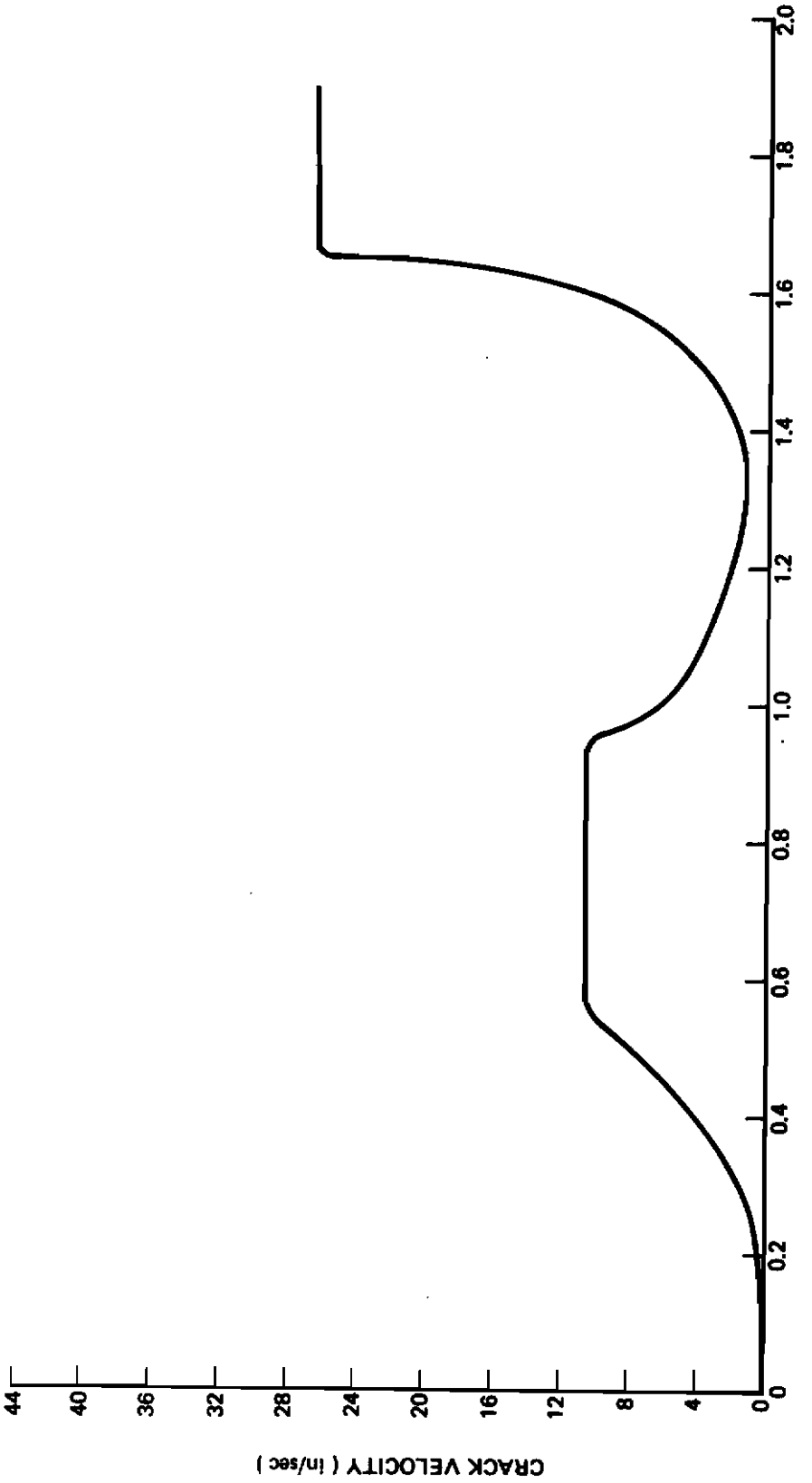

Figure 45: Crack Velocity Versus Distance For The Flared DCB Specimen Of 4340 Steel

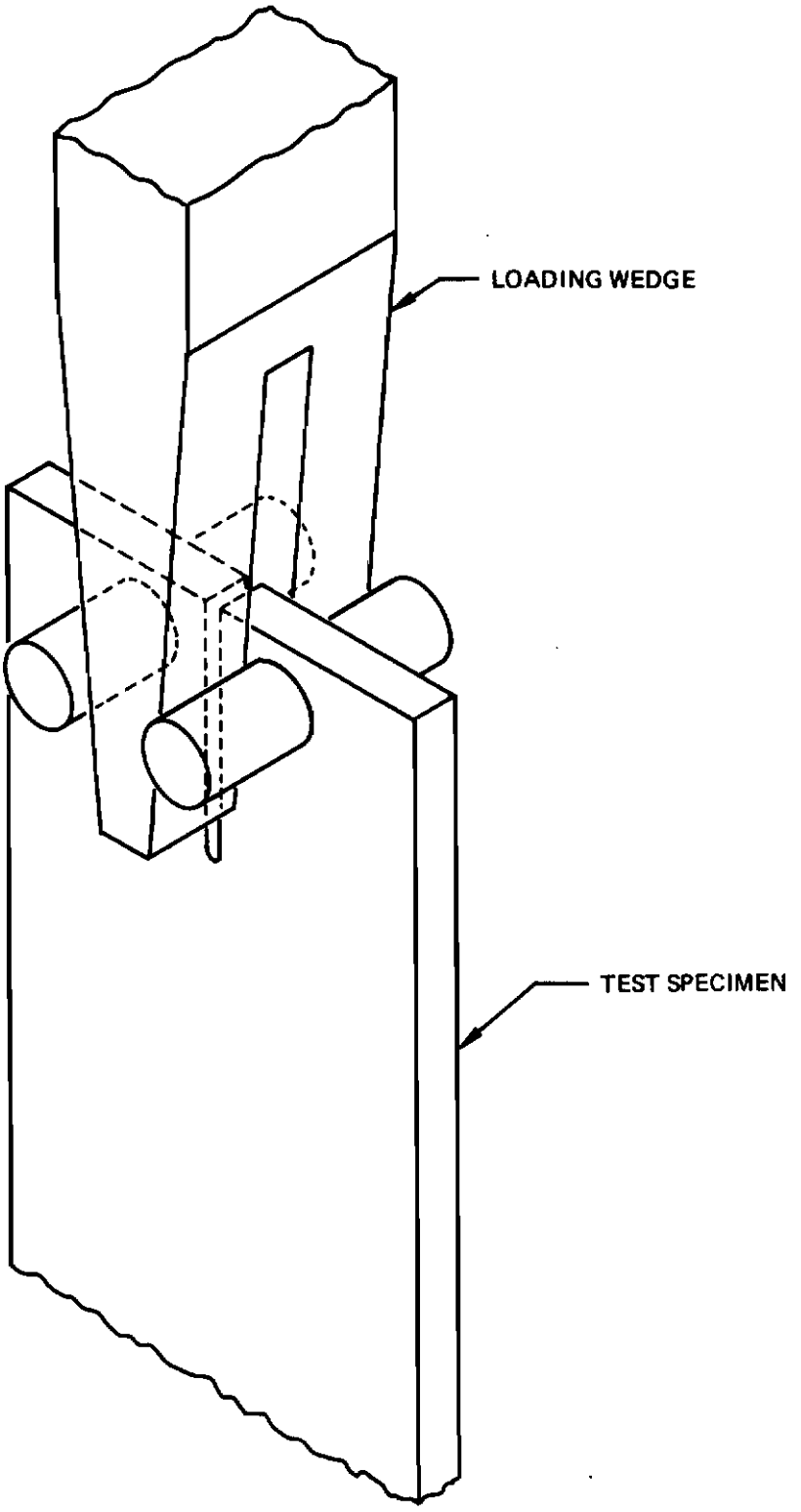

Figure 46: Wedge Loading of a DCB Specimen

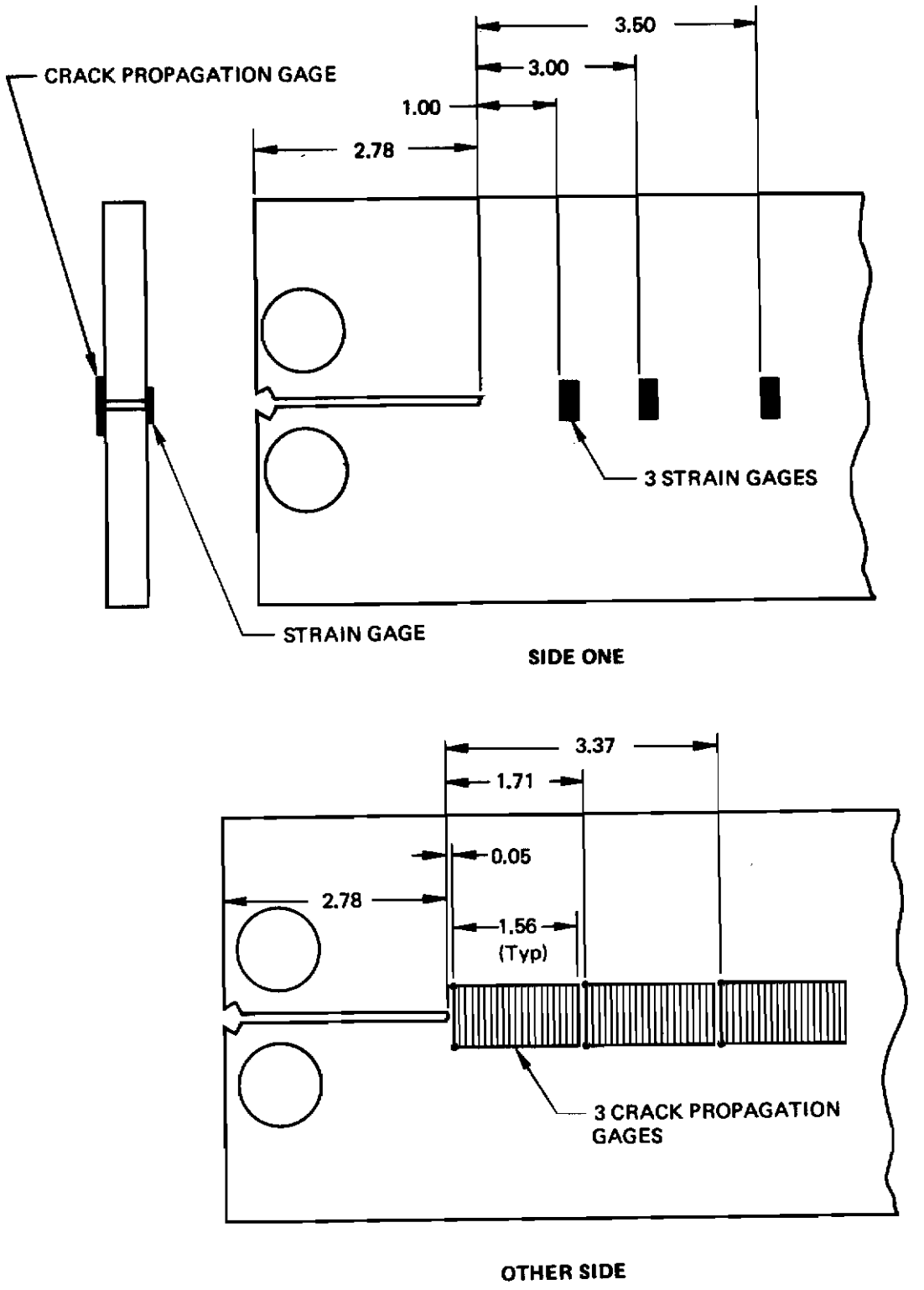

Figure 47: Strain Gage and Crack Propagation Gage Locations for the Notched DCB Specimen

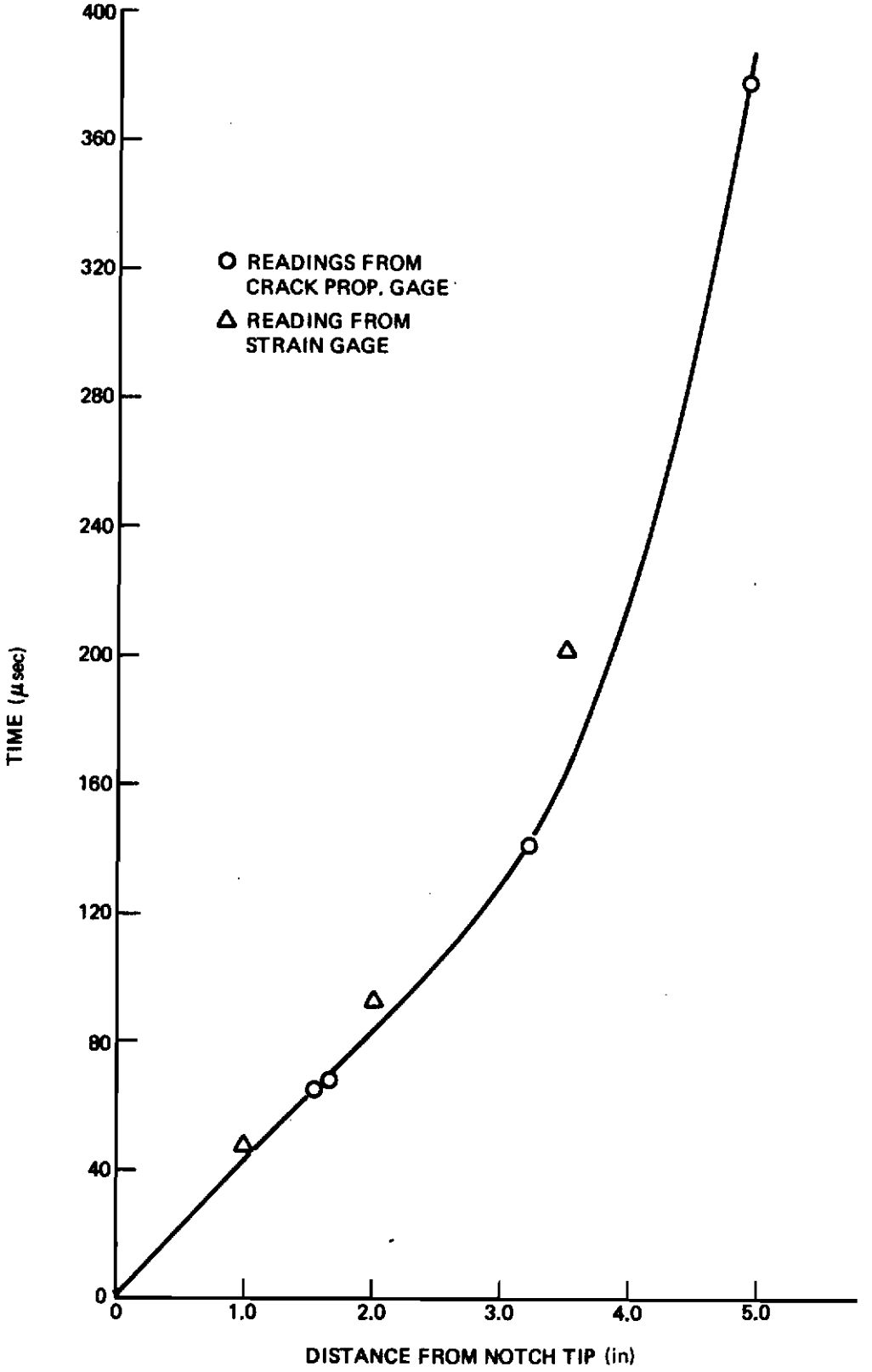

Figure 48: Increase In Crack Length Versus Time For A DCB Specimen Of 4340 Steel Containing A Blunt Notch

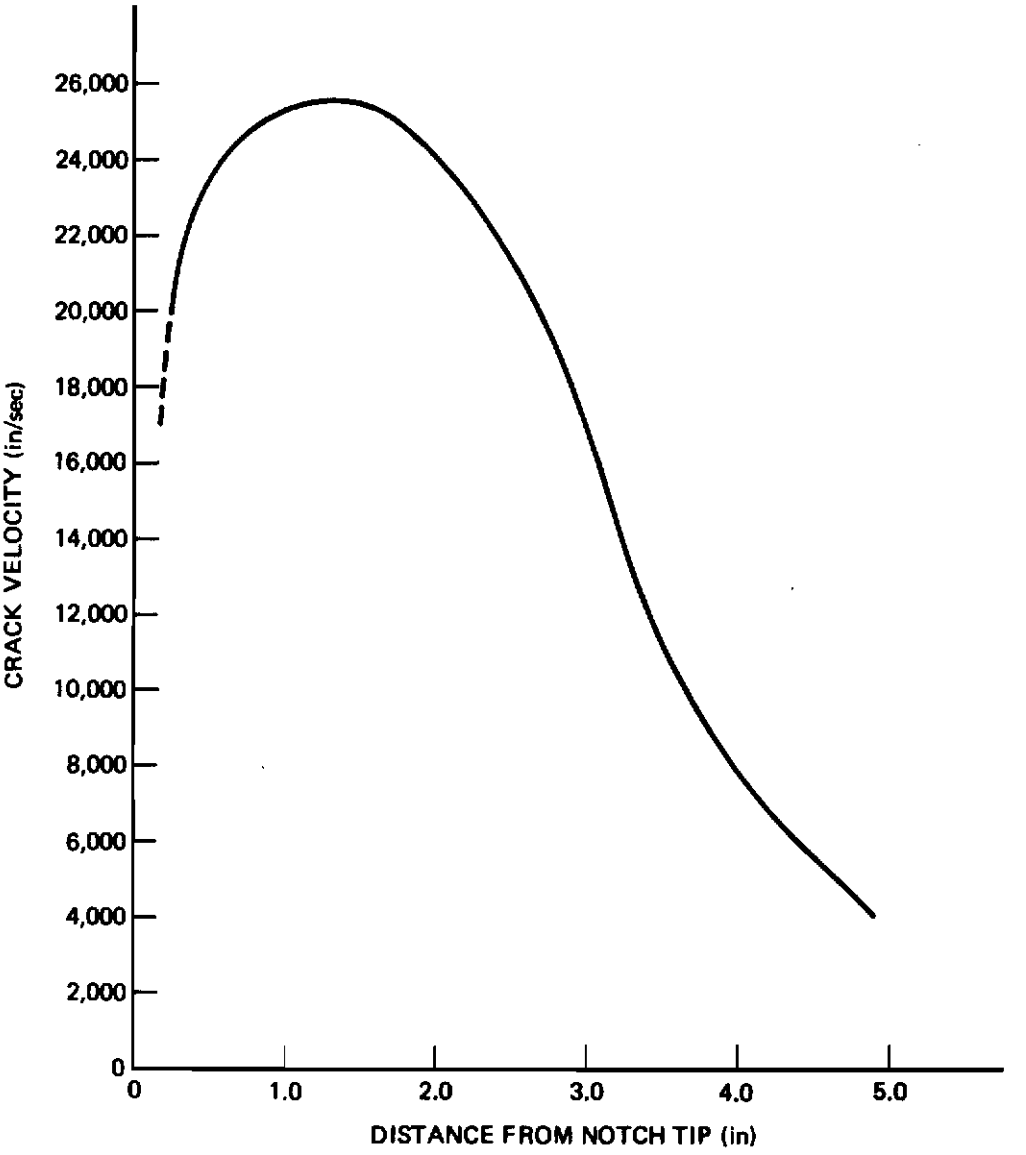

Figure 49: Increase In Crack Length Versus Crack Velocity For A DCB Specimen Of 4340 Steel Containing A Blunt Notch

☆U.S.Government Printing Office: 1974 — 758-433/502